Author/s:
Wang, Kangyan

Title:
Controlled cracking in multilayered graphene films coated on flexible substrates and their electromechanical properties

Date:
2020

Persistent Link:
https://hdl.handle.net/11343/240430

Controlled cracking in multilayered graphene films coated on flexible substrates and their electromechanical properties

By

Kangyan Wang

ORCID: 0000-0003-2677-9422

DEPARTMENT OF CHEMICAL ENGINEERING

THE UNIVERSITY OF MELBOURNE

VICTORIA, AUSTRALIA

A THESIS SUBMITTED FOR THE DEGREE

OF

Master of Philosophy

March 2020

COPYRIGHT NOTICE

Abstract

Cracking in the brittle thin films causes tremendous trouble, but controlling cracking with care brings new opportunities to flexible electronics, particularly the highly accurate strain sensing. However, the complexity of the influencing factors on crack formation poses challenges to research, accurate control, and the full utilization of the novel cracked-thin film strain sensor.

Multilayered reduced graphene oxide (MLG) films, due to their tuneable structural parameters via wet fabrication and high electric conductivity, could potentially serve as a promising material platform to study the cracking behaviours and the corresponding electromechanical properties. In particular, their unique cascading 2D nanostructures may lead to unusual cracking behaviours and advantageous electromechanical properties. Thus, this dissertation aims to explore the cracking behaviours of ultrathin MLG films coated on a stretchable substrate and the electromechanical properties of the cracked thin films.

This project unfolds into three parts. In the first part, the method to coat the vacuum filtrated ultrathin MLG film on a flexible substrate is developed. By utilizing a swelling-induced interfacial effect of graphene oxide, we developed a simple method to manipulate the surface adhesion between the MLG film and the filtration membrane, allowing the MLG film with high surface quality to be readily coated on a series of substrates through a simple transfer printing process. The second part investigates the cracking behaviours of the MLG film transferred on a polydimethylsiloxane (PDMS) substrate. The cracking morphology of MLG films was found to depend on thickness, interlayer distance, and corrugation. An unexpected transformation of cracking morphology from typical “parallel” cracks to random “percolative” cracks was observed when the MLG film is very thin (< 40 layers of reduced graphene oxide). The third part further explores the electromechanical properties of the cracked MLG films. A high gauge factor (GF) of 56521 at ε = 6 % and large stretchability of ε = 60 % when GF = 5.1 were achieved for the parallel cracked and highly percolative cracked MLG

films, respectively. The static and dynamic electromechanical characterization indicates that the percolative cracking could readily reduce relaxation, allowing accurate strain detection. A broad-frequency range accurate strain detection is demonstrated, suggesting their potential applications in human-machine interfacing and neuromuscular disease detection.

Table of Contents

List of Figures

List of tables

List of Abbreviation

Pt	Platinum
Au	Gold
Cr	Chromium
Ti	Titanium
Ag	Silver
ITO	Indium tin oxide
PUA	polyurethane acrylate
PEDOT:PSS	poly(3,4-ethylenedioxythiophene) polystyrene sulfonate
PDMS	Polydimethylsiloxane
PET	Polyethylene terephthalate
PU	Polyurethane
PE	Polyethylene
PI	Polyimide
PMMA	Polymethyl methacrylate
SBS rubber	Styrene-butadiene Rubber
TPU	Thermoplastic polyurethane
MLG	Multilayered reduced graphene oxide
GO	Graphene oxide
rGO	Reduced graphene oxide
0D	Zero dimensional
1D	One dimensional
2D	Two dimensional
NP	Nanoparticle
NW	Nanowire
CNT	Carbon nanotube
ALD	Atomic layer deposition
CVD	Chemical vapor deposition
PVD	Physical vapor deposition
NMP	N-Methyl-2-pyrrolidone
PVP	Polyvinylpyrrolidone
DI water	Deionized water

LFM	lateral force microscope
EMG	Electromyography
MMG	Mechanomyography

Declaration

This thesis is an original work of my research and contains no material which has been accepted for the award of any other degree or diploma at any university or equivalent institution and that, to the best of my knowledge, this thesis contains no material previously published or written by another person, except where due reference is made in the text of the thesis.

Signature: 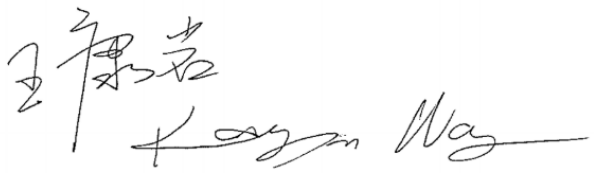

Print Name: Kangyan Wang

Date: 6/03/2020

Acknowledgements

First, I would like to express my sincere gratitude to my supervisor Prof. Dan Li, for his unparallel patience on my personal development, openness to new ideas, and continuous support on my master studies. He imparted a great amount of wisdom via words and deeds on how to have vision, how to create greatness from details, and how to be yourself that you do not have to prove to anyone. I thank him for giving me the opportunities to embark on an adventurous journey. It turned out to be the best two years of my life. Regardless of my future career, the lessons and the good qualities I learnt will be carried on.

Besides, I would like to thank my co-supervisor Assoc. Prof. Zhe Liu, for his insightful comments and knowledge from various theoretical perspectives; his encouragement and motivation. I would also like to thank my committee chair Prof. Frank Caruso, for his high standards, and the important lessons on what makes a good researcher.

My sincere thanks also go to Ms Zijun He, Dr Ke Xie, and Dr Zhiyuan Xiong, who guided me on a series of experimental designs. In a small research direction, many thanks to Ms Zijun He for her guidance and help in the past two years on the material synthesis, critical comments and suggestions. I would like to thank Dr Ke Xie for managing the lab and supported me to carry out experiments safely and accurately. I would like to thank Dr Zhiyuan Xiong for the massive discussions we had over research and life. His unique views on scientific innovations helped to promote my intellectual growth, and his philosophy of life helped me to form a more holistic view of the world.

I am grateful to the fellow groupmates for their friendship and supports on a daily basis. Ms Yang Cao, Mr Xiao Wang, Dr Lianhai Zu, Dr Zhiyuan Xiong, Ms Zijun He, Dr Ke Xie, Dr Hualin Zhan. In the past two years, we have formed deep friendships, which are valuable, especially on the lonely journey seeking new knowledge.

Last, I want to express my deepest gratitude to my family. I could not imagine myself pursuing an advanced degree at a foreign land without their unconditional love and support. I am the man today only because they believed me to be upright, brave, and can do things right; also stood by me no matter what decision I make.

Chapter 1 Introduction

Cracking is a common issue for functional brittle thin films coated on flexible substrates due to their propensity to break, particularly for large-area films or when subjected to large strain. These cracking behaviours pose significant challenges for a range of flexible applications such as flexible display, stretchable epidermal electronics, flexible energy storage, etc. And tremendous collaborative efforts were made to understand the crack mechanisms [1-10] as well as to avoid catastrophic cracks through structural engineering on brittle thin films and stretchable materials' innovation [11-31].

While cracking is conventionally deemed as detrimental, recent studies generated brand new perspectives that carefully controlled cracking can produce unique electromechanical properties—for example, Kang *et al.* [32] produced a platinum (Pt) thin film coated on a polyurethane acrylate (PUA) plastics with "cut-through" parallel nano-cracks (figure 1.1a). These cracks with "parallel" characteristics significantly altered the electric conducting pathways and produced an "on-and-off" switch within 2% strain. As a result, they created an ultrasensitive strain sensor with gauge factor (relative resistance change per unit strain) equals to 2000 in 0-2 % strain range, marking a landmark of sensitive strain sensor which filled the gap of small strain detection. Based on this work, Jaiswal *et al.* [33] designed an ultrasensitive alcohol vapour sensor with quasi-periodic parallel cracked poly(3,4-ethylene dioxythiophene) polystyrene sulfonate (PEDOT:PSS) thin film coated on a polydimethylsiloxane (PDMS) substrate (figure 1.1b). It enhanced the vapour sensitivity approximately 10^7 fold and overcame the feeble changes in electric conductivity in traditional swelling-based vapour sensors. A similar example is the humidity sensor [33]. Choi *et al.* [34] designed a sensitive pressure sensor with a guided crack array of 10 nm chromium (Cr) and 20 nm Pt on top of a hole-patterned PUA film and demonstrate pressure sensitivity of 10^5 at 8-9.5 kPa range (figure 1.1c). The crack-induced rapid change in conductivity also inspired other fields of electronics. For example, Luo *et al.* [35] revisited the detrimental cracks in electronics and innovatively exploited an electric field in a metallic alloy-ferroelectric heterostructure to produce a switchable nano crack and demonstrated a non-volatile high on/off current ratio of $>10^7$. The

revolutionising idea provided brand new opportunities for the development of non-volatile memory and logic.

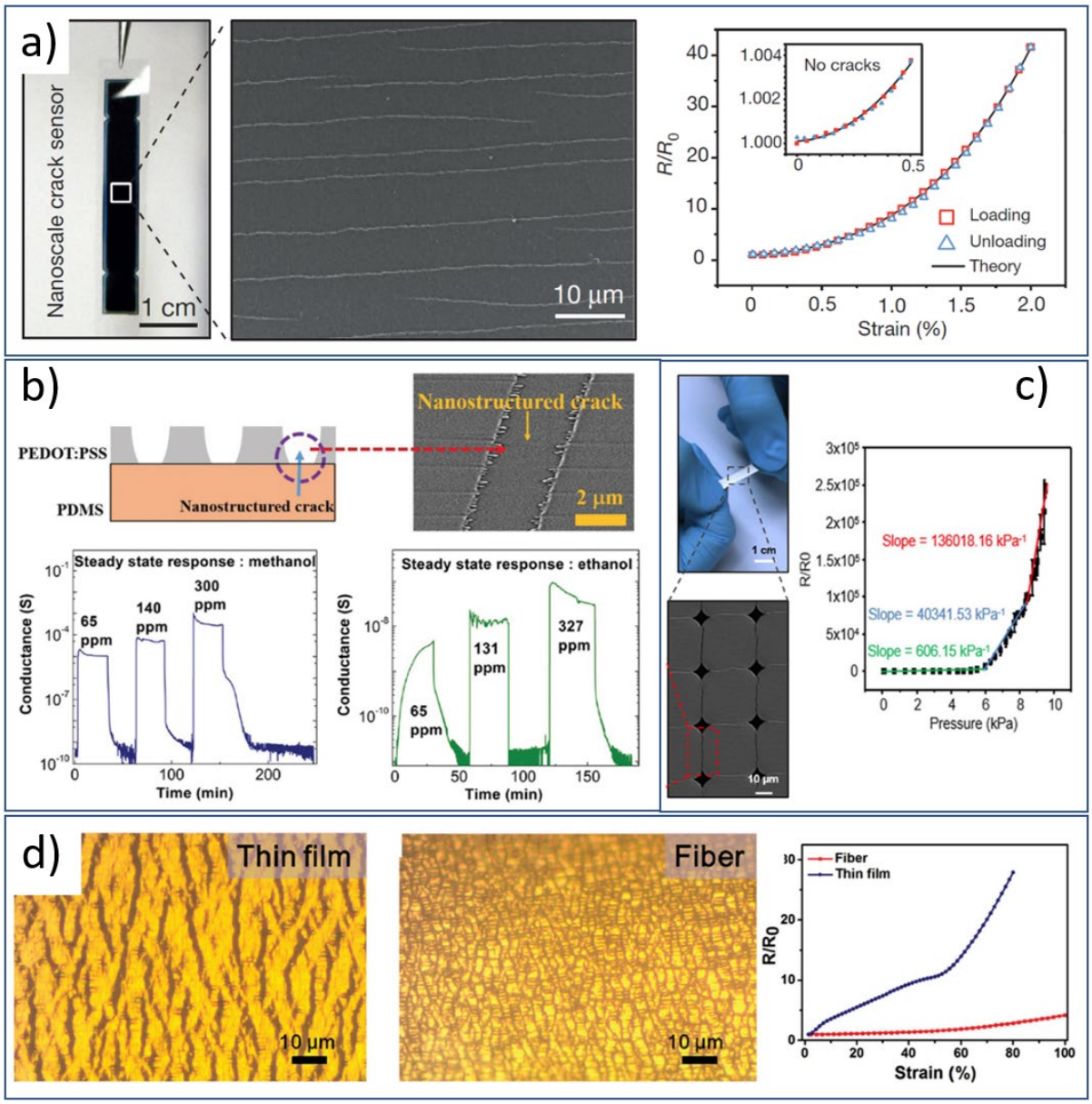

Figure 1.1 *Typical examples of novel electromechanical properties produced by controlled cracking. a) Cracked 100 nm thick Pt film coated on a PUA substrate, as a sensitive strain sensor.[32] b) Cracked PEDOT:PSS thin film coated on a PDMS film, as a sensitive alcohol sensor.[33] c) Guided cracked Pt/Cr thin film coated on a pre-pattern PUA film, as a sensitive pressure sensor.[34] d) Cracked gold thin film and cracked gold fibre that is produced from a gold thin film.[36]*

On the other hand, stretchability also plays an important role in flexible electronics, especially the wearable devices that need to undergo large strains (>30%) due to human motions. While structural engineering is currently the solution to stretchable electronics, they require intricate cutting and transfer printing techniques—instead, Chen *et al.* [36] sought inspiration from the early mechanical studies in stretchable metal films; they produced a gold fibre from gold thin film to show a highly randomised "percolative" crack network with dense small cracks (figure 1.1d), that maintains low electrical resistance of 220 Ω at 100% strain, only four times of the initial resistance. This new strategy in producing stretchable percolative network provides a simple complementary methodology to the stretchable electronics and provides an opportunity in transparent thin film electronics. Other than these typical examples, thin films with different materials and different crack morphologies were examined [37-53] to show various electromechanical properties like large stretchability, high gauge factor, fast response, good cycle stability, etc. All these efforts contributed to the development of thin film flexible electronics.

However, despite the demonstration of novel applications, there remain several fundamental questions. First, the knowledge of crack formation and propagation has not been well established. Second, the effects of cracks on electrical and other physical properties are not well understood. Third, our understanding of how to avoid or utilise cracks for desirable strain sensing performance is limited. The answer to these questions are critical to the accurate control and full utilisation of the novel cracked thin film electronics.

Due to the complexity of crack mechanics, the cracking behaviours can be affected by a variety of factors such as the substrate's surface roughness [54], chemistry [45], modulus [8]; the thin film material's thickness [8, 55], defects [40, 55-57], internal stress [58], stress distribution [59], ductility [5, 6, 8] and the substrate/thin film interfacial adhesion [5, 60]. Therefore, some contradicting experimental results were noted in the literature, and these results are summarised in figure 1.2. In terms of morphology, for example, in Kang *et al.*'s study [32], they compared the cracking behaviour of Pt and Au thin films and claimed that only Pt thin film could form parallel cracks and Au cannot. However, other studies have reported the appearance of parallel channel cracked Au thin film (figure 1.2a) [46, 60]. In terms of electromechanical properties, while most channel cracked networks have low stretchability before losing conductivity [32,

38] (figure 1.2b), and it is a trade-off between high gauge factor and high stretchability [43]. But some recent studies showed excellent stretchability in parallel cracked network [45, 53] (figure 1.2c), showing an unexpected dual high stretchability and gauge factor [43, 53]. The enhancement in stretchability indicates the existence of "bridging structures" that contribute to electric conductivity. Yet, our understanding of the underlying reasons is limited.

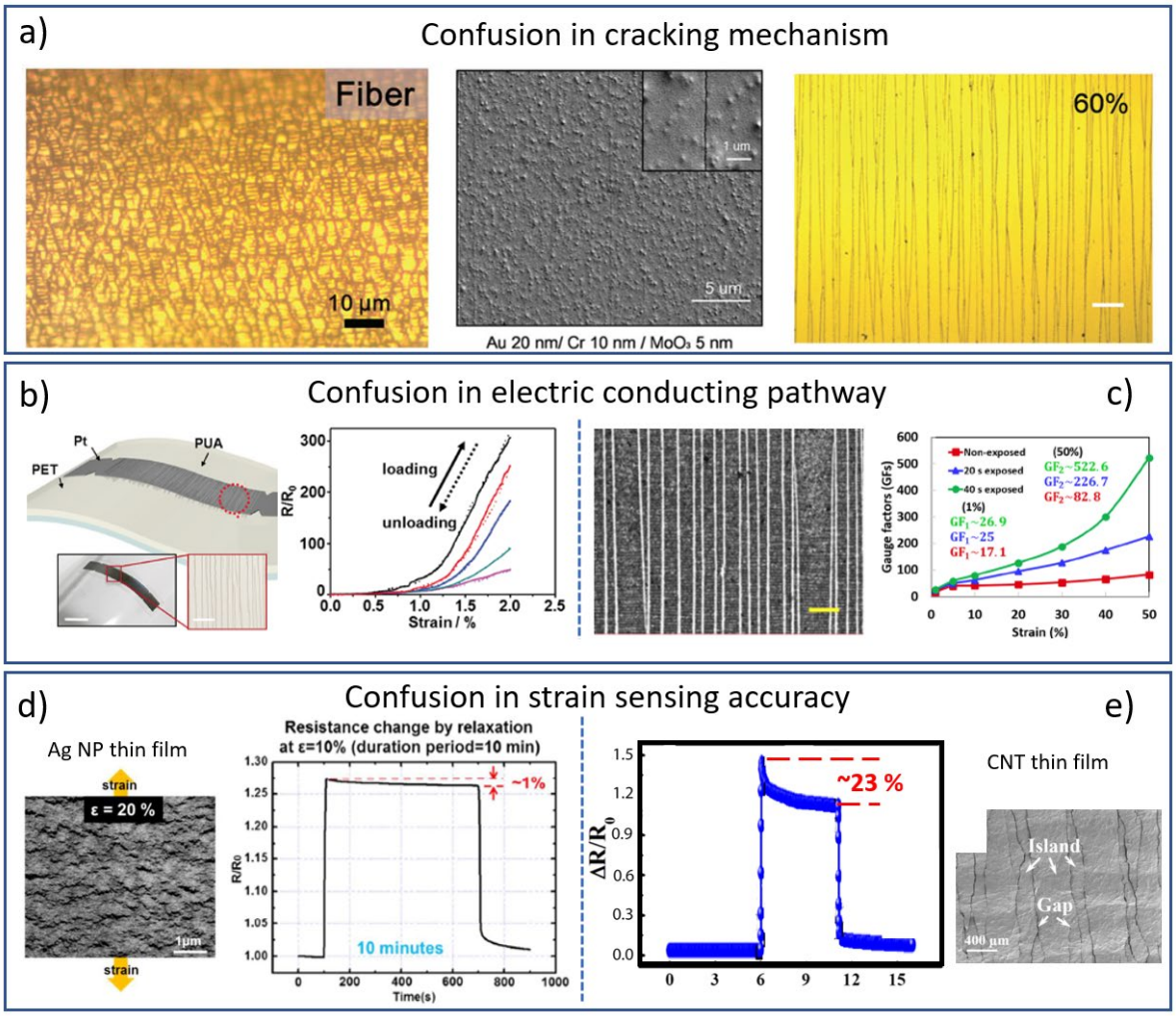

Figure 1.2 *Knowledge gaps in current cracked thin film studies. a) Confusion in cracking mechanism. Left, percolative cracks in Au thin film. Middle, channel crack in Au/Cr/MoO3 multilayer thin film. Right, channel crack in Au thin film. [36, 46, 60] b-c) Confusion in the electrical conducting pathway. b) Morphology and electromechanical property of typical parallel cracked network with low stretchability. [38] c) Morphology and electromechanical property of parallel cracked network with high stretchability. [45] d-e) Confusion in strain sensing accuracy. d) relaxation in Ag nanoparticle thin film. [40] e) Relaxation in CNT thin film. [53]*

Moreover, the stable strain-resistance response is ideal for real-world applications, such as human-machine interface (HMI) [61]. However, the accuracy in strain sensing is questionable due to a propensity to change the resistance, which is named as "resistance relaxation" [40, 43, 62-65], according to the stress relaxation in the polymer substrate. From literature, while the relaxation could be well controlled, for example, Lee *et al.* [40] produced a silver nanoparticle (Ag NP) network on PDMS that has only ~ 1% relaxation in 10 min (figure 1.2d); many other thin films undergo large relaxations within a short time, for example, Zhou *et al*. [53] synthesised a CNT thin film on thermoplastic polyurethane (TPU), which underwent ~23 % relaxation in 6 s. We regard the electromechanical characterisation as an indication of the network's microstructure. Thus the relaxation represents an ongoing structural re-construction. Reduced relaxation is of practical engineering interest; nonetheless, it is usually overlooked, and the underlying reasons for relaxation are not well understood.

Addressing these confusions has important engineering meanings. First, the percolative network produced from Au thin film shed light on a unique cracked morphology, and the prospect of highly stretchable circuitry from simple fabrication is of importance to the development of flexible electronics. Second, the inaccuracy of strain sensing due to relaxation has hindered the development of many future applications such as remote surgery, that requires time-independent accurate strain sensing. Revealing how to achieve small relaxation can support such technological development. Third, the desirable time-independent precise strain sensing also provokes the thinking: Is it likely that cracked thin film has good dynamic sensing ability? Which open the door to the broadband sensing applications such as healthcare monitoring, neuromuscular disorder diagnostics, rehabilitation and sports, etc.

The MLG films that were recently developed in our group provide a new material platform for a systematic study on cracking morphologies and their electromechanical properties. First, the unique layer by layer assembled structure offers a large extent of tunability [66-68]. Due to the colloidal behaviour and the excellent processability of the graphene sheets in solution, the structure of MLG film can be readily tuned via controlling sheet corrugation, sheet size, interlayer distance and overall thickness (figure 1.3) [66-69]. These tunable structural parameters offer a promising opportunity to conduct systematic investigations of the cracking behaviours of MLG film at controlled conditions. Second, the unique interlayer properties in

the cascading 2D MLG film are intrinsically different from grain-interactions in metallic film and thin films made from other 1D or 0D materials. It would be of great interest to study if the cascading MLG film could show unique cracking behaviours. Third, the electrical conducting characteristic of graphene material could facilitate the electromechanical characterization of the MLG films. Moreover, while the cracking behaviour of CVD grown single-layer [70] to few-layer [71-73] graphene have been reported, the knowledge on the cracking behaviour of ultrathin MLG films, particularly when they are coated on a polymer substrate, remain blank. Understanding the cracking behaviours in MLG film can help to the gap, as well as provide insight into the mechanical properties of the 2D material family.

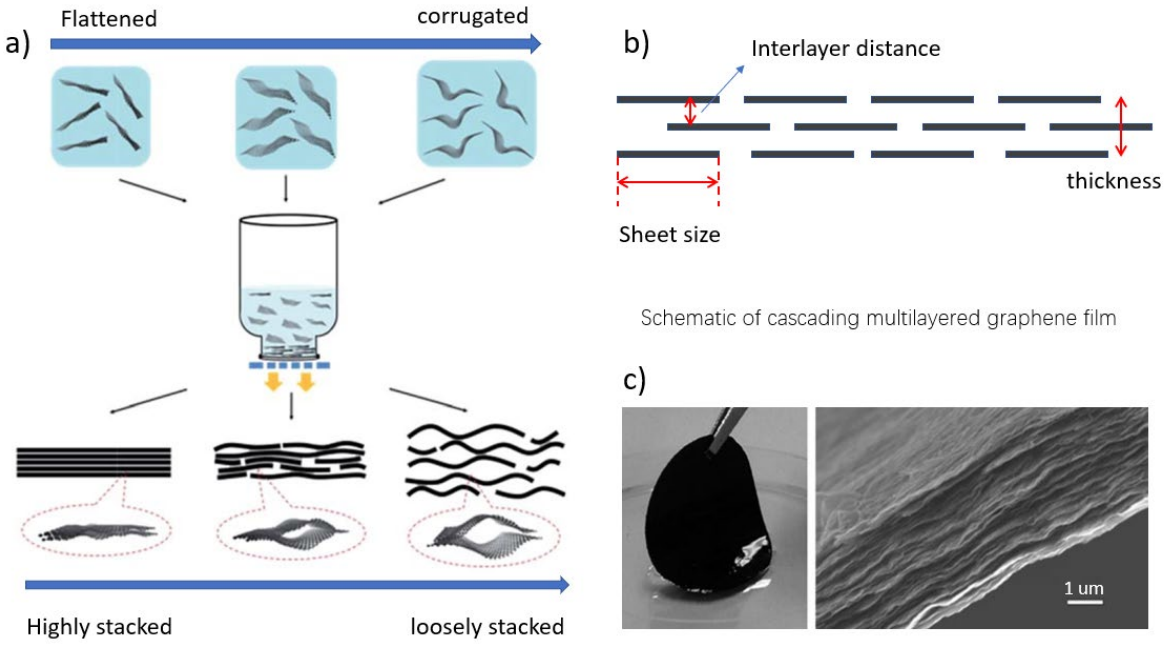

Figure 1.3 *Illustration of structural tunability of MLG film. a) Structural tuning of MLG film via control of CCG corrugation. [66] b) Structural tuning of MLG film via control of sheet size, interlayer distance, and film thickness. c) Macroscopic image of the thick MLG film and cross-section SEM image on the well-stacked MLG sheets. [67]*

In this thesis, we aim to explore the cracking behaviours of MLG film coated on a PDMS substrate via *in situ* optical-resistance characterisation under strain. The effect of a set of material parameters on the cracking behaviours will be examined, and the electromechanical properties of the cracked MLG films with different crack morphologies will be investigated.

We aim to understand how their structural parameters can be engineered to tune their cracking behaviours and the resultant electromechanical properties. And eventually, we aim to examine if the cracked MLG films could offer outstanding electromechanical performances from the engineering perspective.

Chapter 2 reviewed three key aspects that are directly relevant to my project. First, the methodologies to fabricate MLG thin films. Second, the influencing factors that lead to different cracking behaviours in thin films, and the statistical methods to quantitatively describe the crackings. Third, the electromechanical characterisations of the cracked thin films. In the first part, considerable attention is focused on analyzing the problems and limitation of each method in producing thin films with uniform microstructured at the nanoscale. The second and third part provides knowledge background for studying the cracking behaviours of MLG with statistical and electromechanical characterisations

Accordingly, chapter 3 aims at producing MLG thin films coating on different substrates for the subsequent structural and electromechanical characterisations. This chapter will report an interfacial energy modification methods via the swelling effect of graphene oxide (GO) [74], to overcome a general technical barrier in thin film transfer, and produce vacuum filtrated MLG thin films onto various substrates.

Chapter 4 and chapter 5 focus on the exploration of the cracking behaviours and the electromechanical properties of the cracked thin films. Notably, the goal is to examine in detail as to how the unique cascading 2D structure in MLG films can affect thin film cracking. Chapter 4 focus on examining the influencing factors extracted from general studies and the unique influencing factor within the MLG material, on the thin film cracking behaviour. The study discovered that the interlayer properties and thickness of the MLG film have deterministic influences on the cracking behaviour of the MLG film. An unexpected crack morphology transformation from parallel to random percolative is observed when the thickness, interlayer distance, interlayer attraction are altered to a favourable status.

Chapter 5 examined the electromechanical properties of selective thin film network with four typical cracking morphologies. As a result, we discovered unique electromechanical properties in the percolative cracked MLG thin films, to show broadband accurate sensing ability.

Chapter 6 summarises the major contributions to knowledge this dissertation has made. Personal perspectives on the future directions as well as potential opportunities are given in the study of the GO assisted interfacial energy modulated novel electronics fabrication; the in-depth study of cracking mechanisms on polymer supported MLG thin films and other thin films materials; the potential applications such as the precise capture of human bodily motion.

Chapter 2 Literature Review

Studying thin films' cracking behaviour and their corresponding electromechanical properties desires a proper thin film platform that has a series of characteristics. First, the thin film should be flat, reproducible, and uniform. Second, the thickness should have a controllable range from a few to one hundred nanometres, based on the conventional thickness of crack brittle thin films [32, 36, 38, 40, 45]. Moreover, to study the influences on cracking and the crack morphology-electromechanical properties relationship, we desire that the thin film has a broad range of tunability and a reliable interfacing condition with the substrate, as well as good electrical conductivity.

To fabricate MLG films with precisely controllable and reproducible structural parameters coated on a stretchable substrate sets the foundation of this project. The first section of the literature review will introduce the methodologies to fabricate ultrathin MLG films directly or indirectly coated on a polymer substrate. The pros and cons of each method, as well as the challenges and opportunities, are analysed.

Upon having a reliable material platform and since the cracking in MLG is blank in past research. How can we conduct studies in a logical order? What are the possible influencing factors on cracking behaviours? What are the questions we should look at? The second part of the literature review focuses on previous studies on the structural observation of cracks in different thin film systems. The typical cracking networks are summarised first, followed by a review on the effect of various factors on cracking morphologies to date. To quantitively describe the crack morphology, crack statistics methods are summarised.

Exploring the electromechanical properties of cracked thin films is an essential aim of this research. While the electromechanical properties are conventionally used to describe the performance in an application perspective, we also see it as a tool to reveal the network's microstructural dynamic evolution. The third part of the literature review focuses on the electromechanical characterisation of a cracked network, the sensing mechanism, as well as a

set of property criteria, were summarized. The opportunity of using electric characterization method for investigating cracking formation is discussed at last.

2.1 The fabrication of MLG film coated on polymer substrates

Considerable research has been devoted to graphene-based materials due to their excellent electrical, mechanical, tuneable interlayer chemical and physical properties. These properties encouraged the research and application on transparent conductive films, supercapacitors [75], ion sieving membranes [75], field-effect transistors, thermal layers, etc. Freestanding membranes can be utilised as the thickness of MLG film accumulates, but ultrathin film films need to coat on a substrate to maintain structural integrity. There are two well-acknowledged routes for the fabrication of ultrathin graphene films. Namely, the solution-based fabrication methods including spray coating [76, 77], spin coating [78, 79], dip coating [80], drop coating [81], liquid-air interface assembly, vacuum filtration [82, 83], etc. and atomic layer deposition (ALD) based fabrication methods including chemical vapour deposition (CVD) [84] and physical vapour deposition (PVD) [84]. However, to coat the ultrathin films onto a flexible substrate, there might be an extra transfer printing step. This section unfolds into four parts: the solution-based fabrication of MLG film, ALD-based fabrication of MLG film, transfer methodologies, and an overview on the challenges in fabricating nanoscale MLG film with controllable parameters for each method.

2.1.1 Atomic layer deposition-based fabrication of MLG film

Atomic layer deposition (ALD) for the fabrication of ultrathin solid films and lithography are the core techniques in the semiconductor, thin film transistor, solar cell industries [85, 86]. Moreover, since the discovery of uniform single-layer graphene fabrication by Copper (Cu) catalyst in 2009 [87], chemical vapour deposition (CVD) growth of graphene using hydrocarbon molecules in the presence of metal catalyst has been extensively studied to produce large-area uniform single to few-layer graphene thin film at low cost [88]. The detailed scientific and engineering question of ALD growth of graphene is not the scope of this review. For the specific questions such as the initiation graphene growth; ALD process cycles; the effect of temperature, catalyst, substrate, precursor chemistry, *etc*. on the final electric and mechanical properties of graphene film can be referred to other excellent reviews and books [88-92].

While physical vapour deposition has also been demonstrated to produce high-quality graphene film at low temperature [93, 94], the general large scale availability is incomparable to that of CVD. Figure 2.1 describes the growth mechanism of graphene. CH_4 decomposition takes place at the metal catalyst sites, leaving carbon atom at the metal surface. Therefore, the obtained graphene film is a polycrystal material. Once the graphene is formed, transfer methodologies are responsible for transferring the graphene onto the target substrate, which is in section 2.1.3.

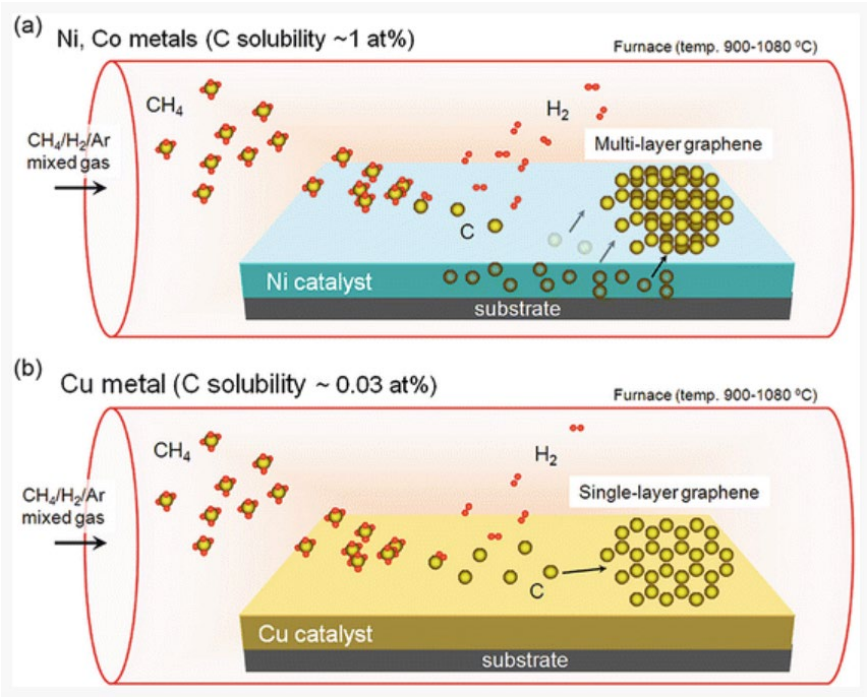

Figure 2.1 *The growth mechanism of graphene in CVD. a) The carbon solubility in Ni catalyst is high, resulting in inhomogeneous growth of multilayer graphene. b) The carbon solubility in Cu catalyst is low, resulting in uniform growth of single-layer graphene only on the Cu surface. [88]*

2.1.2 Solution-based fabrication of MLG film

Recent achievements of homogeneous colloidal suspensions of graphene oxide (GO) [95] and chemically reduced graphene oxide (rGO) [96] in water and various organic solution have facilitated the low-cost and high-volume thin film production of GO or rGO thin films. Here, different methodologies are introduced with typical examples from previous studies. Readers with interest on the background on how to obtain solution-based graphene colloidal suspension can refer to [97]; on the solubility and stability of GO and rGO in solutions can refer to [98].

Spin coating

Spin coating is a technique that the colloidal suspension or viscoelastic liquid is evenly coated onto a substrate due to centrifugal force (figure 2.2a) and it is popularly used to obtain the ultrathin film of viscoelastic polymer substrates. The spin coating of graphene usually starts with depositing drops of GO colloidal solution onto a SiO_2/Si wafer or PET substrate followed by spinning. The solution gradually evaporates and leaving a continuous film of GO plates lying flat on the substrate's surface. The obtained GO thin film can be further reduced with hydrazine (N_2H_4) [95, 99, 100] or HI to produce reduced graphene oxide film. The wafer size production of graphene film has the potential in a set of application in electronics[95], nanoelectromechanical systems (NEMS) [99], gas separation films [75], photovoltaic device [79], supercapacitor [75], etc.

Robinson *et al.* [99] produced a large-area, few-monolayer graphene oxide films that showed excellent mechanical properties. The team found that accelerating the solvent evaporation process by blowing nitrogen gas during spinning can promote the binding of GO sheets and avoid agglomeration [99]. The obtained thin film can be as thin as 4 nm. Yamaguchi *et al.* [100] studied the effect of concentration of GO suspension, suspension volume and spin rate on the quality and thickness of the spin-coated film. And they discovered that aggregation of GO sheets occur when the colloidal concentration is too high, while non-uniform thin film thickness occurs when the colloidal thickness is too low. They also found that a proper spreading of liquid onto the substrate is the prerequisite of a uniform thin film. In their study, the thin film thickness is controlled via the spin rate, that single to 8 layers of GO can be readily prepared, and the maximum thickness can reach up to 30 layers. Zhang *et al*. [100] spin-coated GO oxide film on PET substrate followed by hydrazine vapour reduction to produce graphene electrode. And they controlled the thickness of the rGO film by the volume of the solution.

However, it should be noted that the surface tension of water plays an important role in the surface condition of the obtained thin film. The high surface tension of water leads to an undesirable wetting condition on the substrates' surface, thus creating unevenness, aggregation and defects during the evaporation process. Therefore GO is often made in an organic solvent as colloidal suspension that has better wetting with the substrate [100]. Moreover, this method

might result in accumulated internal stress in the thin film and might result in the propensity to wrinkle or fold during the transfer process [95]. To conclude, the spin coating has advantages in producing uniform ultrathin MLG films (<30 layers, ~10 nm) with efficient and straightforward procedures; however, the synthesis of MLG film up to 100 nm is challenging.

Spray coating

Another facile and low-cost fabrication method is the spray coating, which is widely used in the surface coating industry. It is a technique that atomizes the liquid solution by high pressure at the nozzle, and the liquids can be deposited onto the target surface and achieve a good adhesion onto the surface (figure 2.2b). The key engineering considerations of spray coating are whether the solution can maintain a good dispersion during the coating process? Whether the viscosity of the solution is at the optimal range? And whether a uniform thin film can be achieved with good adhesion? Numerous fundamental studies have suggested several factors to determine the final quality of the spray-coated thin films, such as surfactants, solvent, coating condition, atomising condition, etc. [101]

For graphene thin film, it can be either fabricated from GO solution followed by reduction or directed from rGO solution. For example, Kim *et al.* [76] mixed the GO solution with hydrazine, and the solution is mixed by 80:20 if DI water/EtOH. They produced a highly conductive and flat MLG film with light transmittance equals to 84 %. On the other hand, Hofmann *et al.* [77] sprayed graphene in highly volatile1-methylpyrrolidone (NMP) solvent onto the Polyethylene terephthalate (PET) substrate and produced a percolative 2D graphene thin film as a sensitive strain sensor.

However, the spray coating method face challenges in producing uniform ultrathin films. First, because of the intrinsic non-uniform nature of the spraying amount at different spots in a sprayed thin film, as more liquid is sprayed from the nozzle in the near centre than that of on the peripheral, obtaining in uniform conductive graphene film is challenging at small thickness. Second, the surface coverage of graphene sheets on the substrates heavily depends on the size of atomized liquids sprayed onto the substrate, and it requires an at least >56% coverage to enable electric conductivity according to percolation theory [102-106]. The constant air outlet

and incoming liquid can have a complicate influence on the coated liquid, and large liquid bulbs can agglomerate to prevent uniform coating if not evaporated quickly. Thus, evaporation speed plays a vital role on the surface evenness. Moreover, it usually requires a large amount of coating material to form an electrically conductive network. As indicated in figure 2-2b, the graphene film is nearly opaque to when the thin film reached a desirable electric conductivity. [77] Therefore, while spray coating is a facile and low-cost coating method, it is usually adopted to fabricated thick coatings [107, 108] or require complicated layer-by-layer spray to obtain ultrathin conductive thin films [109, 110].

Vacuum filtration

"From a chemistry point of view, graphene is essentially a conducting polymer with a giant, two-dimensional (2D) molecular configuration" [67]. Because of the colloidal chemistry of graphene, the layer-by-layer stacking behaviours are therefore an interesting scientific topic and facilitate the study of vacuum filtrated fabrication of graphene film (figure 2.2c). The vacuum filtration allows graphene sheets to obtain the maximum extent of $\pi - \pi$ stacking, and therefore can produce thin films with highly order cascading structure [67]. The interlayer interaction can be well-modified by modifying the sheet-sheet interaction from chemical aspect [66, 111] or it can be controlled by the extent of vacuum drying after a hydrogel is obtained [69, 112]. In the past research in our group, the interlayer spacing, interlayer chemical and mechanical properties, mechanical properties of the cascading graphene film, etc. have been extensively studied [66, 69, 113-115]. Moreover, because of the uniform deposition of graphene sheets on the filter membrane and the quantitative usage of rGO solution, ultrathin MLG can be readily produced with precise control on thickness and other parameters. These characteristics makes vaccum filtration the most feasible method to fabricate MLG with controlled parameters.

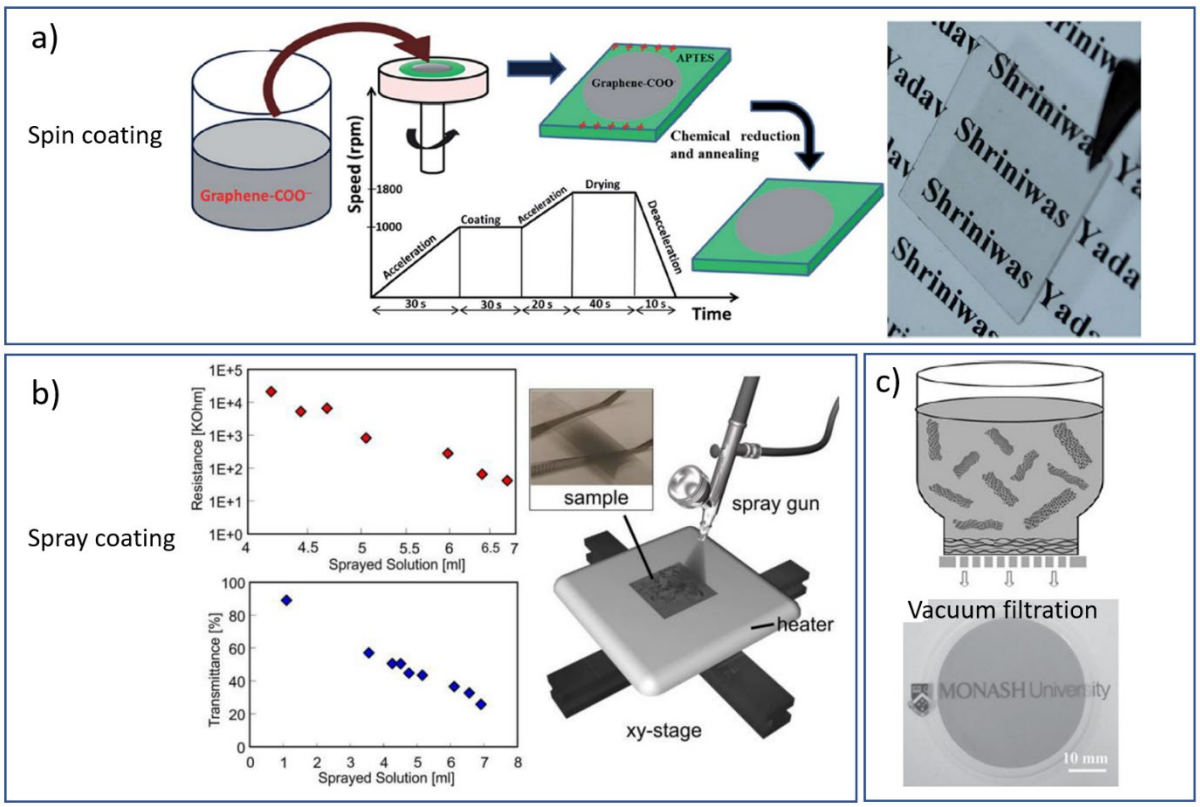

Figure 2.2 *Popular solution-based graphene thin film fabrication methods. a) Spin coating. Left, schematic of the production of spin-coated GO thin film followed by reduction. Right, an optical image of rGO thin film coated on a quartz substrate. [75] b) Spray coating. Left up and down, sprayed volume vs. electric conductivity and light transmittance. Right, schematic of spray coating, inset is the real capture of printed graphene film coated on PET substrate. [77] c) Vacuum filtration. Up, schematic of vacuum filtration. Down, vacuum filtrated rGO film on a filter membrane. [67, 111]*

Air-liquid interfacial assembly

Another potential method to fabrication graphene film with nanoscale thickness control and uniformity is the wetting or surface energy induced air-liquid interfacial assembly of graphene sheets, which received growing interest in recent years [82, 83, 116] (figure 2-3).

Jiang *et al.* [82] directly exfoliated the graphite in N-methyl-2-pyrrolidone (NMP) solvent and obtained a stable few-layer graphene dispersion. The graphene/NMP/polyvinyl pyrrolidone (PVP) dispersion is slowly injected onto the water surface. Due to a distinct difference on

surface tension between NMP/water interface and graphene/water interface, the NMP quickly dissolve into water, leaving a stacked graphene layer on top of the water (figure 2.3a). This method is important as it indicated another thin film assembly method by ingeniously utilizing surface energy. Then a prewetted glass slide is inserted into the water surface, and the graphene film will climb onto the glass slide surface because the glass and graphene have smaller interfacial surface tension. But the graphene will not climb onto the spots where the glass is not prewetted. Therefore, the surface-tension induces thin film fabrication also has implication on patterned thin film fabrication.

Pang *et al.* [116] exploited the idea of selective surface treatment. As a result, Pang et al. selectively produced electronic patterns from the interfacial assembled graphene film, and they used it to fabricate an array of strain sensors. Li *et al*. [83] studied the effect of technical parameters on the interfacial assembly and transfer of graphene thin from an engineering perspective, and they demonstrated a large area of graphene film evenly coated on PET substrate for flexible electronic applications and as a sensitive strain sensor. Readers with interest on self-assembly of graphene oxide at interfaces like Langmuir-Blodgett assembly, the evaporation-induced assembly can refer to [22].

To conclude, the air-liquid assembly of MLG film is an interesting method by a unique utilization of liquid surface tension, and it demonstrates opportunities in the large-scale fabrication of MLG films. However, the extensive use of the volatile solvent is one disadvantage. Moreover, the understanding of the thin film structures from such method is still at an early stage.

Other solution-based fabrication of graphene film

Other methods include dropping coating [117], dip coating [118], electrophoretic deposition [119], etc. Nevertheless, these methods might face challenges like “coffee ring effect”, which represent a non-uniform surface thickness; challenges in controlling surface conditions; or it may involve a complicated interfacial and electrochemical process that we do not fully understand. Nonetheless, readers with interest in the applications of theses method in other fields of surface coating can refer to [120-124].

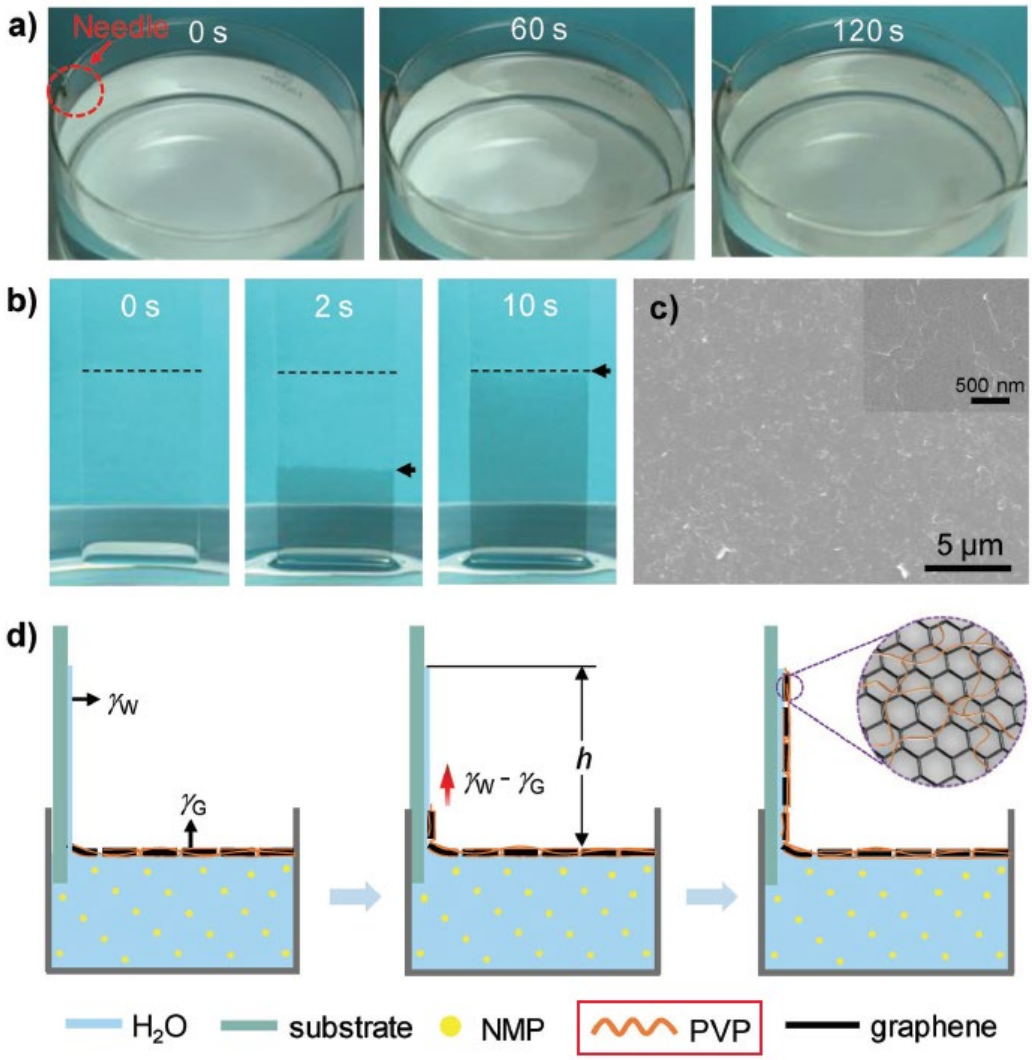

Figure 2.3 *Air-liquid interface self-assembly of the graphene sheet. a) The gradual assembly of graphene sheets due to surface tension. Graphene/NMP/PVP dispersion is gradually injected from the needle. b) Energy difference induced climbing process of interfacial assembled graphene film on the pre-wetted glass slide. The graphene stops to climb at the dashed line, as above which the glass is not pre-wetted. c) SEM image of the climbed graphene film with intact surface morphology. d) Illustration of surface tension difference that drives the assembled graphene film. [82]*

2.13 Transfer MLG film onto flexible substrates

After the ultrathin MLG film is fabricated. Unless directly fabricated on a flexible substrate, the thin film needs to be transferred onto a flexible substrate.

Generally, polymers with good flexibility are chosen for substrate materials in flexible electronics, typical examples include polyurethane (PU) [39], polydimethylsiloxane (PDMS) [37, 125, 126], rubber [127], ecoflex [128], polyethylene (PE) fiber [129], polystyrene-butadiene-styrene (SBS) [130], polyimide (PI) [17] etc. are among the most popular selection for their high elasticity and electric-isolation.

For CVD grown graphene, a universal route to transfer the graphene film from the Cu substrate is illustrated in figure 2.4 [131]. First, the as-grown graphene on Cu is coated with a layer of Polymethyl methacrylate (PMMA), a transparent and rigid plastic. Then the copper substrate is etched away, leaving the PMMA/graphene structure. To coat the graphene onto the target substrate, the graphene side is placed onto the target substrate, and it is sometimes followed by a heating process to enhance the adhesion between graphene and the substrate. Then PMMA is removed with acetone. When the target substrate has good adhesion with graphene such as PDMS, the PMMA can be replaced with PDMS. For example. Kim *et al.* [132] produced graphene patterns on Ni/SiO_2/Si substrate, the patterned graphene on PDMS strain sensor was obtained by etching the Ni/SiO2 substrate. Ruoff *et al.* [17] produced a CVD grown graphene mesh on top of a Cu mesh, and the graphene mesh/PDMS composite is made by adhering the graphene mesh onto a PDMS film followed by etching away the Cu mesh. Similarly, a graphene nanowall network is fabricated by etching away the copper skeleton. After fished by a PDMS film in solution, graphene nanowall/PDMS composite strain sensor is obtained after drying [133]. The disadvantage of such a process is the propensity to induce wrinkles into the graphene film, as well as leaving polymer residuals [134], which might add complexity from the fundamental research perspective.

For solution fabricated graphene film, transfer the graphene film onto the target substrate is widely reported on PDMS substrate [110, 135, 136]. However, the transfer of thin films onto other substrates other than PDMS is rarely found for graphene materials. Thus, we expand the scope to other thin film materials. Still, only limited examples were found that meet the definition of thin film coated on a flexible substrate [62].

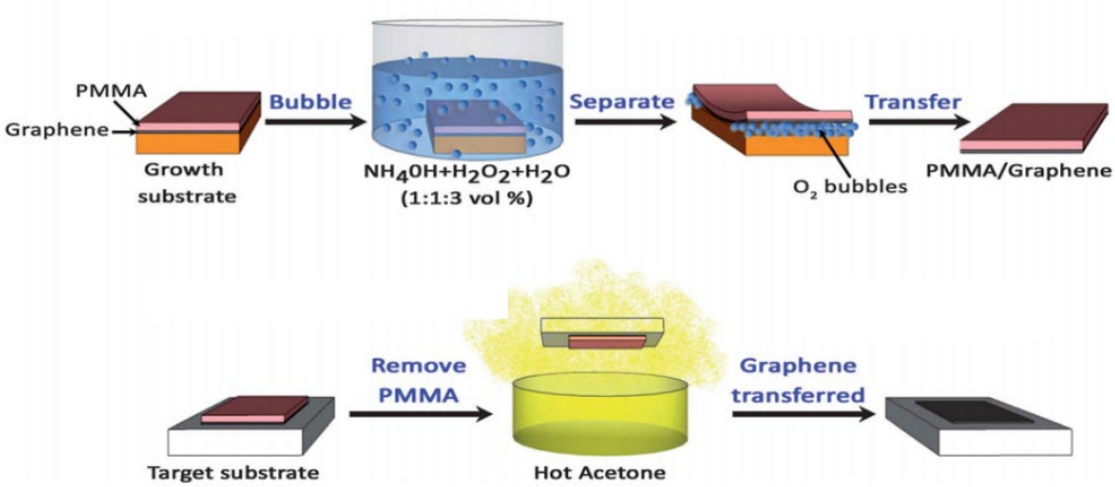

Figure 2.4 *Schematic of PMMA assisted transfer of CVD grown graphene. [131]*

2.1.4 Summary

Producing a thin film uniformly at the nanoscale is somewhat tricky. Moreover, transferring a nanoscale thin film onto a target substrate is also challenging. From a thin film point of view, spray coating faces difficulties in producing a uniform nanomaterial. Spin coating and ALD face challenges to prepare thin film up to 100 nm. At the same time, dip coating and drop coating are not suitable for the fabrication of nanomembrane. Vacuum filtration shows great prospect in producing nano-thin films in a highly controlled manner. However, the filtered thin films face challenges in transferring the thin film onto a flexible substrate other than PDMS. However, as substrates have essential impacts on the cracking behaviour (section 2.2), It would be of great importance to developing a new thin film transfer method to obtain nanoscale MLG coating on a various substrate.

2.2 Structural characterisation of cracking in thin films

In the past research on the controlled cracking in thin films, there appeared two distinct cracked-yet-electrically connected thin film networks, namely “parallel” or “channel” cracking network, and “percolative network”, and some networks have an intermediate cracking morphology (figure 2.5). These cracks in different forms resulted in distinct electromechanical response as introduced in the introduction chapter. The goal for this research is to reveal the cracking behaviours in ultrathin MLG film and the electromechanical properties of the cracked MLG films, so we could aim to create thin films with controlled cracking to meet specific

engineering requirements. Understanding the cracking behaviours in different thin films, especially the effect of different influencing factors on cracking morphology and the mechanical explanation (if possible) is the foundation towards this goal.

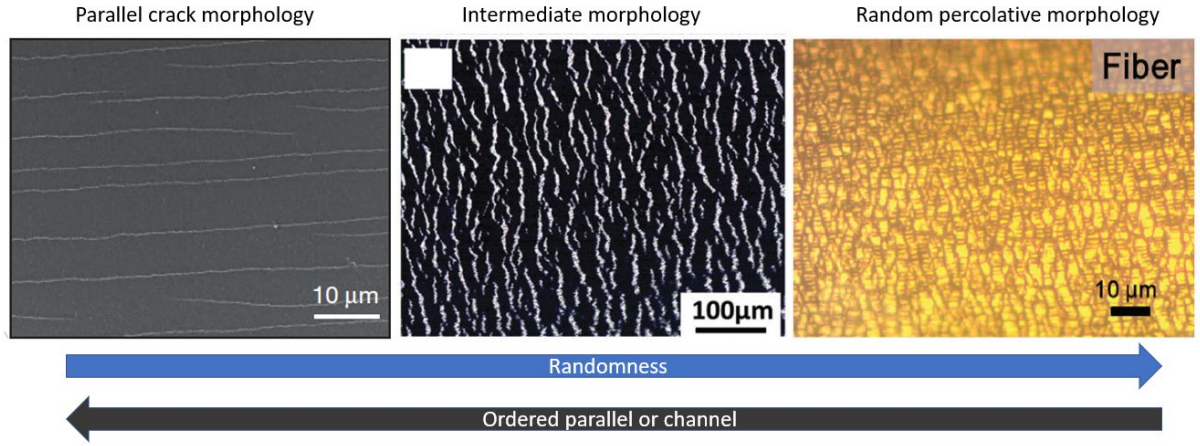

Figure 2.5 *Typical cracking morphologies in thin films coated on the flexible substrate. From left to right are Pt thin film, CNT thin film, Au thin film. [32, 36, 41]*

This section reviews the influencing factors on cracking behaviours from previous articles. Moreover, the statistic methodologies to describe cracks are summarized. Previous studies on the cracking behaviours of MLG film are reviewed, followed by a careful analysis of the challenges and opportunities.

2.2.1 Influencing factors on thin film cracking

Deformation of free-standing films

Measurements on free-standing thin films examine the intrinsic properties of the film material. Both experiment and simulation show low stretchability in free-standing films [4, 5, 137]. Typical metal films like aluminium, copper, steel, etc. have reported fracturing at a tensile strain of <2% [5], free-standing graphene would fracture at low strain (<1%) [138] due to internal defects [139] and the high tensile modulus of graphene sheet [140], while bulk freestanding graphene paper fractures at <7% [141]. Notably, the free-standing films are typically not stretchable, and detrimental fracture usually results from localized stress concentration.

While brittle thin films fracture with a sudden breakage, ductile metal materials such as Au

have slightly different fracturing process, as necking causes a local elongation. Nonetheless, the stretchability of the ductile films is still relatively low [5].

Deformation of substrate-bonded films

Reported back in the early 2000s, Wagner *et al.* [4] showcased that adhering the metallic thin films to an elastomer substrate could suppress the catastrophic fracture in a conventional inelastic metal film. In their study, they found that without proper bonding even after a thin film adheres onto a polymer substrate, large ruptures occur in the gold thin film, whereas well-bonded films show microscale cracks vertical to the strain direction. The same team observed different patterns in crack morphologies via changing thin film thicknesses and bonding conditions [56], which indicated that the thin film materials, interfacial bonding, thickness, etc. might play essential roles in determining the crack morphology. These results are of importance to the future understanding of cracking behaviour in thin films.

The effect of thin film thickness and thin film material

The effect of thin-film thickness on the cracking behaviour in thin films was well reported. For example, for deposited brittle indium tin oxide (ITO) film, when the thick increase from 50 nm to 200 nm, the ductility decreases drastically, Moreover, the crack onset strain is in inverse proportion to the square root of ITO thickness, meaning cracks initiate at smaller strains in thicker films [57]. However, when the thickness of ductile titanium (Ti) film increase from 8 to 50nm, the thin film shows increased ductility [142], and the small short cracks dominate in the network. The comparison between Ti and ITO indicates that it is essential to consider the thin film's intrinsic material properties when analysing the effect of different influencing factors.

Chen *et al.* [55] produced a CNT thin film with a thickness gradient by drop coating. This work is mentioned because it provided a clear observation of crack morphologies from one material, to demonstrate the thickness-induced variation of cracking behaviours (figure 2.6). The "crack wavelength" increased from less than 1 um to over 16 um when the thickness increase from ~20 nm to around 300 nm. While this work had not given mechanical explanations on the thickness-crack wavelength relationship, it confirmed the critical influence of thickness on cracking behaviours.

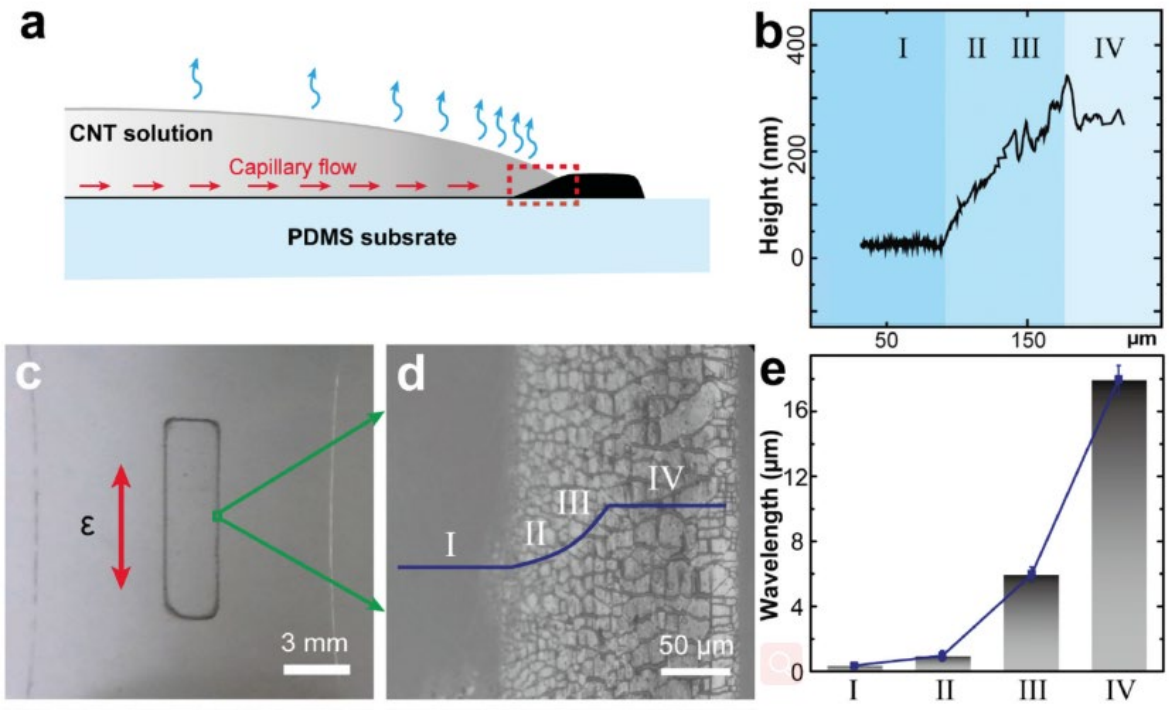

Figure 2.6 *Thickness determined cracking behaviour in CNT thin film coated on PDMS substrate. a) Schematic of the drop coating process to produce a thickness gradient due to the "coffee ring" effect. b) Surface profile on thin film thickness. c) Optical image of the thin film coated on PDMS when stretchable to 60%. d) Microscope image on crack morphologies. e) Statistics on the crack wavelength. [55]*

The effect of substrate, interfacial adhesion, and stress transduction

The substrate is an essential part of the thin film/substrate system. A substrate, in general, has two roles, namely, support the thin film and transduce the deformation to the thin film. After all, cracking is a mechanical phenomenon, and from starting the substrate to forming a cracked network, therefore three steps. Namely, the stress is transduced in the polymer substrate; strain and stress can be transferred to the thin film at the substrate/thin film interface; cracks initiate at stress concentrated spot or thin film delaminates from the substrate. Thus, to analyse the effect of interfacial force transduction is of fundamental importance, and it has a complex contribution from the substrate's surface morphology, interfacial adhesion, shapes, and modulus, etc.

Amjadi *et al.* [45] bar coated a layer of graphite film onto a plasma exposed Ecoflex substrate (figure 2.7); They found that the area after plasma exposure, parallel crack forms in the exposed area when stretched. Moreover, increasing the plasma exposure time would increase the parallel crack density. Unfortunately, the author did not discuss why the selective cracking could happen as well as if this methodologies can be applied to other thin film materials. Nonetheless, this work is important for it indicated the value to study the effect of substrate's chemistry on thin film cracking, and it demonstrated the potential to control cracking via substrate treatment.

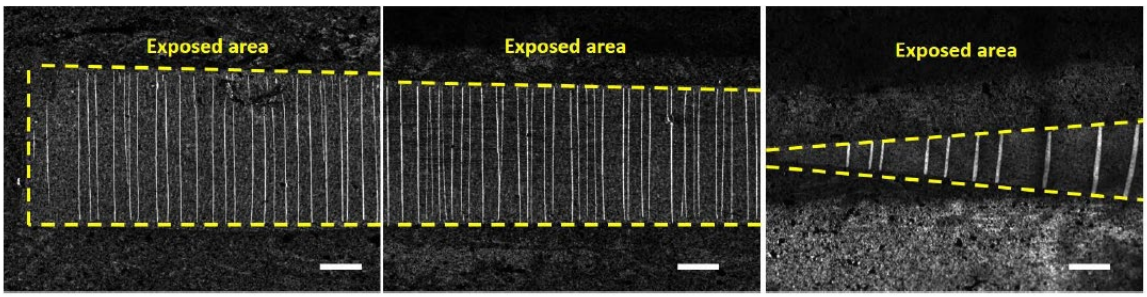

Figure 2.7 *The effect of plasma treatment on the substrate on crack morphology. Scale bar = 100 um.[45]*

The earlier study by Wagner *et al.* [4] found that the rupture pattern of gold can vary with/without proper bonding to PDMS. However, they did not give a clear description of how the bonding is modified. Zhu *et al.* [60] modified the gold thin film/PDMS interfacial adhesion carefully (figure 2.8). In a good bonding condition, before the deposition of gold thin film, the PDMS substrate was first cleaned with Ar plasma sputtering followed by the deposition of 10 nm titanium adhesion layer. And the deposited gold thin film is thermally annealed at 100℃ for two hours to increase the adhesion. In a bad bonding condition, the gold thin film is directly deposited. As a result, a distinct variation on cracking behaviours is observed on the gold thin films. The parallel cracking in this work contradicts the claim made by Kang *et al.* [32], which further indicated the complexity of cracking behaviour in thin films due to multiple influencing factors.

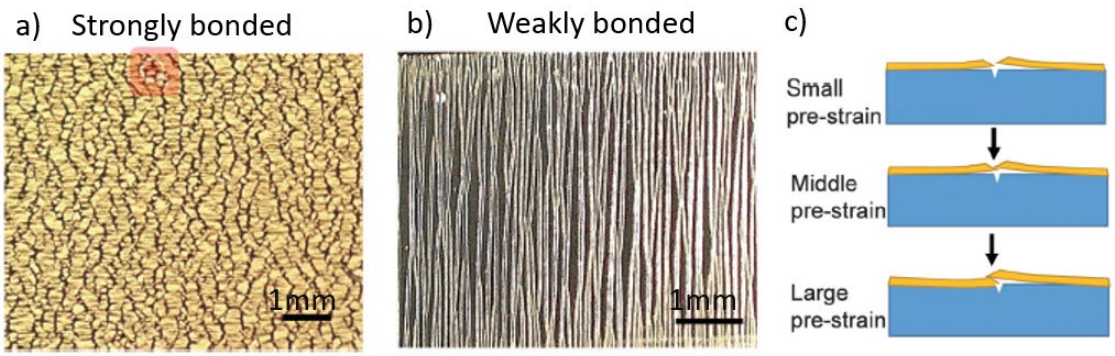

Figure 2.8 *Bonding condition determined cracking behaviours. a) Percolative cracking due to good bonding condition. b) Parallel cracking and surface delamination due to good bonding condition. c) Schematic of surface delamination of the weakly bonded gold thin film. [60]*

However, we should be cautious that the Ti adhesive coating and thermal annealing put extra variables to the direct comparison. In Chen *et al.*'s work [36] on the percolative Au network (figure 2.5), the team attributed the formation of the percolative network to the even transduction of stress when the thin film is scrolled into a fibre. This work provided more evidence on the effect of interfacial stress transduction condition, and further advanced the understanding of the effect of stress transduction. In another work, Chen *et al.* [59] deposited gold thin film on top of a PDMS fibre with bead structures, where they found longer cracking occur at the uniform stress areas (figure 2.9), and the crack length will show more significant variations in crack length distribution. However, the experimental observations can be quite confusing because other parameters such as the deformation of beads in figure 2.9 might also play a role to determine the crack behaviours.

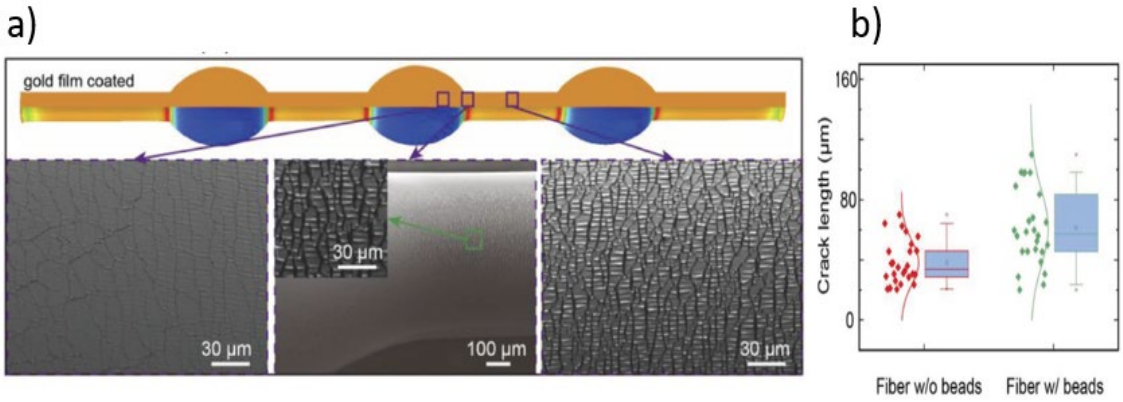

Figure 2.9 *Stress concentration induced cracking behaviours. a) Simulation and SEM images on the stress concentration and cracking morphologies on different places of the PDMS bead. b) Crack length static. [59]*

Here I try to link the cracking phenomena induced by the substrate, interfacial bonding, and stress transduction with classical fracture mechanics. For a thin film coated on a flexible substrate, in fracture mechanics, it describes the channel cracking as an adhesive failure [8]. The energy release rate G, is related with the thin film thickness h, in plane-strain elastic modulus $\bar{E}$ (equation 2-1). The constant Z depending of the elastic mismatch between thin film and substrate, it can be expressed by the plane-strain Dundurs parameters (α, β) shown in equation 2-2.

$$G = Z\frac{\pi}{2}\frac{\sigma^2 h}{\bar{E}}, \qquad \textit{Eq. 2-1}$$

$$\alpha = \frac{\bar{E}_f - \bar{E}_s}{\bar{E}_f + \bar{E}_s}, \quad \beta = \frac{\mu_f(1-2\nu_s) - \mu_s(1-2\nu_f)}{2\mu_f(1-\nu_s) + 2\mu_s(1-\nu_f)}, \qquad \textit{Eq. 2-2}$$

α can be plotted as shown in figure 2.10. From figure 2.10, the constant Z increases rapidly with α, indicating that the more energy will be release if the thin film is stiffer than the substrate, and cracks might occur at a point when the substrate is insufficient to suppress the stress localization. Thus the thin film deforms and ruptures by necking, and the rupture propagates to a channel crack. Nevertheless, the understanding of the influence on thin film cracking is still at its preliminary stage. In future studies, we envisage more effort will be devoted to the understanding of cracking formation mechanisms as well as their detailed controlling methodologies.

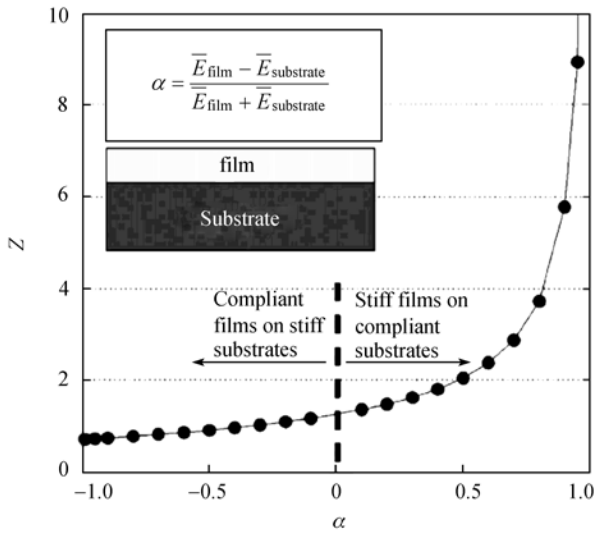

Figure 2.10 *Dundurs parameters, α vs. constraint factor (Z). [143]*

The effect of defects

Due to the fast stress concentration at the defect site when stretched, the defects will serve as crack initiation sites. In an ITO thin film, the crack is observed to initiate and expand at the defect sites [57]. In systems with multiple materials such as the silver nanowire (AgNW)/ silver nanoparticle (AgNP) network, the interfacial junction between AgNW and AgNP can also be regarded as weak points and therefore cracks observed to prone to initiate at these junction sites [130]. Due to the abundant number of initial cracked sites, the thin film shows a homogeneous crack pattern in the percolative network.

Effect the fabrication method

The fabrication method has a huge effect on the internal stress, defect, grain size, mechanical strength, etc. [144, 145] Thus, the fabrication method could potentially create a difference on the crack morphology. For the gold thin films, the thin film produced from the ALD method generally have intact structure, and the cracking morphologies are more dependent on other influencing factors as shown in figure 2.5, and figure 2.8. On the other hand, the thin film produced from solution-based assembly might have less intact structures, and the defects might show a more deterministic effect on crack formation. For example, Lee *et al*. [40] produced an Ag nanoparticle network via spin coating, and the crack initiates from the defect sites (figure 1.2d). As for graphene-based materials, thin films made from different methods show varied craking morphologies. For example, for the CVD-grown single-layer graphene, parallel cracking is observed and shown in figure 2.11a [146]. A laser scribed MLG film show random and large cracks (figure 2.11.b) [147]. A spray-coated MLG film shows the percolative conducting network, and cracks initiate at the boundaries of sheets (figure 2.11.c) [77]. For each fabrication method, the produced thin films might have varied internal structures and interactions with other building blocks. Therefore, the influence of fabrication method is a complex topic and will involve many factors discussed in section 2.2.1, and thus it is discussed later.

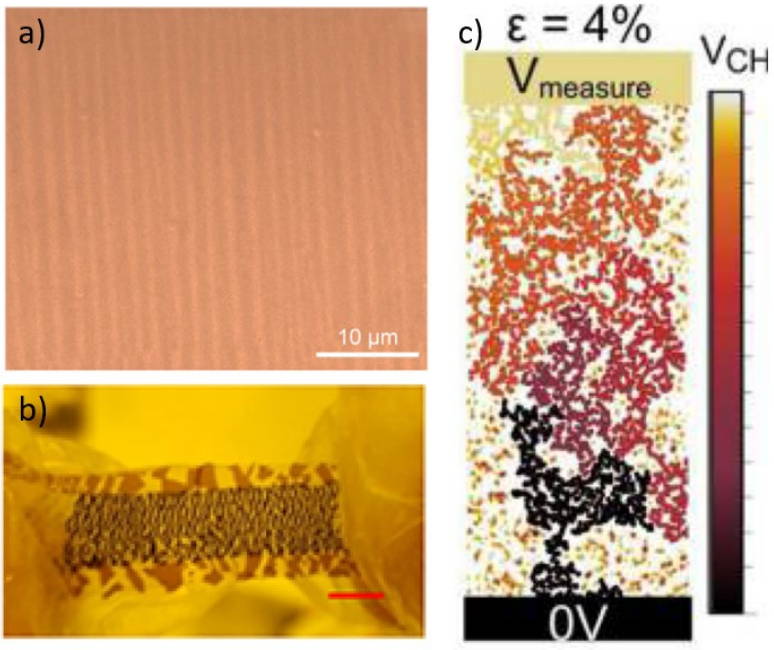

Figure 2.11 *Cracking behaviour in graphene-based films. a) CVD-grown single-layer graphene. [146] b)Laser scribed MLG film. [147] c) Simulation of spray-coated MLG film. [77]*

2.2.2 Statistic methodologies

Traditionally, the cracking morphologies are observed with microscopy and described qualitatively. However, as there is growing interest to control and utilize the unique electromechanical properties of the cracked thin film network. Quantitative descriptive method on crack morphologies and quantitative relationship between crack morphologies and electromechanical properties are desirable. After reviewing previous studies, the methodologies used to quantitively describe crack morphology are summarized in this section.

Chen *et al.* [55] used the term "crack wavelength" to describe the distance between each opposite crack edge (figure 2.7b), in another work, they used the term "crack length" to describe the distance from one end to another end of a discernable crack line (figure 2.9b) [59] Amjadi *et al*. [45] used "crack width" to describe the width of a channel crack. As crack width becomes larger, it indicates that the thin film is being stretched, and when the thin film is not stretched, the crack width is at its minimum value. Leterrier *et al*. [57] used the term "crack density" is describe the number of cracks they observed in a unit area. Zhou *et al.* [53] utilized an image processing technique, and they quantitatively depicted the crack morphology with

"sum of crack area" and "crack area proportion". This work is significant as thin film crack is very complex and making the accurate description very difficult. This work indicated that image processing techniques could facilitate the study of thin film cracking in the future. Lee *et al*. [70]studied the cracking behaviours of CVD grown graphene, they statistically analysed the relationship between "the number of cracks", "average crack length", "crack length of individual crack", number of cracks per unit length", and their result suggested that "average crack length" serves as a good statistic parameter. The terms to statistically describe cracks are summarised in table 2.1.

Table 2.1 *Statistic terms used to describe crack morphology.*

Term	description
Crack wavelength [55]	Distance between each opposite crack edge.
crack length [59]	Distance from one end to another end of a discernable crack line.
Crack density [57]	Number of cracks observed in a unit area
Crack area [89]	The sum of crack areas processed by image processing software
Average crack length [70]	The average length of each individual crack

2.2.3 Summary

To date, different cracking morphologies have been demonstrated, and various studies have individually shown the effect of different influencing factors such as the effect of substrate, thin film thickness, defect, stress concentration, interfacial bonding, thin film mechanical properties, etc. However, due to the complexity of the influencing factor, confusing results can sometimes be observed as the quantitative control of different parameters might differ in these studies, and it is difficult to link the existent research outcomes comprehensively.

Due to the recent development of statistic image-based characterisation on cracking morphologies, and the development of accurate parameter controls in material fabrication, it provides new opportunities in the revealing the systematic relationships between the influencing factors and cracking behaviours on different materials.

2.3 Electromechanical characterisation of cracking in thin films

Ultimately, from material science and engineering perspective, studying the controlled

cracking behaviours in thin films and their electromechanical properties leads to the utilization of the unique electromechanical performance of the proof-of-concept thin film strain sensor. Conventionally, the electroelectromechanical properties are viewed as parameters to describe the functional performance. However, since the electric conductivity is altered by the deformation of the thin film network, we see the electromechanical properties as an alternative pathway to reveal the structural deformation in the thin film network [32]. For example, in Kang *et al*.'s work [32], they utilized a mathematical method to process the electric signals and reveal the rapid "on-off" network evolution at the initiation stage of crack formation. Nakamura *et al.* [148] exploited electrical conductivity measurement to monitor the morphological change of deposited metallic thin films.

In this short section, the strain sensing mechanism of the crack thin film, as well as the assessing criteria on the electromechanical performance, are reviewed first. For real-world applications such as monitoring human motion, the thin film network should accurately refer strain, regardless of the speed and frequency of a movement. Therefore, the particular interest of this review is focused on the static and dynamic electromechanical sensing properties of the cracked thin film. At last, challenges and opportunities are analysed.

2.3.1 Sensing mechanism and assessing criteria

As illustrated in figure 2.12, tensile deformation leads to the initiation of microcracks in the brittle thin film network (figure 2.12a). Theses cracks critically limited the current conduction, thus the increase of resistance. In highly sensitive networks, the high sensitivity is the result of the rapid blockage and redirection of electric current such as the parallel cracked network [32]. While the highly stretchable network is induced by the small influence on electric flow with dense random small cracks [36, 40]. Several key parameters to evaluate the electromechanical performance of the thin film network are as follows:

Gauge factor (GF) and stretchability

Gauge factor (GF) represents the sensitivity to strain or the extent of change in signal output versus the applied strain. It can be expressed as $(\Delta R/R_0)/\varepsilon$ for resistive strain sensor. The higher GF is desired for easy differentiation of data. To obtain a high gauge factor requires a large change in the conducting pathway. On the other hand, stretchability represents the extent the conducting network can be deformed while maintaining the electric conductivity. The

gauge factor and stretchability determine the overall electromechanical sensing range, and there is often a trade-off between the two factors [149]. Thus strain sensors with different functionalities were uniquely designed to achieve different applications such as highly sensitive strain sensor to detect subtle strains [32], or stretchable conductors that can maintain high electric conductivity at large strain [36]. However, for some application such as human motion detection, a combination of large gauge factor and stretchability is desired [53].

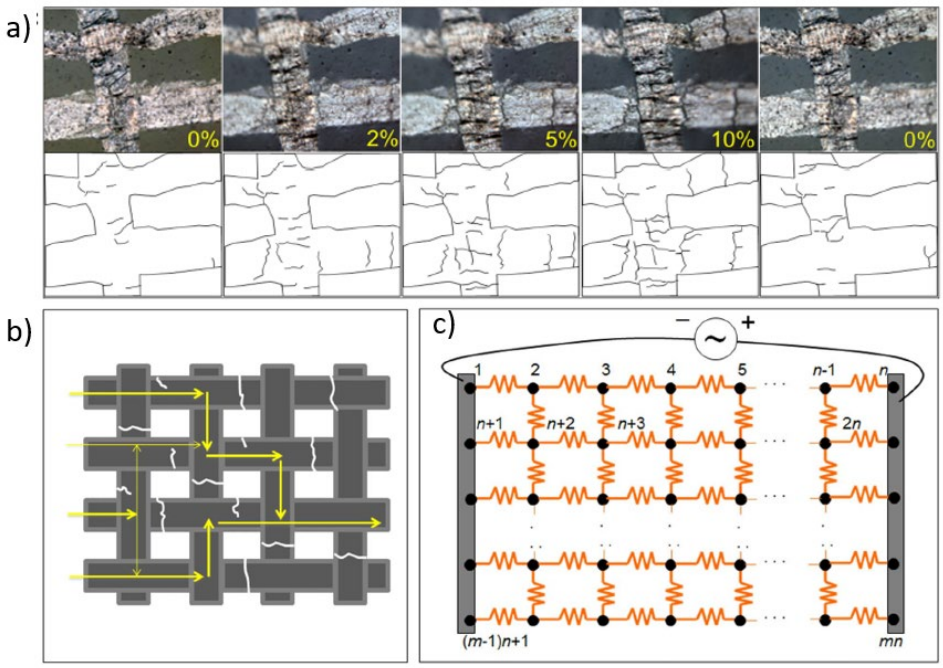

Figure 2.12 *Cracked thin film network of CVD grown graphene mesh. a) Optical image of cracks in the thin film network. b) Illustration of the effect of crack on the alternation of electric current. c) Illustration of the equivalent circuit. [37]*

Structural stability (cycle life)

Structural stability is measured by the irreversible loss of sensing ability at a certain number of stretch-and-release cycles. From a fundamental perspective, this value indicates how well the network can recover to its original form, which involves the process of formation of new crack, interfacial delamination, irreversible structural damage. The structural recovery is affected by many influences such as network's stiffness, environmental impact, humidity, polymer interaction, etc. The proper way to study structural recovery is to characterize with the electromechanical response and microstructural observation.

Response time, hysteresis, and overshooting behaviour

By definition, the response time and hysteresis share similar explanation. However, these two properties are discussed together to bring attention to the differences. Response time stand for the time interval between the application of strain and the detection of electric response in the recording device. This interval might include the time for polymers to deform, the data processing time of the recording device. Small response time is favourable in application perspective as the small response means fast reaction, Hysteresis, is more of a mechanical term, with representing the polymer's intrinsic delay in force transduction and deformation. Overshoot behaviour represents a typical drawback of a strain sensor that the detection can exceed the applied strain, which is due to the hysteresis. The response time, hysteresis, and overshooting are usually large in polymer composite and small in thin film coatings. While little theoretical studies have conducted to explain this phenomenon, the reasonable explanation might due to the viscoelastic mechanical properties of polymers. The conductor that is infused in the polymer matrix inherits the viscoelastic response. However, despite a long history of polymer dynamics discipline, all our understanding and hypothesis are based on empirical studies and hypothetical theories.

Dynamic response

Another critical but sometimes overlooked property is the network's dynamic response-ability. While the influence of hysteresis on the electric response is less vital in a low motion, it becomes hugely influential when detecting a dynamic deformation, especially at high strain rate or high frequency. In the daily application of strain sensing, there are more dynamic motions than static motion, for example, a human is constantly moving, his movements can range from low frequency such as walking, typing, gestures, to high frequency such as the vibration of sound cord, muscle movement, the small movements in a heartbeat, etc. The inaccurate sensing is a typical shortcoming for polymer composite when deformed at a high strain rate. In the mechanical aspect, dynamical mechanical analysis (DMA) has been conducted to study the hysteresis of polymers [150]. From a mechanical point of view, it is known as viscoelasticity. Two parameters, loss modulus and storage modulus, present the portion of energy that is stored as elastic energy and lost during deformation as heat. While no scientist can confirm the loss of energy is due to the sluggish movement of polymer chains, experimental studies give strong evidence that polymers with longer polymer chain typically

has higher hysteresis. The mechanical evidence of hysteresis explains the observable large response time, large hysteresis of the polymer composite. Alternatively, researchers developed surface coating networks, namely, the conducting material is coated on the polymer substrate or partially coated on and partially infused in the polymer. These surface coating network has shown enhanced accuracy in dynamic response.

Relaxation

The accuracy of strain measurement replies on sensitive (gauge factor), hysteresis, overshooting behaviour, dynamic response, and relaxation. Relaxation is the constant change in conductivity after the network is deformed and hold to a certain level. Based on mechanical theories, this is likely due to the propensity to lower the internal elastic energy in the sensing network by structural re-construction, and it is a universal predicament for all strain sensors to move beyond concepts to the real-world wearable application like remote surgery. So far, few studies have focused on the influencing factors on the relaxation, and its discussion is sometimes avoided in previous publications.

2.3.3 Summary

For the thin film cracking network, many studies have demonstrated excellent electromechanical performance. However, the fundamental understanding of what leads to these performances, what are the fundamental unique advantages of each cracked morphologies has not been well defined. Here, we see the electromechanical characterisation not only as the standards to evaluate the properties of strain sensors, but the electromechanical responses can also reflect the structural deformations in the conducting network and indicates the delicate structural evolutions that other characterisation methods cannot observe. In this study, we aim to explore the electromechanical performance of cracked MLG film through a collaboration of structural characterization and electromechanical characterization. The assessing parameters summarised in this section will help to reveal the structural evolution in the cracking process as well as in cracked thin films.

Chapter 3 Interfacial energy modulated intact transfer of MLG film onto flexible substrates

3.1 Design concept

In the material preparation step of the studying the crack behaviours in MLG film coated on a flexible substrate, the MLG film is desired to be flat, evenly distributed, and un-cracked. At the same time, due to the possible thickness-sensitive cracking propensity, the surface of MLG film should be kept as clean as possible. The vacuum filtration provides a simple and controllable route to produce MLG film with desired thin film thickness, interlayer distance, corrugation, sheet size of the single reduced graphene oxide sheet, etc. [66, 151-154] Thus, it is an essential part of the exploration of the cracking behaviour in MLG film coated on a polymer substrate. However, transferring an ultrathin MLG film onto a target substrate is challenging due to the strong adhesion strength between MLG film and the filter membrane. Thus, the process is limited to a selection of materials like PDMS [155, 156]. Moreover, we should be cautious against methods that involve "on membrane reduction of graphene oxide" or hot press technique, as these methods might generate unfavourable wrinkles and cracks [134, 157]. The lack of substrate selection limits the investigation of the thin film cracking behaviour on a flexible substrate.

A careful review is done on "contact printing", "transfer printing", "transfer of graphene". Despite which methodologies, the governing principle for a successful transfer is the inequation of work of adhesion (W^a) [158]. Namely, the work of adhesion between the target substrate and material is higher than doner and the thin film: $W^a_{substrate/thin\ film} > W^a_{donor/thin\ film}$. Therefore, reducing the work of adhesion between the MLG film and the filter membrane is the key desin strategy.

Inspired by the sacrificial layer techniques in many transfer-printing processes of PVD-produced thin films [159, 160], namely, an etchable sacrificial layer coating on the PVD

substrate before depositing the target thin film could facilitate the thin film transfer; we wonder if there is a similar method for vacuum filtrated MLG thin film?

Graphene oxide (GO), the precursor of reduced graphene oxide (rGO) has a similar cascading structure as MLG after vacuum filtration; the GO membrane is widely used in the study of ionic transport, water desalination, etc. [161-163] However, due to the propensity to swell in water, the interlayer distance between GO layers will increase and jeopardize the structural integrity of GO membrane or even make the GO membrane dissolve in water. Can GO membrane be used as a sacrificial layer to transfer MLG? In this chapter, this idea is tested by transferring MLG onto different substrates, and the likelihood to produce an MLG coated on a flexible substrate in a controllable manner is examined.

3.2 Experimental section

3.2.1 Fabrication of graphene oxide (GO) and reduced graphene oxide (rGO)

Graphene oxide solution is prepared by Hummer's method. The rGO solution of lowly oxidized GO solution is made via hydrothermal reaction. Namely, 25 ml 0.05mg/ml GO solution, 1.8 ml NH_3H_2O, 0.625 ml (1/125) N_2H_4 are mixed and reduced at 100℃ for 1 hour. The obtained clear black solution is quenched in ice-water after reduction and then stored a 4℃ fridge for later use. The mass concentration is obtained by filtering sufficient solution and weighing the filtered product.

3.2.2 Preparation of GO and MLG film

GO membrane is prepared via vacuum filtration. 10 μg of GO in solution is vacuum filtrated on the target filtration membrane with diameter equals to 37 mm. The MLG film is made by filtrating rGO solution via a vacuum filtration set (Buchi V-700 vacuum pump; Millipore glass funnel, 300 mL, 47 mm). The thickness of the thin film is determined by mass equivalent to 20, 40, 80, 160, 320 layers of rGO sheets. The estimation method is in 3.2.3. The rGO solution is either directly filtered on the filter membrane or filtered on top of a filtered dry GO membrane.

3.2.3 The estimation of the number of layers in rGO thin film via mass

The number of layers in this work is estimated by using the parameters of graphite, assuming that the singer layer rGO sheet has similar mass density and interlayer distance as graphite. In this work, the interlayer distance (d_G) is 0.335 nm [164], and the density of graphite (ρ_G) is 2.09~2.23 g/cm^3, according to the parameter of graphite flakes we used to produce graphene oxide. Therefore, with the diameter of the filtered membrane equals 3.7 cm, a single layer of graphene is weighted approximately:

$$m = \rho_G \cdot d_G \cdot \pi \cdot (3.7cm)^2/4 \qquad \textit{Eq. 3-1}$$

3.2.4 Transfer MLG onto target substrate with GO interlayer

First, 50 μg of graphene oxide solution is vacuum filtrated onto the filter membrane to form a uniform GO membrane. Then a certain amount of rGO solution is filtrated on top of the GO membrane. After an rGO hydrogel membrane is formed, the filter/GO/rGO membrane is peeled off from the vacuum filtration system and placed onto the target substrate. After a good wetting between the rGO layer and the target substrate is formed, deionized (DI) water is dropped on the filter membrane, and the MLG/substrate can be obtained after peeling off the filter membrane. GO precursors of rGO solution were chosen for the interlayer film due to the same sheet size and thus a similar cascading structure. The GO membrane layer will dissolve into water, leaving a clean MLG layer on the target substrate. The whole process is schematically illustrated in figure 3.1.

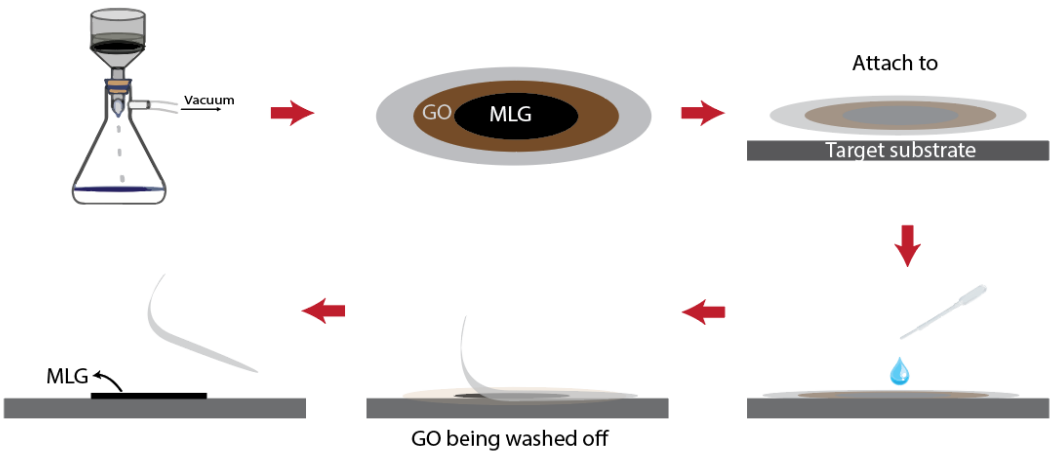

Figure 3.1 *Schematic illustration of transferring a vacuum filtrated MLG film onto target substrates.*

3.2.5 Transfer MLG onto target substrate without GO interlayer

The process is similar to transfer MLG onto the target substrate with GO interlayer; only no GO participates in this process. The transfer process face challenges to transfer rGO onto other substrates than PDMS.

3.2.6 Contact angle measurement

The wettability of membranes is measured by Dataphysics Model OCA 20 tensiometer. Sessile drop and ellipse fitting are chosen. The contact angles of 15 μl testing liquid are measured at 20℃. The testing liquids are CH_2I_2 and DI water [165-167].

3.2.7 Sheet resistance measurement

The sheet resistance is measured by Keithley Model 2400 SourceMeter® under 4-probe ohmmeter mode. The testing current was 100 mA.

3.3 Results and discussion

3.3.1 Transfer of MLG film without GO interface layer

Based on previous methodologies from earlier publications, the direct transfer of filtered MLG film onto various substrates was examined, and the result can be summarized as table 1. Two conventional filter membranes were chosen to vacuum filtrate MLG film onto five different substrates. PDMS (polydimethylsiloxane) and Ecoflex ™ (soft silicone rubber) are popular elastic polymers in flexible electronics, while petri dish, glass slide, and silicon wafer are other conventional substrates. It is obvious that only PDMS yield a good thin film quality after the transfer, but the transfer of MLG film onto other substrates were not feasible or were difficult to obtain an entire film.

The possible route to facilitate the transfer process is either increasing the adhesion strength between the target substrate and MLG film or reduce the adhesion strength between the filter membrane and the MLG film. Increasing the adhesion strength between the target substrate and MLG was conducted by heating the target substrate on a hotplate [168], which showed

little enhancement on the transfer process, likely due to the enhancement brought by heat is insufficient to overcome the large difference in the adhesion strength. On the other hand, reducing the adhesion strength between filter membrane and the MLG face challenges as well. From literature [131, 134, 157], only chemical modification is feasible for filter membranes. First, the filter membranes can not be regarded as "viscoelastic material", therefore the kinetic surface energy modification is not feasible. Second, modify the adhesion via unique structures is difficult for commercial filter membranes. Therefore, we seek methods from chemical modifying interlayers.

Table 3.1 *The direct transfer of MLG film without GO interfacial layer.*

	Ecoflex	PDMS	Petri dish (polystyrene)	Glass slide	Si wafer
MCE	X	O	X	X	X
PC	X	O	X	X	X

O = Yes, X = No.

In this study, a thin layer of graphene oxide is introduced in between the filter membrane and MLG film, via controlling the sequence of vacuum filtration. The outcomes for transfer are summarized in table 3.2 and table 3.3.

3.3.2 Transfer of MLG film with GO interface layer

After the addition of GO interlayer, two sets of tests were conducted. First, after the filter membrane/GO/MLG film is placed on the target substrate, the film is peeled off without the addition of DI water. Second, DI water is dropped onto the filter membrane to wet the GO membrane, as shown in figure 3.1. The wetting of GO will induce the swelling effect of GO membrane, which increases the interlayer distances of the GO membrane [74].

Intriguingly, without the addition of water, the transfer condition is the same as when without GO interlayer (table 3.2). Moreover, because of the addition of GO interlayer, we observe the trace of GO membrane contamination on the transferred MLG on PDMS. This result is non-

ideal. However, after the DI water is applied to wet the GO, we observe a significant expansion of the range of transferrable surface, as summarized in table 3.3. The sudden expansion of transferrable substrate indicates a rapid change at the filter membrane/MLG interface.

Table 3.2 *Transfer of MLG film with dry GO interfacial layer.*

	Ecoflex	PDMS	Petri dish (polystyrene)	Glass slide	Si wafer
MCE	X	O	X	X	X
PC	X	O	X	X	X

O = Yes, X = No.

Table 3.3 *Transfer of MLG film with wet GO interfacial layer.*

	Ecoflex	PDMS	Petri dish (polystyrene)	Glass slide	Si wafer
MCE	O	O	O	O	O
PC	O	O	O	O	O

O = Yes, X = No.

Figure 3.2 shows the macroscopic image of the transferred MLG film on PDMS. From figure 3.2, highly intact reflective MLG films are observed for MLG film assembled from rGO sheets with different sheet sizes, and from 20 layers to 320 layers. The highly reflective optical properties of the MLG indicates a well-stacked cascading structure [112]. The microscope image on the surface condition of the transferred MLG is shown in figure 3.3. The images in figure 3.3 are well-focused, which indicates that the obtained MLG films have flat surface conditions without wrinkles. The flat and intact surface condition is desirable for the study of thin film cracking, as they provide a simple and reliable material platform.

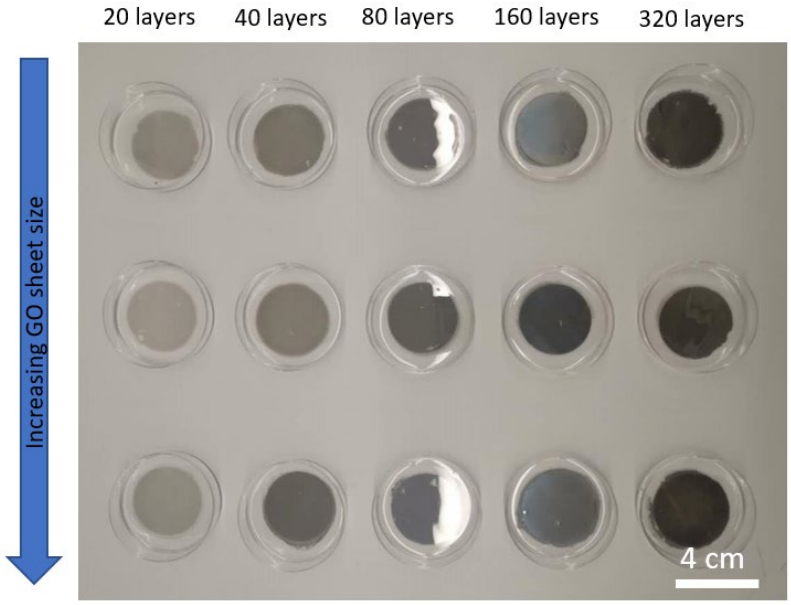

Figure 3.2 *Macroscopic capture of transferred MLG graphene films on PDMS.*

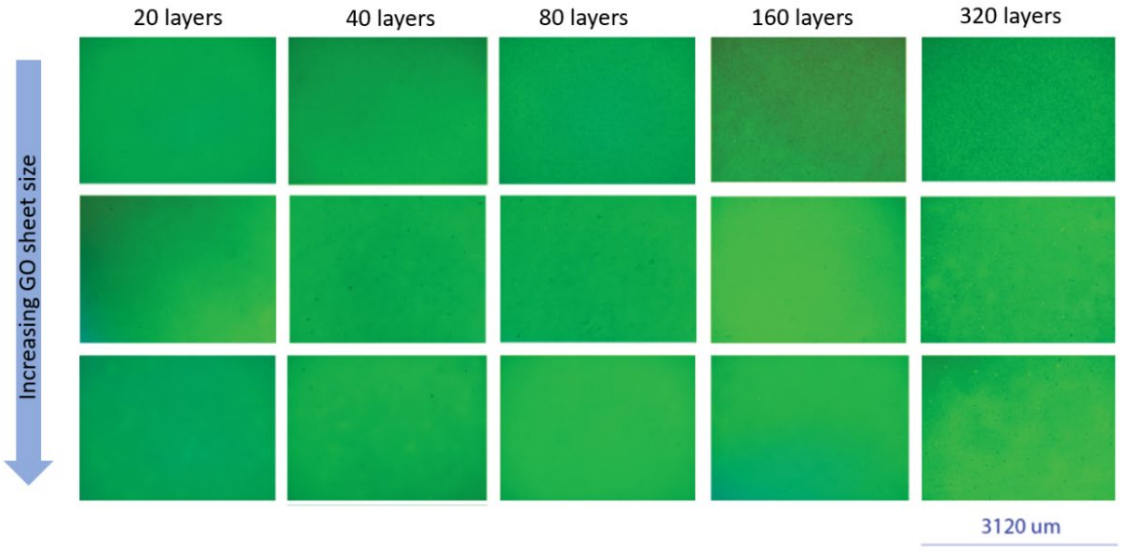

Figure 3.3 *Optical observation of the transferred thin films on PDMS.*

Upon the experimental finding, we are curious about what is the effect of the swelling of GO on the interfacial adhesion between the GO membrane and MLG film? Section 3.3.3 will focus on revealing the underlying reasons.

3.3.3 GO swelling induced interlayer modification

To understand why GO interlayer played an important role. We referred to the theory of solid surface energy, particularly the solid-solid adhesion [166, 167].

3.3.3.1 Solid-solid surface adhesion

Over the years, a variety of characterisation methodologies were utilized to probe the different chemical and physical properties of solid surfaces, which contributes to the understanding of the basic material characteristics. Among different aims, the measurement of surface work of adhesion of the solid surfaces provides a good understanding of the surface interactions between solid surfaces, and it can be measured via contact angle and the use of Young-Dupre equation and Fowke's equation [166, 167, 169].

When a drop of liquid is on a solid surface, a classic 3-phase diagram can be drawn in figure 3.4, which illustrate how energy is balanced in a solid-liquid-air system that leads to Young's equation:

$$\gamma_{sv} = \gamma_{sl} + \gamma_{lv} cos\theta \qquad Eq.\ 3\text{-}2$$

Here, γ represent the surface tension or surface free energy, the subscripts sv, sl, and lv refer to the solid-vapour, solid-liquid, and liquid-vapour interfaces, respectively. γ in physical concepts, is the free energy G per unit area. θ stands for the contact angle.

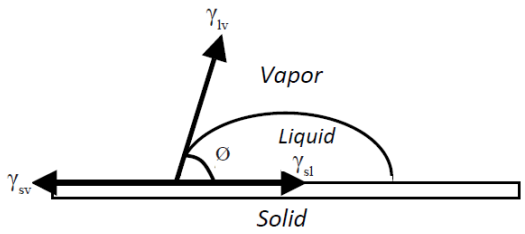

Figure 3.4 *Schematic of the three-phase surface energy balance.*

For the convenience of understanding surface hydrophilicity and hydrophobicity, Eq. 3-2 can be written as:

$$cos\theta = \frac{\gamma_{sv}-\gamma_{sl}}{\gamma_{lv}} \qquad Eq.\ 3\text{-}3$$

The value of $cos\theta$ is solely determined by the values of surface tensions, γ_{sv}, γ_{sl}, γ_{lv}. When $\theta > 90°$, the surface is deemed as "liquid-phobic", which indicate the bad wetting condition, i.e., the liquid will not wet the surface. On the contrary, if $\theta < 90°$, the surface is deemed as "liquid-philic", which indicate that the liquid will wet the surface, a perfect wetting is when the contact angle is zero. From a mathematic perspective, a supplementary rule is applied to Young's equation: if $\gamma_{sv} - \gamma_{sl} > \gamma_{lv}$, keep $cos\theta = 1$. At this point, it can be qualitatively understood that solid surfaces with high energy and liquid with low energy will result in a better wetting.

The work of adhesion W^a was introduced by Dupre [170], a dynamic thermal concept related to the free energy G. When two separate surfaces with different natures are tightly bonded together at the interface, such a process is called adhesion. The change in free energy per unit area at the interface, ΔG^a, is the negative of the work of adhesion W^a. For two separate materials i and j,

$$\Delta G_{ij}^a = \gamma_{ij} - \gamma_i - \gamma_j = -W_{ij}^a \qquad Eq.\ 3\text{-}4$$

Therefore, combining Eq. 3-2 and Eq. 3-4, we obtain the Young-Dupre equation:

$$\Delta G_{sl}^a = -\gamma_{lv}(1 + cos\theta) \qquad Eq.\ 3\text{-}5$$

$$W_{ij}^a = \gamma_{lv}(1 + cos\theta) = \gamma_i + \gamma_j - \gamma_{ij} \qquad Eq.\ 3\text{-}6$$

The adhesion strength between two surfaces in close contact can be calculated once the surface energies are measure. The surface energy can be determined by the Owens-Wendt equation:

$$\gamma_{sl} = \gamma_{sv} + \gamma_{lv} - 2\sqrt{\gamma_s^d \gamma_l^d} - 2\sqrt{\gamma_s^p \gamma_l^p} \qquad Eq.\ 3\text{-}7$$

γ_s^d and γ_s^p represent the contribution of dispersion and dipole-dipole interaction. The total surface energy is the sum of both energies.

The surface energy between two surfaces in close contact can be calculated by Wu's equation [171]:

$$\gamma_{12} = \gamma_1 + \gamma_2 - 4\frac{\gamma_1^d \gamma_2^d}{\gamma_1^d + \gamma_2^d} - 4\frac{\gamma_1^p \gamma_2^p}{\gamma_1^p + \gamma_2^p} \qquad \textit{Eq. 3-8}$$

Therefore, the work of adhesion between surface surfaces can be determined when the surface energy of each surface is measure by contact angle measure via a polar and non-polar testing liquid.

3.3.3.2 GO swelling induced surface energy alternation

To understand the effect of the GO swelling on the interfacial energy status. We chose CH_2I_2 and DI water as the standard testing liquid for contact angle measurement [166]. The different filter membranes and substrate were chosen as samples. The wetting condition of GO membrane is rather complicated due to the strong propensity to dissolve in water. Therefore, the wetting condition of GO membrane is simulated by placing the filter membrane/GO membrane on top of a water drop in a sealed and humid petri dish. During the contact angle measurement, the volumes of the standard testing liquids in each test (H_2O, CH_2I_2) were 15 ul. The surface energies are calculated. All results are listed in table 3.4.

From table 3.4, we see that the MLG film and the filter membranes have relatively high surface energies, while the target substrates like PDMS, petri dish, glass slide have relatively low surface energies. These values roughly explain the difficulty of transferring ultrathin MLG films from the filter membrane. As for the GO film, the excellent wetting condition of water indicates that the GO film is extremely hydrophilic. Moreover, as wetting continues, the swelling took place and alters the chemical properties of the GO/water composite. However, it should be noted that the measurement of swelling subjects can lead to inaccurate results [167]. Therefore, the contact angle measurement was conducted quickly to minimize the influence of

swelling as well as evaporation. For the detailed analysis, the work of adhesion between MLG film and other surfaces are calculated and illustrated in figure 3.5.

Table 3.4 *The surface energy of membranes.*

Material	CA (H_2O)	CA (CH_2I_2)	γ_s^d (mJ/m^2)	γ_s^p (mJ/m^2)	γ_s (mJ/m^2)
MCE membrane	63.63	36.25	1.9	83.5	85.5
PC membrane	52.58	28.14	4.2	88.1	92.4
Glass slide	31.14	65.41	29.0	38.8	67.8
PDMS	92.00	66.00	0.02	53.6	53.7
Petri dish	94.74	87.72	1.7	26.5	28.2
Si	78.50	34.50	41.6	2.0	43.6
MLG film	83.00	38.35	0.2	88.8	89.0
Dry GO membrane	15.00	49.38	26.1	56.5	82.6
Dry GO membrane + 1 min. wetting	11.76	55.00	30.2	49.4	79.6
Dry GO membrane + 10 min. wetting	9.31	78.00	48.9	22.9	71.9
Dry GO membrane + 30 min. wetting	6.93	95.00	67.3	8.9	76.2
Note: MCE = mix cellulose ester (MF-Millipore™); PC = polycarbonate (Isopore™) H_2O: γ_l^d=21.8 mJ/m^2,γ_s^p=51 mJ/m^2, γ_l= 72.8 mJ/m^2, γ_l^p/γ_l^d=2.36 CH_2I_2: γ_l^d=48.5 mJ/m^2,γ_s^p=2.3 mJ/m^2, γ_l= 50.8 mJ/m^2, γ_l^p/γ_l^d=0.05					

From figure 3.5, the PC and MCE filter membranes show the highest adhesion strength with MLG, while the dry GO and PDMS also have relatively higher adhesion than other substrates. At the same time, silicon wafer has a very low adhesion strength with MLG. These results are in agreement with previous studies that PDMS is used as the stamp to fetch other thin films in flexile electronics and other graphene thin films. As expected, the GO/rGO interfacial adhesion reduces rapidly as swelling take place. The swelling in this experiment is roughly controlled. Because the graphene oxide used in this experiment is extremely hydrophilic, the addition of water is hard to control; therefore, the extent of swelling is controlled qualitatively, rather than quantitively. As GO swells, the electrostatic repulsion on each GO sheet will facilitate the collapse of membrane structure, and the extreme case is to leave a layer of water between the

MLG film and the filter membrane. This notion is similar to the sacrificial layer techniques in atomic layer deposition [159]. Interestingly, the adhesion between MLG film and filter membrane in this experiment is even higher than the adhesion strength between MLG and PDMS; this is counterintuitive as our experimental observation suggested otherwise. Thus, another transfer experiment was conducted for completely dried MLG on the filter membrane by 20℃ air dry for one day. After intense drying, the MLG adhered firmly to the filter membranes, and could not be transferred. Therefore, it is likely due to the water molecule between the MLG and the filter membrane decreased their adhesion strength, which was proved in other cases [172].

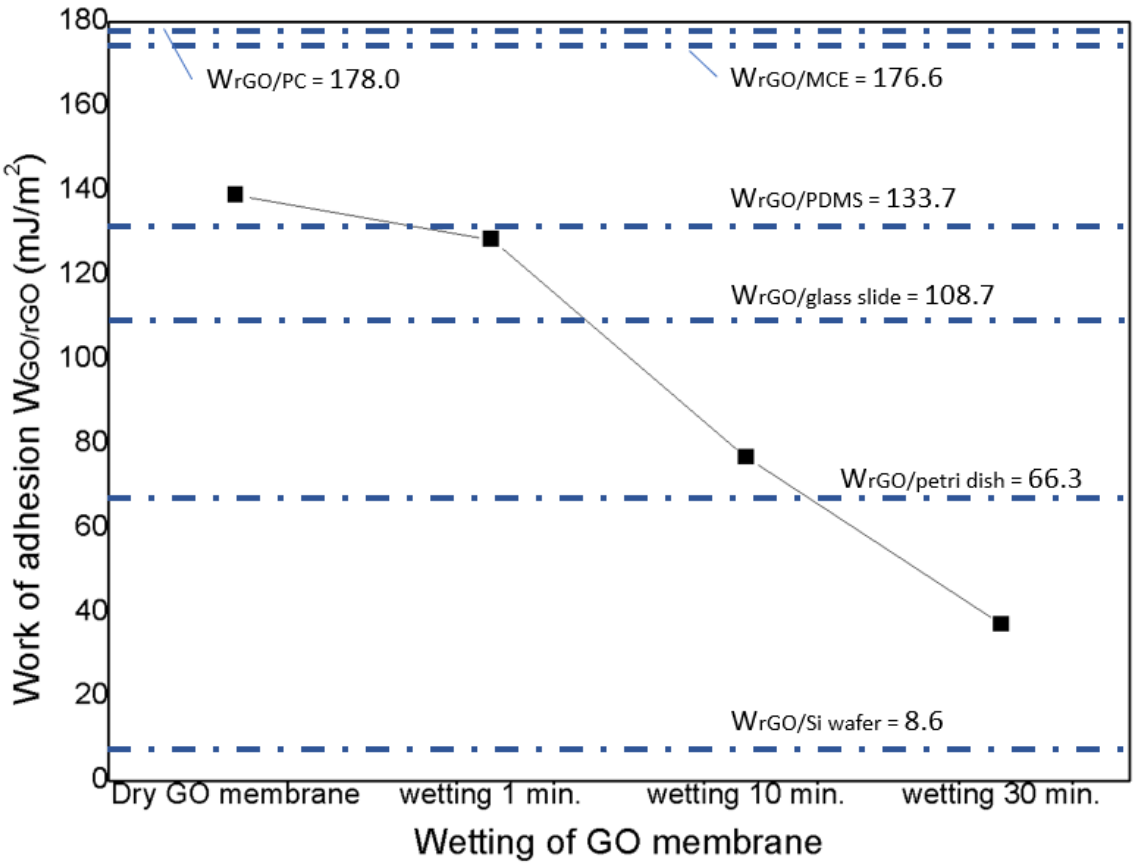

Figure 3.5 *GO swelling induced reduction on GO/rGO interfacial work of adhesion.*

Furthermore, as conductive thin films, the electrical properties of MLG film with different thicknesses are of interest. From table 3.4 and figure 3.5, we choose PDMS and petri dish to coat MLG with different thickness. The sheet resistance was measured via 4-probe ohmmeter

by Keithley Model 2400 SourceMeter®, and the results are shown in figure 3.6. The sheet resistance of MLG film after filtration (on MCE), MLG film directly transferred to PDMS, MLG film transferred to PDMS with the aid of GO interlayer, and MLG film transferred to a petri dish with the assistance of GO interlayer are measured. The comparison is shown in figure 3.6. From figure 6, it indicates that an increase in sheet resistance is unavoidable for the transfer process, which is likely due to the microcracks. However, as compared to the direct transfer of MLG to PDMS, the GO assisted transfer shows a slight improvement on the electric conductivity. The improvement might be attributed to less stress is applied on the thin film surface during the GO assisted transfer. Moreover, figure 3.6 shows that the GO can facilitate the transfer of MLG film onto a Petri dish with high quality. This outcome of this work demonstrates the potential of a simple thin film transfer technique that could contribute to the field of flexible electronics and transparent conductors.

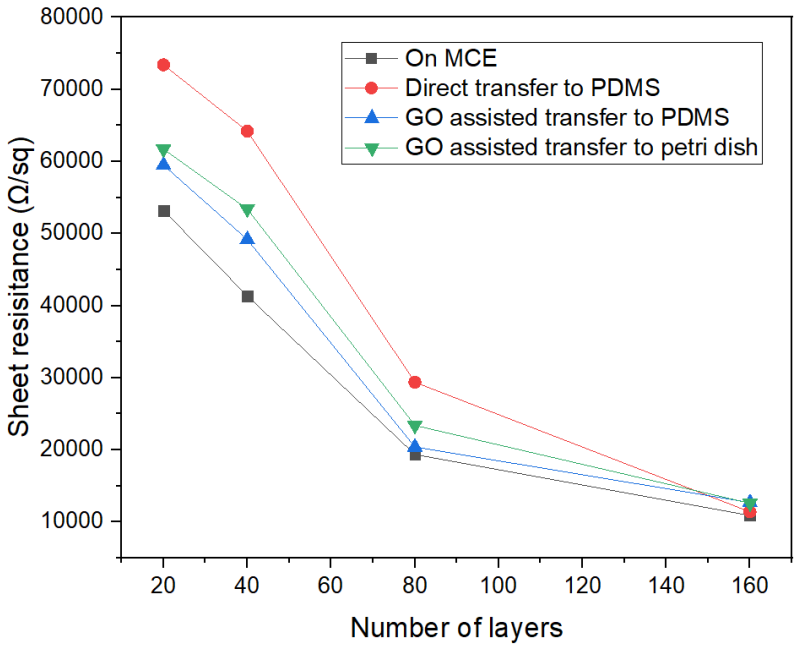

Figure 3.6 *Comparison of sheet resistance of MLG films before and after transferred to PDMS and petri dish substrates.*

3.4 Conclusions

In this study, we examined the effect of GO swelling on the interfacial transfer of vacuum filtrated MLG film and discovered that the GO interfacing layer could readily reduce the

adhesion strength between the GO membrane and the MLG film. Therefore we largely expanded the feasible range of graphene coating and demonstrated coating MLG film onto a variety of substrates. The unique contributions of this work are two-fold:

First, we confronted a significant technical barrier the solution-based fabricated thin films can only transfer to a limited selection of substrates due to the weak surface adhesion between thin films and the target substrate. This work solves the issue by innovatively utilizing the swelling effect of graphene oxide and provided a reliable fabrication method to enable the systematic study of the material-crack morphology-electromechanical property relationship. While in this work, the swelling of GO is controlled qualitatively, it demonstrated a promising prospect in the application of pattern transfer of thin film electronics. And it implies a future research direction in the accurate control of interfacial adhesion via accurate humidity or chemistry modification.

Second, we revisited the swelling effect of graphene oxide and showcased a unique application of the swelling effect. While the structural collapse of the GO membrane is conventionally deemed as an undesirable phenomenon for functional of GO membranes, this work innovatively endowed GO with another favourable usage and could promote the further development in the field of functional GO membranes.

Chapter 4 The cracking behaviour of MLG films on PDMS substrate

4.1 Design concept

As summarised in section 2 of Chapter 2, the cracking of thin films coated on flexible substrates is determined by multiple influencing factors. In the past research on the cracked thin film-based strain sensors and thin film electronics [8, 15, 32, 36, 38-40, 45, 55, 59, 60], various effects such as the mechanical mismatch between the thin film and substrate, interfacial bonding, thin film thickness are reported to impact the cracking behaviours. These studies provide essential knowledge backgrounds for the investigating of the cracking behaviours in new materials such as MLG films.

MLG films, due to their large structural tunability, easy and reliable control on structural parameters, could achieve accurate modulation on thickness; corrugation, sheet size, which in term lead to different extent of defects. Moreover, the unique interlayer properties as compared to the traditional metallic materials or thin film assembled from particles or 1D materials also makes it a unique and interesting material platform [66, 69, 111, 152, 173]. At the same time, in the past studies on graphene-based functional films, researchers mainly focused on their functional properties. However, the mechanical cracking behaviour is another important fundamental material characteristics, and studying the cracking behaviours in MLG film could potentially contribute to the future material designs for flexible energy storage membranes, *etc.* While the mechanical properties and crack behaviours of single-layer graphene and few-layer CVD-grown graphene, as well as bulk graphene-paper, have been reported [73, 141, 174-177]. The cracking behaviour of nanoscale MLG films and MLG films coated on a polymer substrate remain blank. These reasons are the driving force to conduct exploration on the cracking behaviours of MLG film coated on polymer substrates due to various influencing factors.

In chapter 3, we have demonstrated a highly controllable and reliable method to fabricate MLG films onto various substrates. However, in this project, we use PDMS as the substrate due to its high stretchability, high interfacial adhesion with an MLG film, and transparency [178]. We

first examine the common encapsulation and the substrate parameters from the literature. Then, our primary goal is to explore whether the interlayer properties in MLG film could be tailored to induce unique cracking behaviour and if these cracking behaviours could lead to advantageous electromechanical properties for thin film strain sensor. Chapter 4 focuses on the first question.

4.2 Experimental section

4.2.1 Fabrication of PDMS substrate

Sylgard 184 PDMS is used. Mass ratio = bass: curing agent = 20:1. The mixture is violently stirred with Heidolph stirrer (model) at 200 rpm for 10 minutes at room temperature. Then the well-mixed PDMS liquid is degassed in a vacuum chamber. To fabricate the PDMS substrate, the pre-mixed PDMS liquid is poured into a petri dish with a certain amount of weight to make PDMS films with thicknesses equal to 200 μm, 400 μm, 600 μm. The mixed liquid is cured at 80℃ for 1 hour. The 20: 1 ratio for PDMS is selected due to its small mechanical hysteresis within 100% [179]. For the comparison on the effect of PDMS thickness and modulus, PDMS with base liquid: curing agent = 5: 1 and 10: 1 were fabricated with the same method.

4.2.2 Fabrication of MLG films coated on PDMS

The MLG film coated on the PDMS substrate is fabricated via the method reported in Chapter 3. Mixed cellulose ester (MCE) membrane is used for its ideal flexural modulus. For polycarbonate (PC) membrane is too soft to handle during transfer, while anodic aluminium oxide (AAO) membranes are too stiff to obtain a compliant contact with the PDMS substrate. The MLG films are air-dried at 20℃ for 2 hours. For comparison, PDMS encapsulation is done by curing another layer of PDMS with the same thickness as the substrate on top of the MLG/PDMS surface. To fabricate MLG films with reduced interlayer distance, the MLG film is dried at 80℃ overnight. To fabricate MLG films with increased interlayer distance, the MLF films are produced as hydrogels, followed by a quick air blow to dry the thin film's surface.

4.2.3 Fabrication of soft electrode

The conducting gel is made by mixing Ecoflex liquid (part A and B, Smooth-On, 00-10) and carbon black (mass ratio 5:5:1) [180]. The same weight of n-hexane is poured into the mixture, and the slurry is violently stirred with Heidolph stirrer at 200 rpm for 5 minutes in a fume hood. The slurry is stirred at a sealed condition.

4.2.4 Fabrication of MLG/PDMS conductor

With the MLG coated on PDMS and the Ecoflex/carbon black slurry, 100-200 μm of the slurry is blade cast onto the two ends of MLG film in two steps. First, 100 μm of the slurry is blade cast onto the MCE surface; then carbon fibre is adhered to the casted slurry to make the electrode. The product is then cured in room temperature for 5 min. Then another layer of 100 μm of slurry is cast onto the electrode to cover the carbon fibre. The electrode is cured at room temperature for 10 min. Then another layer of PDMS encapsulation poured on top of the overall product. After the PDMS is cured at 80℃ for 1 hour, the whole layer of PDMS substrate is carefully peeled off from the petri dish first to avoid deformation-induced cracking in the MLG film. Then the sample is cut into a rectangle shape with L * W = 5 cm * 2 cm.

4.2.5 Uniaxial mechanical stretching

The mechanical stretching is done with lab-made stretchers from micrometres. Two sets of micrometres (purchased from Parker Hannifin) are fixed onto a lab-designed and 3D printed frame. The sample is carefully clamped on the lab-made stretcher, and the length of the sample within the two clamps is measured with a digital calliper. The step-resolution of elongation depends on the micrometre; in our study, the step-resolution of elongation is 0.01 mm. And the stretching of the sample is conducted manually at a "quasi-static" rate of 0.5 cm/min. to avoid inaccuracy due to strain rate.

4.2.6 Optical microscope characterisation on thin film morphology

Due to the optical transparency of MLG film, the morphologies, including wrinkle, crack, folding, etc. could be readily observed with an optical microscope (Leica ICC50 W) in our experiment. The objective lens are 4x/0.1 POL, 10x/0.25 POL, 20x/0.4 POL, 63x/0.75 POL.

4.2.7 Image processing

The captured images are processed with "Image J". The crack length, crack gap distance, and wrinkle distance are captured and processed in this work. For each image, 50 data points are collected. For the measurement of crack gap distance, three measurements are carried out for each crack gap. The definitions of the parameter are illustrated in figure 4.1.

4.2.8 *In-situ* mechanical-optical-resistance characterisations

The thin film morphology and resistance are monitored *in-situ* on the lab-made stretcher. The stretcher is designed to fit onto the optical microscope, and the electromechanical response was monitored by eDAQ ER466 integrated potentiostat system.

4.3 Results and discussion

4.3.1 Influencing factors from literature

The effect of encapsulation

The encapsulation of thin film, namely, having another layer of the substrate coated onto the thin film and have it sandwiched in the substrate has reported suppressing stress localisation to create uniform stress distribution and avoid surface delamination most effectively [15, 36, 181-183]. Since the uniform stress distribution and localised stress concentration can lead to distinct cracking behaviours [5, 6, 10, 36, 56, 60], we first examine the effect of encapsulation on the MLG coated on PDMS.

In our experiment, we stretched the thin films to 20% of strain, and the thickness is controlled from 20 layers to 320 layers. The number of rGO layers is calculated and controlled by mass in chapter 3. The value range is selected as previous mechanistic studies on the cracking behaviour of thin films mainly focused in the range of 5 to 100 nm [4, 9, 10, 32, 36, 46, 184], and these films were mainly stretched from 15% to 40%, except for the highly sensitive strain sensors. Therefore, we think 20% is a reasonable strain to observe the effect of influencing factors reported in past studies. And the number of layers is chosen from 20 to 320 as the interlayer distance of cascading MLG film is approximately around 0.35 nm [69, 185].

For samples without encapsulation and with encapsulation are shown in figure 4.1 and figure 4.2. From figure 4.1, wrinkles and cracks are readily observed. In the optical image, the white lines are due to more lights passing through the cracks in the thin film. The dark lines are attributed to the wrinkle. Compared to the flat surface of the unstretched MLG film (Chapter 3), the surface morphology in figure 4.1 underwent large changes. The wrinkles can be explained by the mismatch of Poisson's ratio between the thin film and the PDMS substrate [186]. Thin films with smaller Poisson's ratio than then PDMS will not shrink on the transverse direction; therefore, wrinkles are formed to accommodate the mismatch.

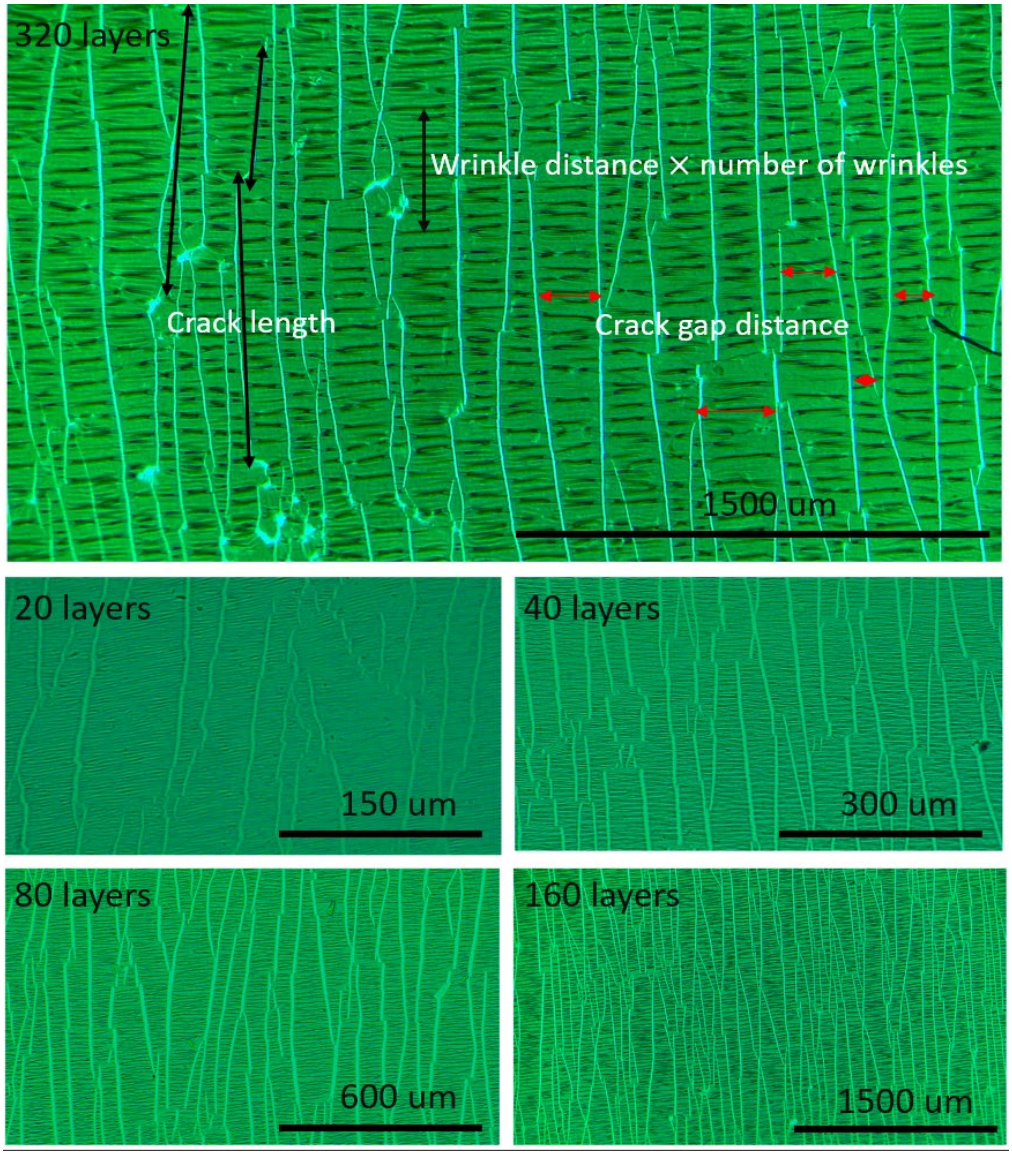

Figure 4.1 *Unencapsulated thin film morphology of stretched MLG film with different thickness. Substrate thickness = 400 μm.* $\varepsilon = 20\%$.

Cracks that are perpendicular to the applied strain direction are observed. Moreover, as the thickness of the MLG films gradually reduces, the crack lines seem to become more random. To have a quantitative view on the effect of thin film thickness, we measured the crack length, crack gap distance and the wrinkle distance, which represents the distance between each wrinkle. The statistic results are illustrated in figure 4.2.

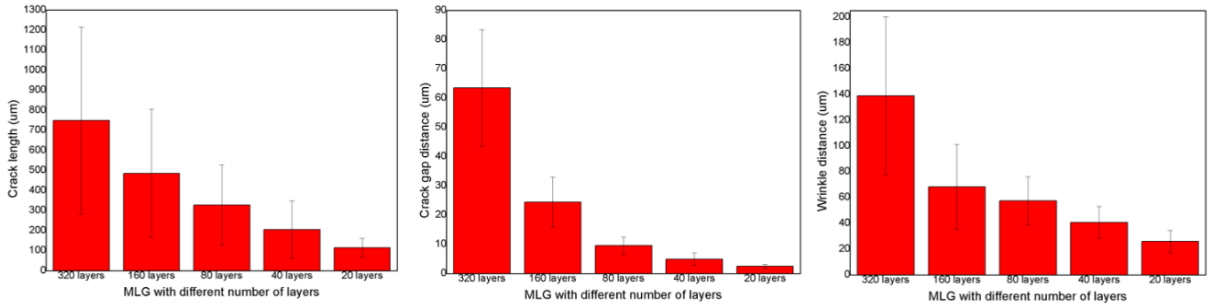

Figure 4.2 *Statistic on crack morphologies of unencapsulated MLG films coated on PDMS substrates.*

From figure 4.2, an apparent trend is observed that as the thickness of MLG film gradually decrease, wrinkle distance, crack length, crack gap distance all decreased accordingly. The wrinkles observed in the unencapsulated MLG films indicated surface delamination. From figure 4.1, a much greater extent of surface delamination is seen for thin films with larger thicknesses. Moreover, as the thickness decrease, a decrease in the proportion of standard deviation can also be observed, which indicates that the cracking is more uniform when thin MLG is thinner.

To interpret the effect of thin film thickness, we referred to the classical fracture mechanics. From the energy point of view [187-189], when a thin film is being stretched, the strain energy per unit area accumulated is expressed as:

$$U_\varepsilon = \frac{1}{V}\int f\,dx = \int \frac{f}{A}\frac{dx}{L} = \int \sigma\, d\varepsilon \qquad \textit{Eq. 4-1}$$

When the energy accumulates above a critical value, cracks will be formed to release the system' s energy. In an idealized situation illustrated in figure 4.3a, the released energy is estimated by

two triangle regions near the crack tip, of width a and height βa, the remaining parts still benefactress σ. Parameter β should agree to Inglis equation and found $\beta = \pi$.

Thus the total released energy per unit thickness is:

$$U = -\frac{\sigma^2}{2E} \cdot \pi a^2 \qquad \textit{Eq. 4-2}$$

When cracking is formed, it also creates two surfaces. The surface energy S is:

$$S = 2\gamma a \qquad \textit{Eq. 4-3}$$

Where γ is the surface energy (Jm^{-2}). Therefore as shown in figure 4.3b, the total energy due to crack is the sum of the absorbed surface energy and release strain energy. Thus, as the crack propagates with longer a, a quadratic dependence of strain energy on crack length upon a critical length a_c, where the total energy is at max. Below a_c, extra stress is the need for crack growth. Therefore It is observed that most cracked networks can reach saturation. However, if above a_c, the crack can continue to grow spontaneously to lower the system's total energy.

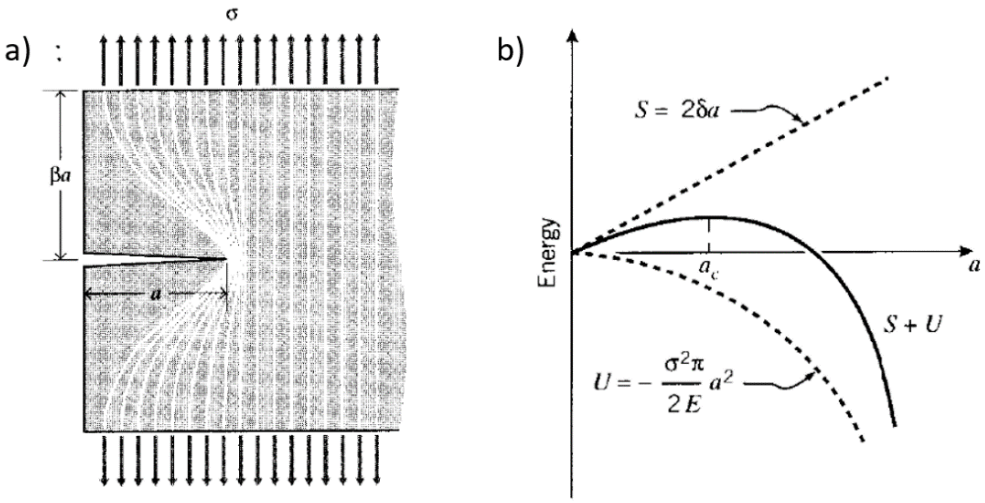

Figure 4.3 *Griffith's energy-balance theory on the brittle thin film. a) The idealization of an unloaded region near the crack tip. b) The fracture energy balance. [187]*

Our finding appears to be in consistence with the Griffith theory. In MLG films with smaller thickness, localized energy is less prone to accumulate to a critical value that leads to unpredictable detrimental cracks. Therefore, both the optical observation and statistics suggest that thinner MLG film shows a more uniform crack formation, which is favourable for controlling cracks [188].

After the MLG film is encapsulated with another layer of liquid PDMS and cured at 80℃ for 1 hour, the crack morphologies are significantly altered, as shown in figure 4.4. First, the wrinkles are well suppressed after PDMS encapsulation. However, we could still observe wrinkles on the sample of 320 layers. The suppression of wrinkles is a sign of improved surface stability. Nonetheless, the cracking observed in the 320 layers of MLG is interesting, as the wrinkles are seemingly to "bridge" the thin film part on the two sides of a crack. Admitted, the wrinkles are important phenomena for thin films, and it might contribute to certain properties that we do not yet understand; nonetheless, the wrinkle represents the surface delamination [183, 190], and delamination might gradually lead to irreversible structural damages and failures. A reliable investigation of cracking behaviours relies on a stabilized thin film system. Thus we desire the suppression of wrinkles, and encapsulation should be applied in our further investigations.

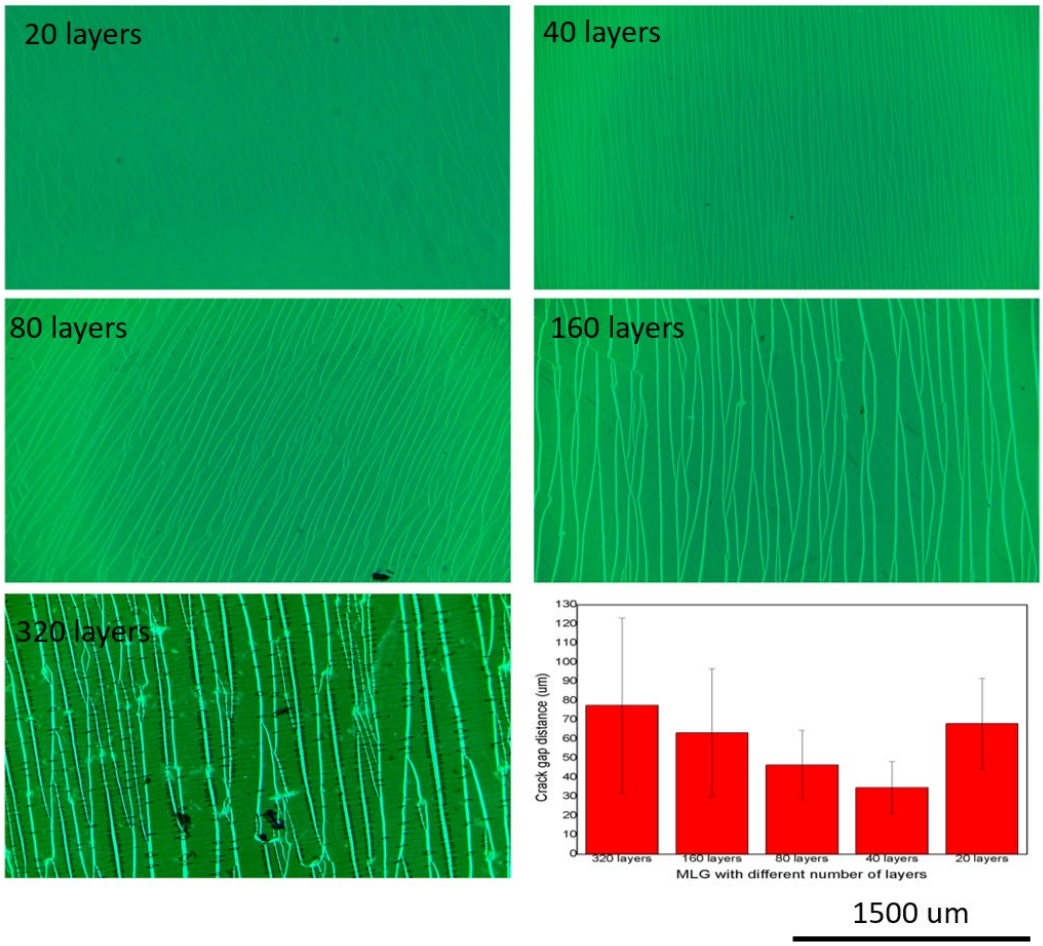

Figure 4.4 *Encapsulated thin film morphology of stretched MLG film with different thickness. Substrate thickness = 400 μm, encapsulation thickness = 400 μm. ε = 20%. Scale bar = 1500 μm.*

Moreover, the crack length is largely increased as we could no longer observe the crack length from the optical microscope. The cracks show apparent parallel crack morphology, similar to the brittle, thin films [32, 45]. The increase crack density as crack length might be the result of the suppressed wrinkle. As surface delamination cannot take place, the energy has to be released in the form of cracks, which can be explained by energy-balance theory.

To reveal a clear relationship between thickness and crack gap distance, we statistically calculated the crack gap distance, as shown in figure 4.4. As expected, the crack gap distance gradually reduced with reducing thickness, which is also well demonstrated in many other thin films with parallel cracking morphologies [55, 57, 142]. However, an interesting increase in

crack gap distance is observed when the thickness is 20 layers. Also, from figure 4.4, the thin film morphology of the 20 layers MLG film does not show obvious channel cracks as observed above 40 layers, the abnormality observed here for the ultrathin MLG (20 layers) might be induced by the intrinsic mechanical properties of the cascading multilayered structure. But we cannot confirm at the moment. Repeated tests show similar results.

The effect of the substrate' thickness and modulus

The mechanical mismatch between the substrate and the thin film has a considerable impact on the stress transduction and localization as introduced in the literature review chapter [8]. Due to our scarce understanding of the mechanical properties of the ultrathin MLG films, as well as our little knowledge on how exactly stress is transduced on the PDMS/MLG film/PDMS interfaces. A set of experiment is designed to study whether the effect of the substrate's thickness and modulus will influence the cracking behaviours of the MLG film.

As per our experimental finding that the 320 layers of graphene will lead to surface delamination, we choose the 160 layers MLG film as the sample with highest mechanical strength, and 20 layers as the sample with lowest mechanical strength [191, 192]. Meanwhile, for PDMS, the modulus of PDMS can be readily modified via changing the ratio between base and curing agent [179], and the total force needed to deform can be multiplied by increasing thickness [193]. Similarly, the observation is conducted at 20% strain. And thin film morphologies are illustrated in figure 4.5.

In our experiment, the PDMS base: curing agent = 1:20. As shown in figure 4.5, for 160 layers MLG thin film with 1: 20 PDMS, increasing the thickness of PDMS substrate and encapsulation from 200 μm to 600 μm, the average crack gap distance increased; however, because of the overlapping of error bar, we should be cautious as to claim the changes in the network.

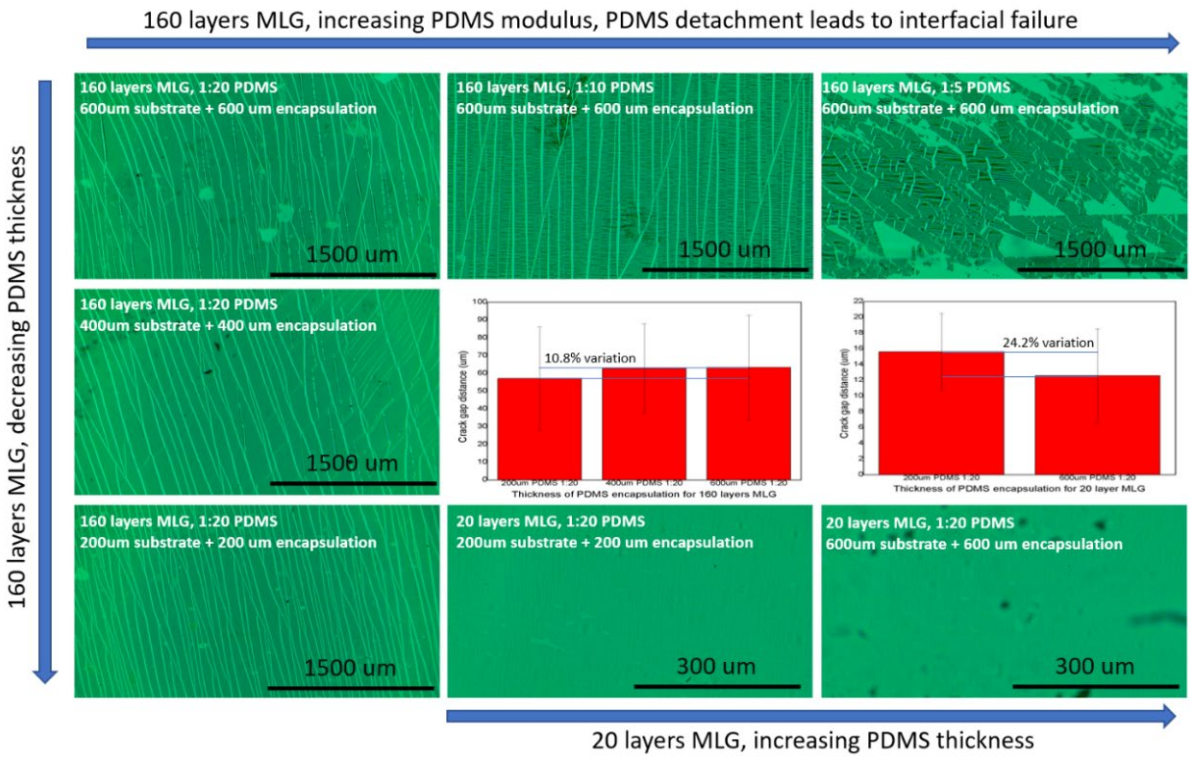

Figure 4.5 *The effect of the substrate's thickness and modulus.*

For 160 layers MLG film, it is observed that increasing the modulus of the thick 600 μm PDMS would result in cohesive interfacial failure. The modulus of PDMS is controlled by the ratio [194]. When the base: curing agent ratio increase from 20: 1 to 10: 1, the PDMS become stiffer, obvious wrinkles can be observed. The occurrence of wrinkle indicated that the encapsulation layer for the substrate layer is detached from the MLG thin film. Further increasing the ratio to 5: 1, interfacial failure can be observed macroscopically. The PDMS layer will delaminate and cause catastrophic damage to the thin film. The interfacial failure can be explained as the interfacial attraction between MLG and PDMS is insufficient to sustain the MLG/PDMS interface as the substrate or encapsulation layer has the propensity to shrink to its high Poisson's ratio.

For 20-layer MLG films, increasing the substrate and encapsulation thickness changes the crack morphology. Comparing figure 4.4 and figure 4.5. The value of crack gap distance for 160 layers remain near the same; however, from 200 μm to 400 μm. The crack morphology of the 20 layers MLG is inconsistent. From 200 μm to 600 μm. The network showed a

transformation from small gap distance parallel crack to large gap distance semi-random crack, to small gap distance random crack. Both figure 4.4 and figure 4.5 indicated that the MLG has unique mechanical properties at ultrathin thickness. Nonetheless, changing the substrate's mechanical properties induces multiple variations. Since this project aims to explore the unique cracking behaviours of ultrathin MLG film, we envisage constructing a mechanical model to study the cracking behaviours in ultrathin MLG films in future studies.

Upon the experimental examination of the traditionally studied influencing factors, we discovered that the MLG film shows brittle, thin film-like mechanical behaviours when the thickness is or more than 40 layers, However, interesting cracking morphologies starting to take place when the thickness is reduced to less than 40 layers. Upon the finding in this section, the standard substrate parameter is determined to minimize the surface delamination, that future studies are conducted with PDMS thickness and encapsulation = 200 μm, PDMS bass: curing agent = 20: 1. The key influencing factors due to the interlayer properties in MLG film will be examined based on the standard substrate condition.

4.3.2 Key influencing factors in cascading MLG film

Upon the discovery of the abnormal cracking behaviours of MLG film at the nanoscale thickness, this section explores the unique influencing factors of the cascading MLG film. They are the controllable interlayer mechanical and chemical properties and the controllable sheet size of the single rGO sheets.

The effect of interlayer attraction and sheet size on crack formation

One of the major difference between cascading MLG film and other thin film materials is its controllable interlayer properties [151], and it can be assembled from rGO sheets with different sizes or even different chemistries. In this experiment, the interlayer attraction is modulated via drying condition [112], namely, a set of samples were prepared with extensive drying of the as-prepared MLG film/PDMS at 80℃ overnight to enhance the interlayer attraction. Another set of samples are obtained by fabrication MLG hydrogels, which maintains the hydration between graphene interlayers and reduces the interlayer attraction. Both sets of

samples are encapsulated and cured at 80℃ for 1 hour. The sheet size is controlled by the sonication, followed by centrifuge [195].

As per results in 3.1. Stretching the thin films to the same strain provides directly comparable cracking morphologies, and it is an important method for mechanical analysis. However, this research aims to explore the cracking behaviours of MLG film and the electromechanical properties of the cracked-yet-electrically conducted thin film. Their detrimental cracks should be avoided. Therefore, in this study, we conducted an *in-situ* study to test the continuity of the electric current in the cracked film. The cracking images are captured when the thin film network lose conductivity. And the crack morphologies at the critical points were summarised in figure 4.6 and 4.7, for films with enhanced and reduced interlayer attraction, respectively. L, M. S represent large sheet size, medium sheet size, and small sheet size. The sheet sizes are controlled by distinct sonication conditions.

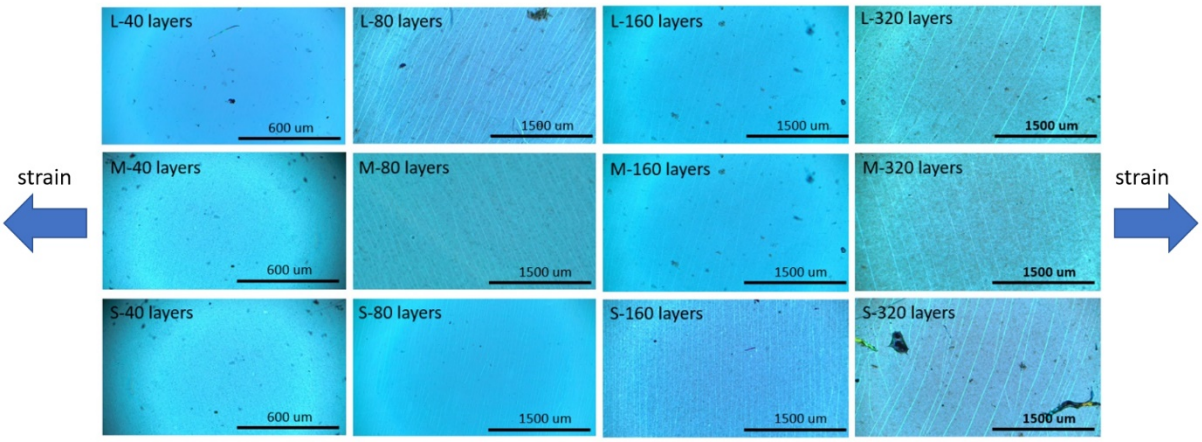

Figure 4.6 *Crack morphology of MLG film coated on PDMS with enhanced interlayer attraction.*

Enhancing or reducing the interlayer attraction alters the mechanical characteristics of the MLG and will increase the thin film strength [112]. As a result, the MLG films with reduced interlayer distance show obvious channel crack properties, as shown in figure 4.6. Meanwhile, reducing the interlayer attraction is seemingly leading to more random crack morphologies. On the other hand, the cracking morphologies of the MLG films with increased interlayer show

slightly different cracking morphology, as shown in figure 4.7. While the samples with increase interlayer distance still show parallel cracks when the MLG films are assembled with large sheet size and when the MLG is thicker than 40 layers. Based on the previous investigation on the cracking behaviours of single-layer graphene film [146], and few-layered graphene film [72, 73], we expect parallel cracking morphologies in the MLG films. However, from figure 4.7, it will show unexpected cracking morphologies that are more random when the thickness is smaller than 40 layers. For a direct comparison, the crack gap distance is extracted, and the statistic on cracks for the two sets of samples is illustrated in figure 4.8.

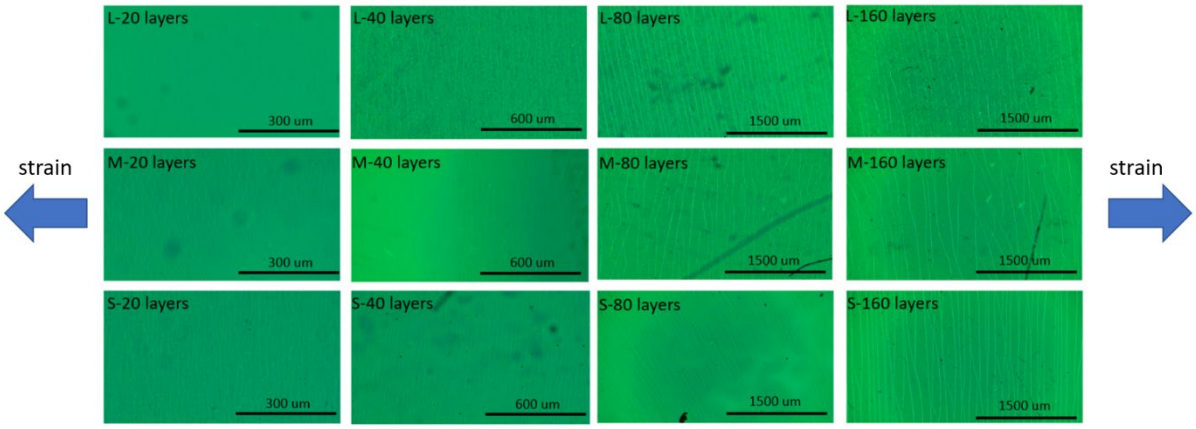

Figure 4.7 *Crack morphology of MLG film coated on PDMS with reduced interlayer attraction.*

From figure 4.8, a clear crack gap distance vs. thickness relationship is observed for the MLG films with reduced interlayer distance. An obvious increase in crack gap distance with thickness indicated that when the thin film network losses electric conductivity, MLG films with larger thickness will statistically have lager crack gap distance. Meanwhile, an interesting trend is observed that as the MLG film is assembled by rGO sheets with smaller sheet sizes, the MLG will statistically show smaller crack gap distances. However, on the other hand, the MLG films with increased interlayer distance have relatively confusing results. First, the increase of crack gap distance does not necessarily show in the small sheet size samples. Second, the decreasing trend on crack gap distance with decreasing sheet size does not necessarily show. These confusing results can hardly be interpreted along. However, when considering the maximum conducting strain, a correlation between the stretchability and crack morphologies can be generated in figure 4.9.

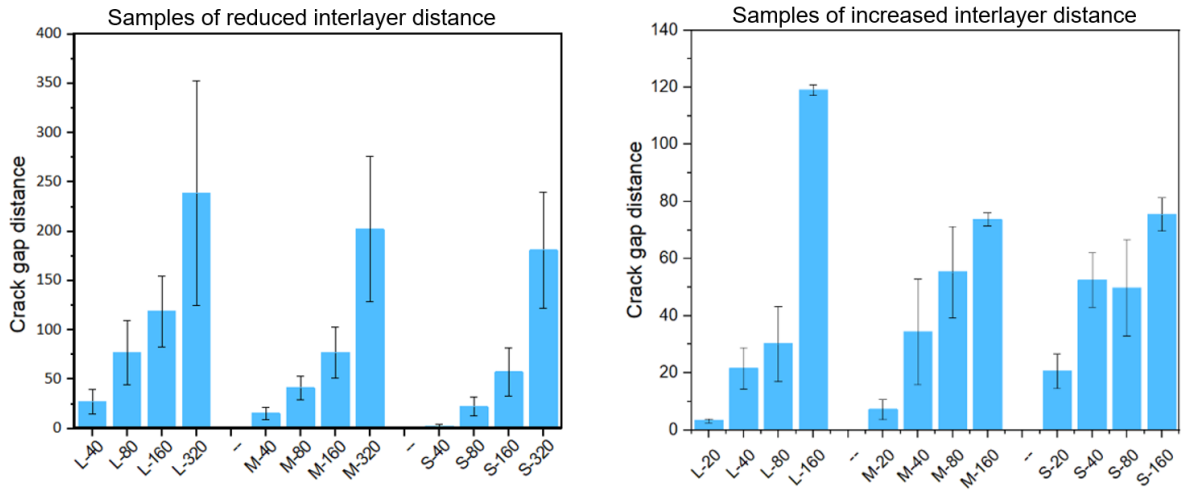

Figure 4.8 *Statistics of cracked thin films at the critical strain.*

In figure 4.9, the y-axis is the maximum strain when the thin film losses electric conductivity, and each dot represent a thin film sample. Clearly, for MLG films with reduced interlayer distance, a correlation between crack gap distance and stretchability can be found, that thin films with reduced crack gap distance will exhibit larger stretchability. The reliance of stretchability on crack gap distance is also observed in other brittle thin films [32, 46], which indicates that the MLG film with reduced interlayer distance might have similar mechanical properties as the reported materials. However, the MLG films with increased interlayer distance will not fit into the curve of the MLG film with reduced interlayer distance, it will deviate as the network starts to form cracks with more random cracks that is similar to the percolative cracking behaviours in gold fibre, gold nanoparticles, and CNT thin films [36, 40, 41]. This intriguing transform of crack deformation indicates a unique underlying deformation mechanism due to the cascading structure. Possible explanations include interlayer sliding [190, 196] and defects induces cracking [197, 198]. Or it might be related to other unexpected mechanisms. We foresee a mechanical modelling on the cascading structures would contribute to the understanding of such a unique phenomenon.

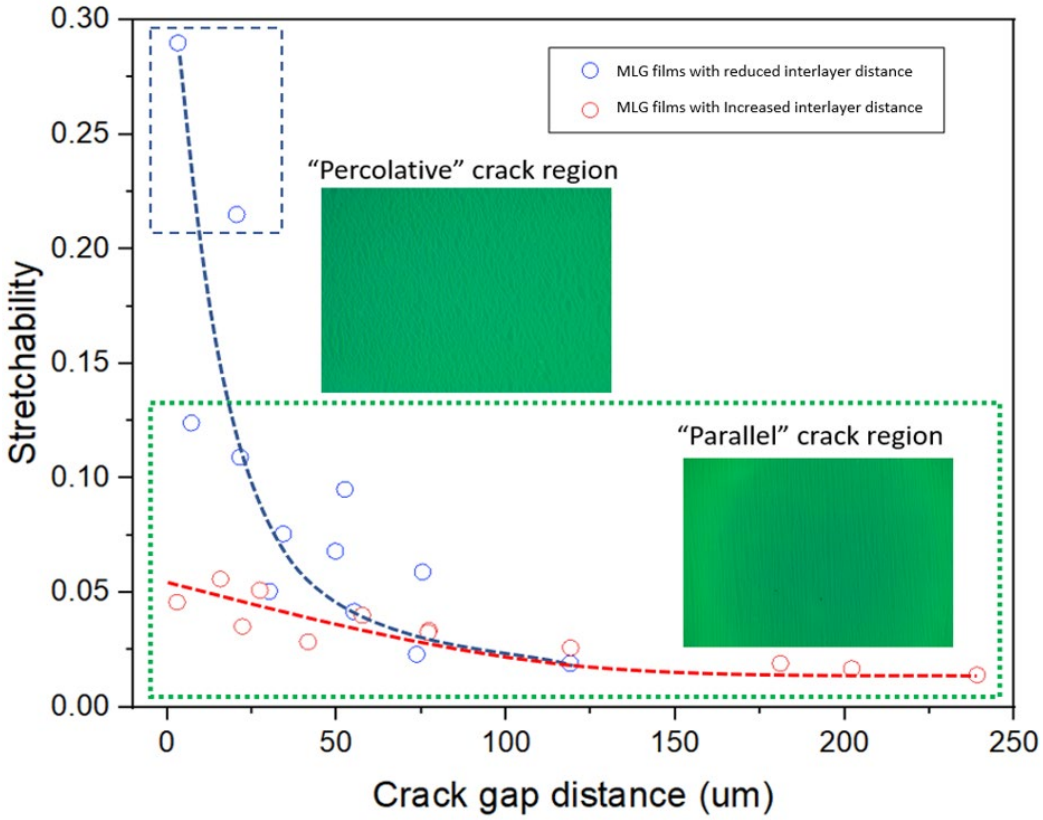

Figure 4.9 *Crack gap distance vs. maximum stretchability.*

The effect of sheet corrugation on crack formation

To further explore how would the unique interlayer properties influence the cracking behaviours of MLG film, We enhanced the extent of corrugation of the single rGO sheets by excessive hydrothermal reduction on two samples, namely, the L-20 and S-20 from figure 4.8. To our surprise, both networks show much more random cracking behaviours, as shown in figure 4.10. While we could still observe the crackings in the L-20 sample, the cracks become too small to be observable for optical microscopes in the S-20 sample. Moreover, the *in-situ* electrical continuity experiments were carried out, and both thin films retained electric conductivity at 70% of strain. It should be noted that while increasing the extent of corrugation, the graphene sheet might also agglomerate, thus the agglomerated particles might serving as a new defect site. Moreover, the control of corrugation in this study is only qualitative.

At the moment, we do not understand as to why the MLG film will undergo the different cracking processes due to the effect of thickness, interlayer distance, and corrugation. Further investigation is necessary.

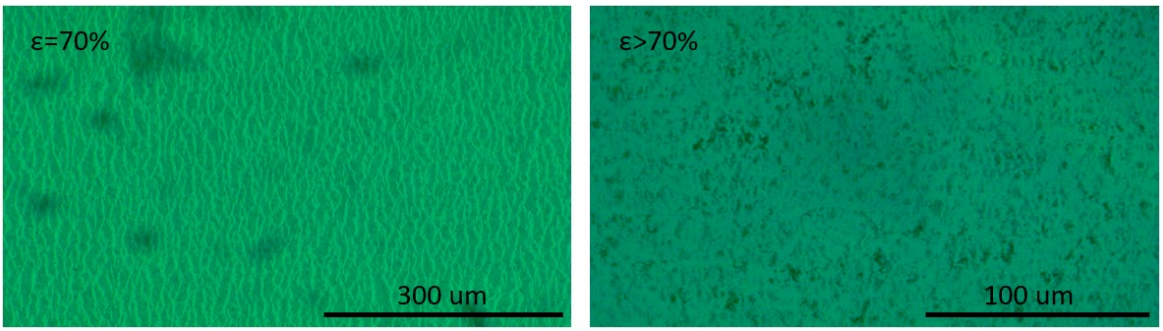

Figure 4.10 *Percolative cracking network in MLG film. Left, large sheet-20 layers, Right, small sheet-20 layers.*

4.4 Conclusions

In this chapter, we explored the cracking behaviour in MLG film coated on the PDMS substrate. Influencing factors from previous studies were examined first, and the unique influencing factors originated from the cascading 2D structure were also examined.

We discovered that the MLG film shows multi-phase cracking behaviours when changing thin film thickness, interlayer distance, and the extent of corrugation. The thick MLG film demonstrates brittle mechanical behaviours and mainly crack in parallel manners. The ultrathin MLG film (~20 layers) shows ductile mechanical behaviours and starts to form cracks as a percolative network. For statistic analysis, we can obtain the crack gap distance-stretchability relationship for the cracked network with parallel morphologies.A "brittle-ductile" transition is observed on the MLG films with enhanced or reduced interlayer attractions. Moreover, a chemically induced "defect" by assembly MLG film with corrugated rGO sheets extensively increased the randomness of the cracking morphology. The significant increase in stretchability indicates the "bridging effect" of the percolative network. These discoveries demonstrate huge potentials for the ultrathin transparent MLG thin in the flexible electronics applications.

However, we do not fully understand the reasons for the transform of cracking behaviours discovered in this project. And we envisage a theoretical mechanical model to reveal the cracking process in the ultrathin cascading 2D structure; we also envisage applying image-processing based machine learning for future characterisation on the percolative network.

Chapter 5 Electromechanical properties of the cracked MLG thin film network

5.1 Design concept

As summarized in section 3 of the literature review chapter, the field of flexible strain sensor value electromechanical properties like sensitivity or gauge factor (relative signal change to strain), stretchability (maximum tensile strain before disconnection), static sensing accuracy (deviation of signals in a given time) and dynamic sensing accuracy (deviation of signals during dynamic deformations) [32, 38, 62, 127, 149]. But often there is a tradeoff between properties, for example, the tradeoff between gauge factor and stretchability. Achieving high sensitivity and high stretchability had always been a challenge and of interest in past years [38, 39, 43, 45, 62, 149, 199-201]. Graphene, based on its high electric conductivity, might be an ideal material to achieve dual functionality [147].

Upon cracks formulated in thin films, the electromechanical behaviours are determined [32, 37], and any alternation on the electromechanical response indicates structural deformation. As discussed in the literature review chapter, we view the electromechanical characterisation to have a two-fold definition—first, the characterisation of strain sensing properties from an engineering perspective; second, the electromechanical response is also a reflection of the thin film's microstructure. Chapter 4 explored the cracking behaviour in MLG film and discovered that the unique cascading 2D structure and the tunable interlayer interactions could lead to unusual percolative cracking. This chapter continues to examine the electromechanical properties of cracked MLG film.

5.2 Experimental section

5.2.1 Fabrication of MLG/PDMS conductor

With the MLG coated on PDMS, 100-200 μm of the Ecoflex/carbon black slurry is blade cast onto the two ends of MLG film in two steps. First, 100 μm of the slurry is blade cast onto the MCE surface; then carbon fibre is adhered to the cast slurry to make the electrode. The product

is then cured in room temperature for 5 min. Then another layer of 100 μm of slurry is cast onto the electrode to cover the carbon fibre. The electrode is cured at room temperature for 10 min. Then another layer of PDMS encapsulation poured on top of the overall product. After the PDMS is cured at 80℃ for 1 hour, the whole layer of PDMS substrate is carefully peeled off from the petri dish first to avoid deformation-induced cracking in the MLG film. Then the sample is cut into a rectangle shape with L * W = 5 cm * 2 cm.

5.2.2 *In situ* uniaxial mechanical stretching-resistance measurement

For accurate control on the deformation, the tensile stretching experiment is operated on an Instron 5944 microtester. The rectangle samples were clamped by the sample clamps. The electromechanical response is monitored by eDAQ ER466 integrated potentiostat system. During the tensile test, the stretching is controlled by the strain, and the strain rates are set as 0.1 %/s, 10 %/s, 100 %/s. The maximum conducting strain is obtained by stretching the sample at 0.1 %/s until the current becomes too small for the potentiostat, or when signals become unstable. For potentiostat, the sample rate is 100 points/second.

5.2.3 Formation of a cracked thin film network

For any un-cracked thin film conductor, the maximum conducting strain is measured first. Strain rate = 0.1%/s. Then another un-cracked thin film conductor is stretched to 90% of the maximum strain and released. The same process is repeated for several times until crack saturates that the strain-resistance curve becomes stable. Strain rate = 0.1%/s.

5.2.4 Static electromechanical characterization

The static electromechanical characterization is conducted under the creep/relaxation mode in Instron. The sample is stretched to a certain strain and hold for 200 s to observe the change in resistance. The strain rates are chosen as 0.1%/s, 10%/s, and 100%/s. The strains are 30%, 60%, and 90% of the maximum conducting strain.

5.2.5 Dynamic electromechanical characterization

The dynamic electromechanical properties are measure on a lab-made dynamic testing setup. Type 4810 mini-shaker is purchased from BRÜEL & KJÆR. The sample is placed in a lab-made sample holder, and it is dynamically stretched and release by the mini-shaker. The dynamic deformation parameters are set by Keithley Model AFG 2000 arbitrary function generator. The waveform is set as Sinusoidal, and the frequency is set from 1Hz to 200 Hz. A current pre-amplifier controls the shaker's deformation amplitude.

5.3 Results and discussion

From chapter 4, we selected four samples with four distinct crack morphologies. And they are illustrated in figure 5.1. These samples were chosen due to their distinct crack morphologies. Sample a shows a near parallel morphology with large gap distance. At the same time, the MLG assembled by corrugated sheets induced unevenness into the thin film, which is indicated by the colour difference observed in the thin film. Sample b shows a typical parallel crack morphology. Sample c shows a typical percolative network. And sample d has a unique microstructure with indiscernible cracks.

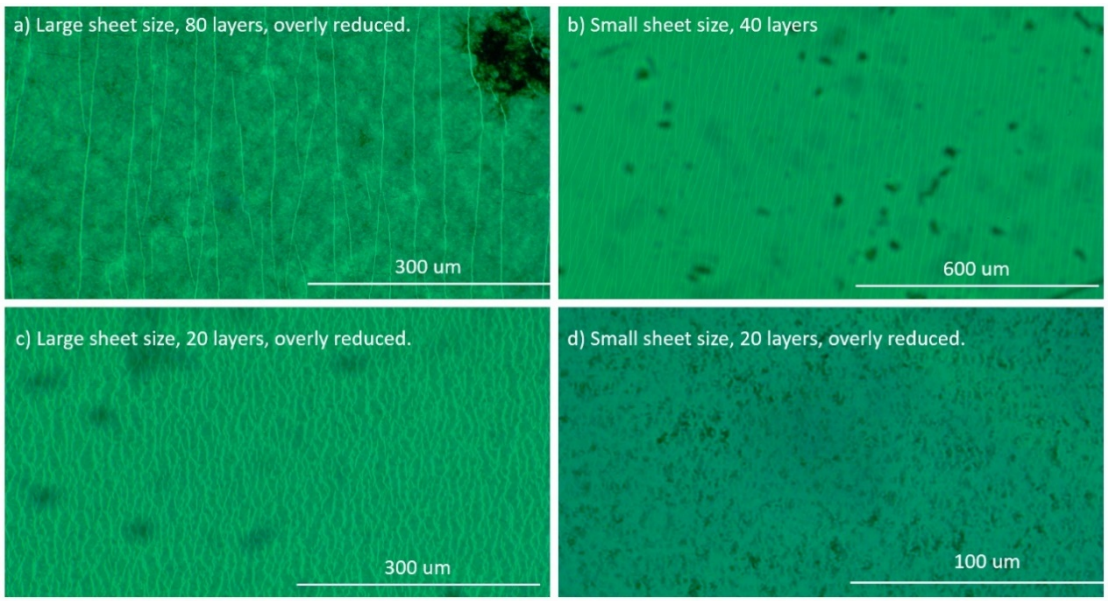

Figure 5.1 *Selection of networks with typical crack morphologies.*

5.3.1 Strain-resistance response

The strain-resistance curve presents an overview of the sensing range, including stretchability and gauge factors [48, 149, 202]; which gives the most direct information on the sensing properties of a strain sensor. For the cracked MLG films. After the maximum conducting strain is measured, another MLG/PDMS composite is repeatedly stretched to 90% of the maximum strain at 0.1%/s strain rate and released, to form the cracked network. The electromechanical properties of the crack-yet-electrically connected network are examined after the crack saturate that two consecutive cycles of the strain-resistance curve are identical.

For the four samples from a to c in figure 5.1, the maximum conducting strain are 6 %, 15%, 70%, respectively. However, for sample d, the network remained conductive over 70%. However, due to the high pressure at the clamp to ensure samples' stability, stress concentration will occur at the clamp edges and cause damage to the substrate. Thus, even though sample d might show greater stretchability, we set its maximum conducting strain equals to 70%.

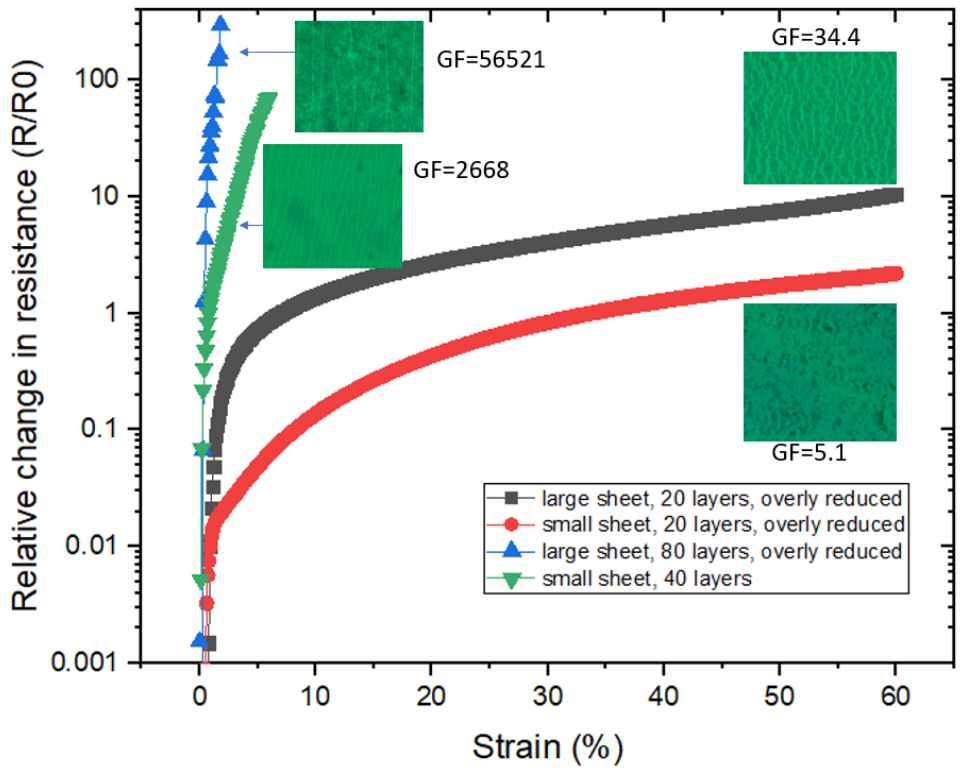

Figure 5.2 *Strain vs. relative change in resistance for thin films with different cracked morphologies. The gauge factors in the figure are the maximum gauge factors.*

Figure 5.2 presents the strain vs. relative change in resistance relationship for thin films with different cracking networks. Interestingly, these four typical cracked networks show distinctively different sensing ranges. A thin film with large parallel cracks (sample a) results in high strain-responsive sensitivity; while a thin film with small percolative cracks (sample d) results in a high stretchability. Meanwhile, the thin films with morphology in between the two typical crack networks indicates a trade-off effect. In figure 5.1, the x-axis is the tensile strain applied on the thin films, and the y-axis is the relative change in resistance (R/R_0), where, R is the realtime resistance and R_0 represent the resistance at strain = 0 %. An apparent two-stage change in resistance can be observed for each thin film, the slope is large in the first stage, and becomes smaller in the second slop. It should be noted that the y-axis in is exponential scale; thus, the fine linearities observed for each thin film at the second stage indicates the exponential growth of resistance. The exponential increase in resistance is a good agreement with the percolation theory, and it suggests that the network is deforming evenly [203-207].

The maximum gauge factors were calculated based on the mean relative change in resistance in the last 1 % strain deformation. And the calculated the gauge factors of the four different thin films are 56521, 2668, 34.4, 5.1, respectively. These values are comparable to the landmarks in the current field of flexible strain sensors [36, 45, 53], and it has implication on broad range sensitive strain sensors. How do the gauge factors and stretchabilities vary significantly raises interesting questions, especially as these properties were produced from the same material? Therefore, it is natural to wonder what kind of cracks alters the electric conduction most distinctively? And what is the unique reason for MLG film to exhibit the ultrahigh sensitivity? What kind of crack helps thin film's elongation yet maintains the current flow? At the moment, we do not yet have answers to these questions; but we hypothesise that the cascading structure provides a "face to face" contact mode in the thin film network. On the one hand, in the highly sensitively parallel crack network, the disconnection of sheet surface to sheet surface might create large loose in conductivity as compared to the disconnection of "point to point" or "point to face" contact.

On the other hand, in the highly percolative network, the sliding between rGO sheets [190, 208] might contribute to the elongation, and it can maintain electric conductivity. However, further investigation is needed. Since the characterisations of sheet sliding have been demonstrated by

Raman spectroscopy [209] and lateral force microscope (LFM) [70], we envisage future investigations to examine our hypothesis. Nonetheless, the large sensing range determined by different cracking morphologies of MLG film suggested important implication on the strain sensing applications.

5.3.2 Static electromechanical properties

After the overall strain-resistance curve have been determined, the static electromechanical performances are examined. As mentioned in the introduction and literature review, the static electromechanical characterization gives critical information on whether the deformed thin film network can remain structural stability, and it is a crucial property for realistic strain sensing applications. In this section, the static electromechanical performances of different thin films are examined with different strain and strain rate.

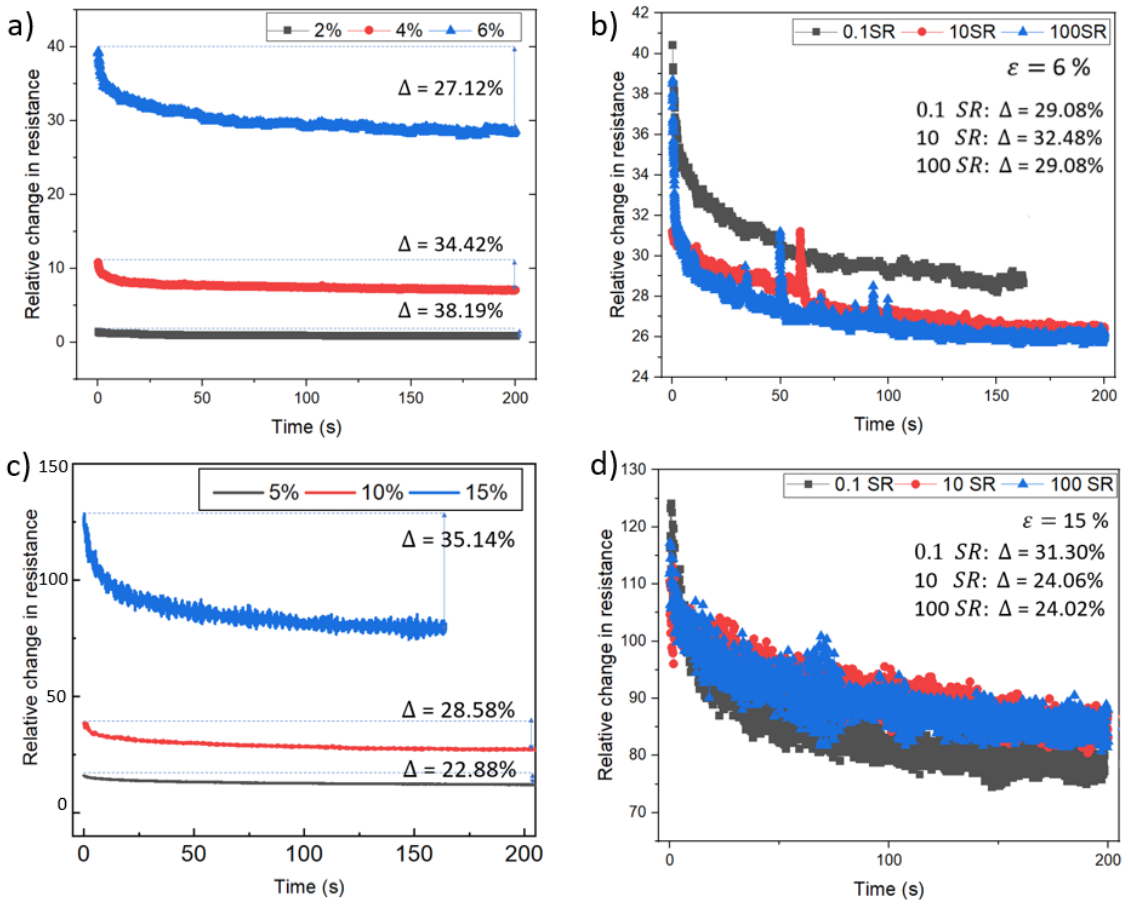

Figure 5.3 *Static electromechanical properties of cracked thin films with large parallel cracks. a-b) Large sheet size, 80 layers, overly reduced. c-d) Small sheet size, 40 layers.*

The static electromechanical performance of the large parallel cracked thin films are demonstrated in Figure 5.3. Obvious relaxation occurred in these thin films. In each test, Δ is used to quantify the extent of signal loss, it is calculated as $((R/R_0)_{t=0s} - (R/R_0)_{t=200s})/ (R/R_0)_{t=0s}$. The relaxation occurs due to the propensity to release the internal stress-energy by structural reconstruction [64]. The effect of strain is demonstrated in figure 5.3a and figure 5.3c, and the effect of strain rate is demonstrated in figure 5.3b and figure 5.3d. When examined the effect of different strain rate, the sample is stretched to the 90% of maximum conducting strain. The extent of relaxation is severe in these two samples, as a large shift in resistance took place despite strain or strain rate. Moreover, as strain increase, the noise starts to increase; large noises are observed when the thin films were stretched to 6 % for sample a and 15 % for sample b.

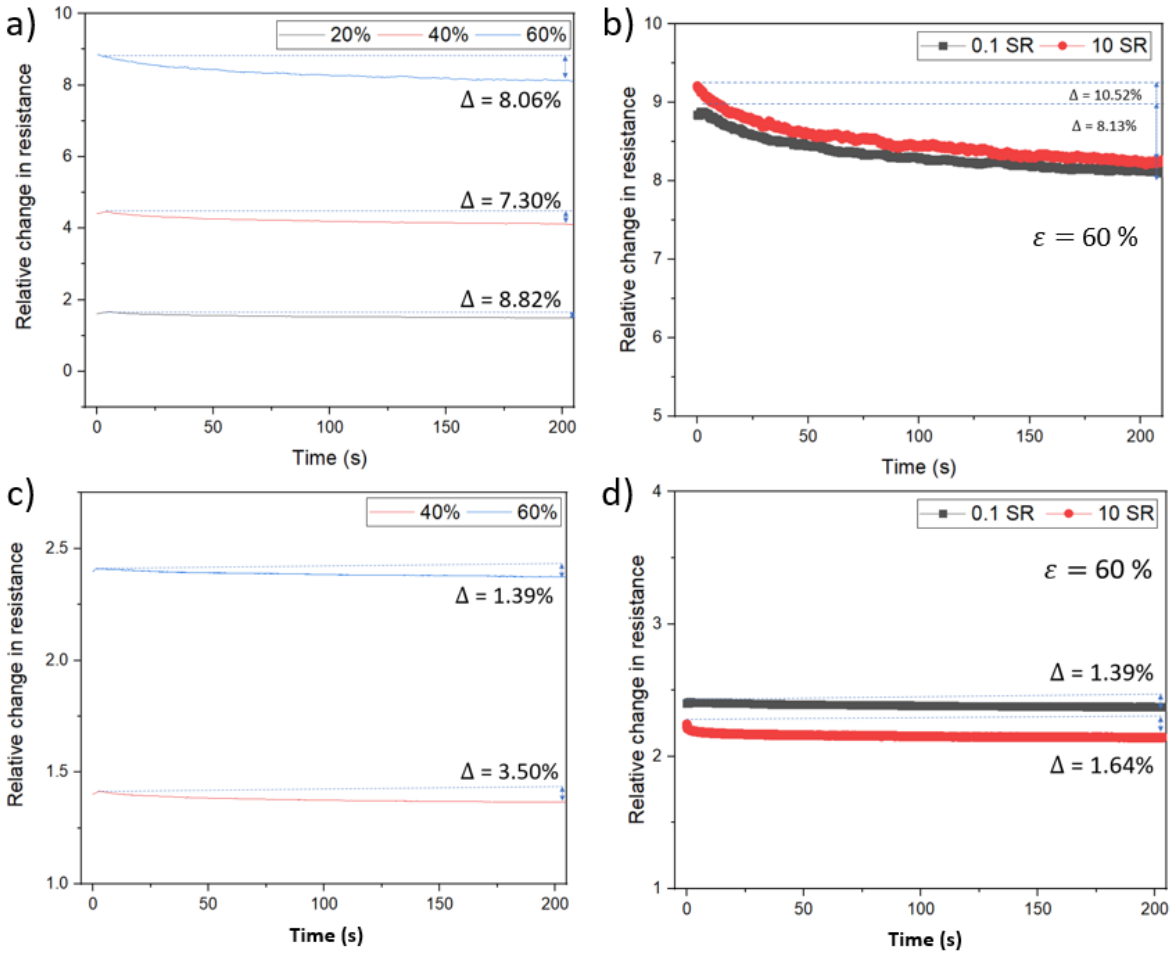

Figure 5.4 *Static electromechanical properties of cracked thin films with small percolative cracks. a-b) Large sheet size, 20 layers, overly reduced. c-d) Small sheet size, 20 layers, overly reduced.*

The static electromechanical properties of sample c and d are demonstrated in figure 5.4. Unlike sample a and b in figure 5.3. The extent of relaxation is largely reduced when stretched up to 60 %. For both thin films with percolative networks, the extent of relaxation still vary. While in sample c, the relaxation of ~ 8 % is observed in 200 s, sample d exhibited only ~ 1.5 % relaxation in 200 s, which is comparable to the lowerest relaxation from the literature [40].

As discussed, the relaxation can indicate structural reconstruction due to internal energy. Thus, it is reasonable to suspect that the evenly distributed microcrack in the percolative network can readily dissipate the strain energy during a deformation, hence the trend for structural reconstruction is low. This hypothesis is backed up by the reduced noise, as shown in figure 5.4. The strain-resistance relation is a rather clean line for sample 4. We wonder if the easy release of strain energy is one of the intrinsic advantages of thin films coated on polymer substrate material systems. Nonetheless, we have not yet constructed a mechanical model to examine our hypothesis theoretically, but we envisage it in our future studies.

To discuss further on the experimental finding, the understanding of the underlying reasons for this unique cracking phenomenon-induced electromechanical performance should be further investigated in two directions. First, as also summarized in Chapter 4, the signs of graphene agglomeration are observed in sample 4. We are not clear if the percolative network results from the sliding, the defects, the further reduced interfacial attraction. The following strategies could be considered for future research. The first strategy is to carefully synthesis and produces cracked thin films with sufficient characterizations on sheet size and the extent of agglomeration via AFM or SEM; the interlayer distance shall be quantitatively controlled via liquid exchange method [69]. Second, the advance on machine learning-based image processing techniques should also be considered, as the current statistic descriptions fail to establish a quantitative relationship between crack morphology and the electromechanical properties. On the other hand, we believe that the electromechanical characterization can provide valuable insight into the structural evolution of the conducting network—for example, Kang *et al.* [32] processed their electric signals during cracking and revealed the cracking evolution process at crack onset points. Thus, the third strategy is to develop data processing techniques, which will not only benefit the thin film's network but also help to understand the structural evolution in other electric conducting systems.

5.3.3 Dynamic electromechanical properties

Upon realizing the static electromechanical properties of thin films. We conducted a dynamic stretching experiment to investigate the thin films dynamic strain response. The sample we chose was sample d.

Figure 5.5 illustrates the dynamic testing device and the high-frequency strain-resistance response. The tensile deformation is conducted by clamping the MLG film/PDMS conductor between a stable holder and the mini shaker. The amplitude of the shaker is measured to be 1.4 cm. From figure 5.5, a clear periodic electromechanical response is observed for the thin film. From the Y-axis, the amplitude of shaker gradually reduces with increasing deformation frequency. However, it can be calculated from the current that the strain is around 13% at 200 Hz.

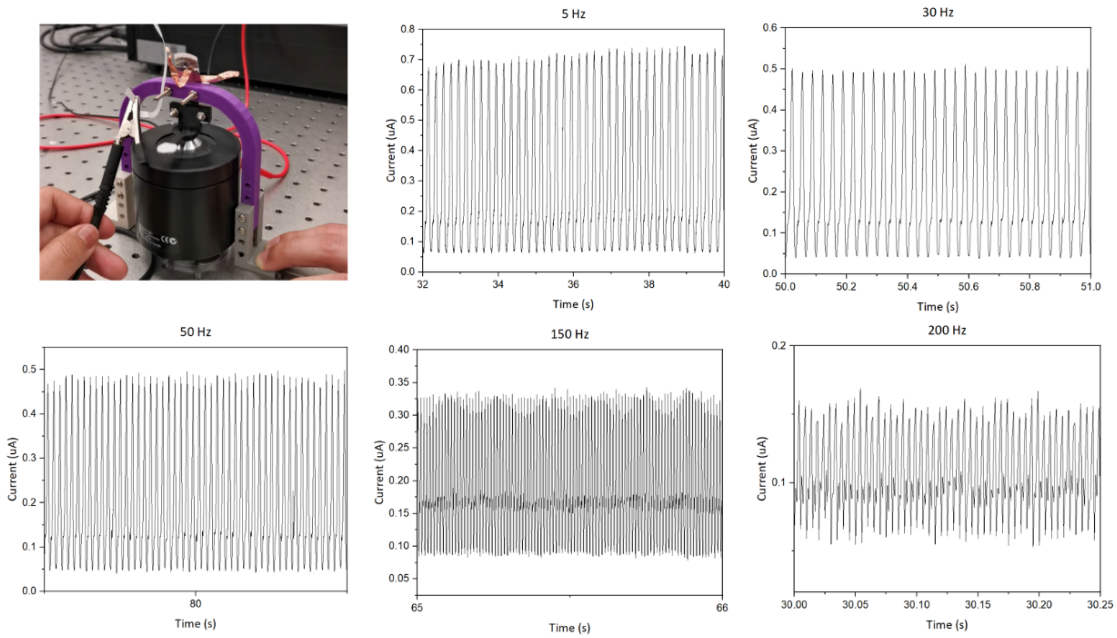

Figure 5.5 *The dynamic electromechanical response of cracked MLG thin film. The high-frequency deformation is carried out from 5 Hz to 200 Hz.*

The result from dynamic response shows that the cracked MLG thin film has benign sensing at all frequencies. Combining with the static sensing performance, the cracked MLG exhibit broadband sensing ability. Moreover, we conducted a long circle test at 200 Hz; the thin film

performed stable sensing for more than the testing time of 1 min., which suggested the excellent Durability. Comprehensive comparison on the critical performance (gauge factor, stretchability, and dynamic frequency) of various strain sensors that demonstrated dynamic sensing performance is listed in table 5.1. The relaxation is not compared due to the less direct report on such data. From table 5.1, it can be found the thin film sensors produced in this work exhibit excellent overall electromechanical sensing performance that can demonstrate a wide range of sensing performances at 0-200 Hz. While the underlying reasons for the excellent electromechanical sensing performance are not well understood, the results imply the potential for the high precision broadband strain sensor, which might lead to the future development of HMI, neuromuscular disease detection, human motion ID, muscle fatigue detection, etc.

Table 5.1 *Overview of the properties of several strain sensors.*

Material	Gauge factor	Stretchability	Application & Elastic frequency (Hz)	Ref.
CNT film array on PDMS	0.82	280%	Knee joint movement; 1 Hz	[39]
CNT fiber/ Ecoflex	0.56	900%	Finger motion; 1.5 Hz	[210]
Buckled fibres	21.3	1135%	Throat, forearm; 21Hz	[211]
Graphene woven fabrics	10^6	30%	Hand motion, breath, pulse, phonation, blink; 5Hz	[199]
AgNW/PEDOT:PSS/PU	12.4	100%	Breathing, coughing, drinking, eating, swallowing; 5Hz	[212]
Low density graphite film	522.6	50%	Body large motion, sound vibration detection; 14Hz	[45]
3d graphene film	2.67	50%	Finger movement; 4Hz	[213]
Graphene putty	>500	100%	Pulse, blood pressure; 3Hz	[214]
TiO2 NM/Au NPs	0.5	25%	Limb tremor, 1Hz	[16]
Multilayer graphene paper	673	10%	Pulse, joint movement; 1.25Hz	[147]
overlapping graphene sheets/PDMS	400	7.5%	Pulse, winkle; 2.5Hz	[215]
Crack-based Pt film/PUA	2000	2%	Small sound vibrations; 1400Hz	[32]
Graphene/rubber composite	35	6%	Finger, sound, dynamic vibration; 160Hz.	[127]
CNT/PEDOT composite	62.3	20%	Finger, facial motion; 1Hz	[216]
ZnO nanowire/ PDMS	116	50%	Finger movements; 2Hz	[217]
CNT/TPE composite	8.3	76%	Fast bending; 23Hz.	[107]

5.4. Conclusions

In this chapter, the electromechanical performances of thin films with different cracking morphologies are examined. We discovered that cracked MLG film could show large sensing range from highly sensitive (GF =56521, ε = 7 %) to highly stretchable (GF = 5.1, ε = 70%) with thin film networks of different cracking morphology, which covers a wide application scope as strain sensors. Moreover, the percolative cracked MLG film shows the ability to reduce static relaxation and reduce signal noise. An interesting “non-relaxation” and “time-independent” electromechanical sensing performance is demonstrated, as the highly percolative cracked thin film showed only ~1.5 % relaxation when stretched at 60 % strain for 200 s, and demonstrate highly accurate strain sensor at 200 Hz around 13 % strain; These electromechanical properties have important implication on broadband strain sensing applications. Nonetheless, our current understanding of why could MLG film exhibit large sensing range, why could percolative cracking network reduce the extent of the relaxation are scarce; revealing these underlying reasons is one of our goals for future studies.

Chapter 6 Conclusions and Future Work

6.1 Conclusions

Carefully controlling the cracking behaviours in brittle thin films provides opportunities in flexible electronics. The tuneable structural parameters and the unique interlayer properties in cascading MLG films make it a promising platform to study the cracking behaviours and the corresponding electromechanical properties.

The primary purpose of this study has been three-fold:

1. To controllably synthesis MLG film coated on polymer substrates.
2. To explore the cracking behaviours of MLG film on PDMS substrate.
3. To explore the electromechanical properties of the cracked MLG thin films.

The first aim has been achieved by transferring vacuum filtrated MLG film onto the target substrate. The challenge in transferring the thin film onto flexible substrates is due to the high adhesion strength between the filter membrane and the MLG film. This study confronted the challenge by utilizing a swelling-induced interfacial effect of GO and manipulated the surface adhesion between the MLG film and the filtration membrane is a simple method. We revisited the swelling effect of GO that usually cause a structural collapse in the functional GO membranes, and endowed it with a new application. The produced thin films are flat and have high electric conductivity, which might lead to future applications in the fabrication of thin film electronics.

The second and third aims have been achieved. In this study, we explored the cracking behaviours of nanoscale thick MLG film for the first time. Unlike single-layer graphene and bulk multilayer graphene membranes, we discovered that the interlayer distance and corrugation have huge impacts on the cracking behaviours of MLG film for thin films with thickness below 40 layers. An unexpected tailorable transformation in cracking morphologies from ordered “parallel” crack to random “percolative” crack is discovered in MLG films when increasing interlayer distance and the extent of sheet corrugation below 40 layers. This finding

leads to other interesting mechanical and material questions, such as what is the effect of defects in cascading structure on thin film's cracking behaviours.

The electromechanical characterisation demonstrated that cracked MLG films with different morphologies have a broad sensing range. A high gauge factor (GF) of 56521 at ε = 6 % and large stretchability of ε = 60 % when GF = 5.1 were achieved for the parallel cracked and highly percolative cracked MLG films, respectively. The high gauge factor set a new landmark for strain sensor within 0-6 % strain range and demonstrates the potential for sensitive strain sensing. Meanwhile, the transparent graphene thin film conductor with stretchability $\geq$ 60 % is demonstrated for the first time. The stretchability of 60 % with GF $\leq$ 5.1 is comparable to literature and has interesting implications in flexible electronics. An unusual broad-frequency range accurate strain detection is demonstrated with the highly percolative cracked MLG film, that it shows only ~1.5% relaxation when ε = 60 % for 200 s; and accurate strain sensing up to 200 Hz when $\varepsilon \geq$ 13 %. The "time-independent" electromechanical performance shows the ability to meet the needs in real-world applications such as human-machine-interface. The findings in this work also gave a clue to many fundamental questions, like how to reduce relaxation in strain sensors? And how to achieve high-frequency dynamic response? Nonetheless, due to limited time, this work is still at a preliminary stage, future study is needed.

6.2 Future Outlook

This work has carried out a systematical investigation on the cracking behaviour of ultrathin MLG film and revealed its unique static and dynamic electromechanical properties. Although due to the limitation of time, some of the discoveries are preliminary and not fully-understood, they still suggest few areas worthy of being further investigated.

6.2.1 Interfacial energy modulated novel electronics fabrication

Transferring intact vacuum filtrated-MLG films on to different types of substrates via altering the interfacial interactions between graphene and an interfacial layer of graphene oxide seems to provide a promising strategy to transferring not only graphene but also other different types of vacuum filtrated thin films (i.e. MoS_2, CNT) onto required substrates. For examples, our preliminary trails on 1t phase MoS2 have demonstrated the intact transfer of MoS_2 onto various substrates and obtaining an ultrathin free-standing MoS_2 membrane. Illustrating the great

potential for synthesis ultrathin freestanding membranes or heterojunction materials for fundamental material research or the relevant applications. Moreover, by tuning the chemistry (wettability) of the interfacial layer materials via controlled humidity, heating, or lasering, it could potentially provide new clues to the cost-effective fabrication of thin film electronics.

6.2.2 In-depth study of cracking mechanism of polymer-supported thin film material

The PDMS-supported MLG film has demonstrated the unique cracking behaviour and extraordinary electromechanical sensing performance, indicating the possibility for future strain sensing applications. However, due to the limitations of time and experimental strategies, many problems remain.

For examples, the crack morphologies are roughly depicted with currently available image process techniques. Therefore, it was difficult to establish a clear influencing factor-crack morphology-electromechanical property profile, such as the difficulty faced in figure 4.9. Benefit from the novel techniques such as machine learning, our research group is currently adopting a machine learning technique on data processing to predict the performance of supercapacitors. We foresee that modern computing power can provide us with a shortcut to revealing the abovementioned profile. For another example, this study failed to apply precise data processing techniques on characterizing the crack formation process. Ideally, electromechanical characterizations could provide delicate information that the observational methodologies struggle to obtain. Therefore, developing data processing techniques could potentially help us to reveal the underlying cracking mechanisms of the MLG film or other materials; otherwise, we would reply on massive experimental characterisations. Both strategies suggested here are of practical feasibility, which will help us march towards transforming the cracked thin film electronics into real-world applications. Moreover, how would other factors such as deformation methods, materials' microstructure, thin film's wetting condition are also important aspects that are under consideration for further examination.

6.2.3 Precisely capturing human bodily motions

Through the elaborate control of assembling structure of PDMS-supported MLG film, the cracked MLG with unprecedented static and dynamic sensing capability has been developed.

This material holds great potential in precisely capturing human bodily motions with extreme broadband ranges. For example, the finger movements are a combination of quick and slow motions, achieving steady strain-resistance output could enable applications in the remote control system, such as remote surgery and remote military robotics, etc. Extreme accuracy is required in these future situations. For another example, the human body consists not only low-frequency motions but also high-frequency motions such as muscle tremblings. As movements are defined by their motion pattern, frequency and amplitude, an enormous amount of physiological information could be gathered if these motions can be captured and analysed. For example, muscle activity detection and analysation could lead to applications in assessing athletic performance, neuromuscular health conditions, etc. Moreover, strain sensors could collaborate with commercial techniques such as electromyography (EMG), and mechanomyography (MMG) for motion detections.

Currently, we are working towards this goal by an ongoing experiment at the St. Vicent hospital.

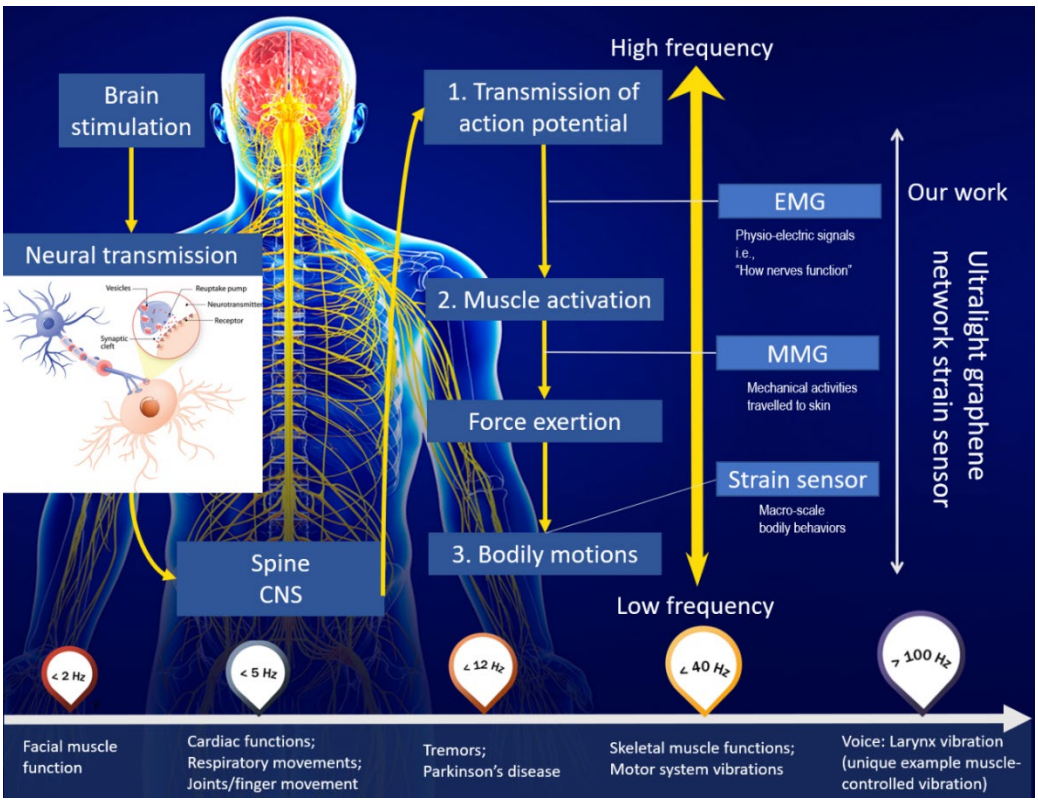

Figure 6.1 *Human bodily motion in frequency order.*

List of References

1. Bouchbinder, E., J. Fineberg, and M. Marder, *Dynamics of simple cracks.* Annu. Rev. Condens. Matter Phys., 2010. **1**(1): p. 371-395.
2. Hutchinson, J.W. and Z. Suo, *Mixed mode cracking in layered materials*, in *Advances in applied mechanics*. 1991, Elsevier. p. 63-191.
3. Pan, T.S., et al., *Experimental and Theoretical Studies of Serpentine Interconnects on Ultrathin Elastomers for Stretchable Electronics.* Advanced Functional Materials, 2017. **27**(37): p. 8.
4. Li, T., et al., *Stretchability of thin metal films on elastomer substrates.* Applied physics letters, 2004. **85**(16): p. 3435-3437.
5. Li, T. and Z. Suo, *Deformability of thin metal films on elastomer substrates.* International Journal of Solids and Structures, 2006. **43**(7-8): p. 2351-2363.
6. Li, T. and Z. Suo, *Ductility of thin metal films on polymer substrates modulated by interfacial adhesion.* International Journal of Solids and Structures, 2007. **44**(6): p. 1696-1705.
7. Lu, N., et al., *Failure by simultaneous grain growth, strain localization, and interface debonding in metal films on polymer substrates.* Journal of Materials Research, 2009. **24**(2): p. 379-385.
8. Niu, R., et al., *Ductility of metal thin films in flexible electronics.* Science in China Series E: Technological Sciences, 2008. **51**(11): p. 1971-1979.
9. Suo, Z., J. Vlassak, and S. Wagner, *Micromechanics of macroelectronics.* China Particuology, 2005. **3**(06): p. 321-328.
10. Tsay, C., et al., *How stretchable can we make thin metal films?* MRS Online Proceedings Library Archive, 2005. **875**.
11. Sekitani, T. and T. Someya, *Stretchable, Large-area Organic Electronics.* Advanced Materials, 2010. **22**(20): p. 2228-2246.
12. Miyamoto, A., et al., *Inflammation-free, gas-permeable, lightweight, stretchable on-skin electronics with nanomeshes.* Nature Nanotechnology, 2017. **12**(9): p. 907-+.
13. Sekitani, T., et al., *A rubberlike stretchable active matrix using elastic conductors.* Science, 2008. **321**(5895): p. 1468-1472.
14. Schwartz, G., et al., *Flexible polymer transistors with high pressure sensitivity for application in electronic skin and health monitoring.* Nature Communications, 2013. **4**: p. 8.
15. Lipomi, D.J., et al., *Skin-like pressure and strain sensors based on transparent elastic films of carbon nanotubes.* Nature Nanotechnology, 2011. **6**(12): p. 788-792.
16. Son, D., et al., *Multifunctional wearable devices for diagnosis and therapy of movement disorders.* Nature nanotechnology, 2014. **9**(5): p. 397.
17. Wang, S., et al., *Mechanics of epidermal electronics.* Journal of Applied Mechanics, 2012. **79**(3): p. 031022.
18. Sun, Y.G., et al., *Controlled buckling of semiconductor nanoribbons for stretchable electronics.* Nature Nanotechnology, 2006. **1**(3): p. 201-207.
19. Ray, T.R., et al., *Bio-Integrated Wearable Systems: A Comprehensive Review.* Chemical reviews, 2019.
20. Mack, S., et al., *Mechanically flexible thin-film transistors that use ultrathin ribbons of silicon derived from bulk wafers.* Applied Physics Letters, 2006. **88**(21): p. 3.
21. Kim, D.H., et al., *Stretchable, Curvilinear Electronics Based on Inorganic Materials.* Advanced Materials, 2010. **22**(19): p. 2108-2124.
22. Huang, X., et al., *Epidermal Impedance Sensing Sheets for Precision Hydration Assessment and Spatial Mapping.* Ieee Transactions on Biomedical Engineering, 2013. **60**(10): p. 2848-2857.
23. Heikenfeld, J., et al., *Wearable sensors: modalities, challenges, and prospects.* Lab on a Chip, 2018. **18**(2): p. 217-248.

24. Xu, B.X., et al., *An Epidermal Stimulation and Sensing Platform for Sensorimotor Prosthetic Control, Management of Lower Back Exertion, and Electrical Muscle Activation.* Advanced Materials, 2016. **28**(22): p. 4462-+.
25. Wu, J., et al., *Mechanics of reversible adhesion.* Soft Matter, 2011. **7**(18): p. 8657-8662.
26. Wang, H.L., et al., *Vibration of mechanically-assembled 3D microstructures formed by compressive buckling.* Journal of the Mechanics and Physics of Solids, 2018. **112**: p. 187-208.
27. Won, S.M., et al., *Recent Advances in Materials, Devices, and Systems for Neural Interfaces.* Advanced Materials, 2018. **30**(30): p. 19.
28. Kim, D.H. and J.A. Rogers, *Stretchable Electronics: Materials Strategies and Devices.* Advanced Materials, 2008. **20**(24): p. 4887-4892.
29. Han, M., et al., *Three-dimensional piezoelectric polymer microsystems for vibrational energy harvesting, robotic interfaces and biomedical implants.* Nature Electronics, 2019. **2**(1): p. 26.
30. Kim, D.H., et al., *Materials and noncoplanar mesh designs for integrated circuits with linear elastic responses to extreme mechanical deformations.* Proceedings of the National Academy of Sciences of the United States of America, 2008. **105**(48): p. 18675-18680.
31. Ko, H.C., et al., *Curvilinear Electronics Formed Using Silicon Membrane Circuits and Elastomeric Transfer Elements.* Small, 2009. **5**(23): p. 2703-2709.
32. Kang, D., et al., *Ultrasensitive mechanical crack-based sensor inspired by the spider sensory system.* Nature, 2014. **516**(7530): p. 222.
33. Sarkar, B., D.K. Satapathy, and M. Jaiswal, *Nanostructuring mechanical cracks in a flexible conducting polymer thin film for ultra-sensitive vapor sensing.* Nanoscale, 2019. **11**(1): p. 200-210.
34. Choi, Y.W., et al., *Ultra-sensitive pressure sensor based on guided straight mechanical cracks.* Scientific reports, 2017. **7**: p. 40116.
35. Luo, Q., et al., *Nanoelectromechanical Switches by Controlled Switchable Cracking.* IEEE Electron Device Letters, 2019. **40**(7): p. 1209-1212.
36. Zhang, B., et al., *Stretchable conductive fibers based on a cracking control strategy for wearable electronics.* Advanced Functional Materials, 2018. **28**(29): p. 1801683.
37. Li, X., et al., *Stretchable and highly sensitive graphene-on-polymer strain sensors.* Scientific reports, 2012. **2**: p. 870.
38. Park, B., et al., *Dramatically Enhanced Mechanosensitivity and Signal‐to‐Noise Ratio of Nanoscale Crack‐Based Sensors: Effect of Crack Depth.* Advanced materials, 2016. **28**(37): p. 8130-8137.
39. Yamada, T., et al., *A stretchable carbon nanotube strain sensor for human-motion detection.* Nature nanotechnology, 2011. **6**(5): p. 296.
40. Lee, J., et al., *A stretchable strain sensor based on a metal nanoparticle thin film for human motion detection.* Nanoscale, 2014. **6**(20): p. 11932-11939.
41. Wang, S., et al., *Network cracks-based wearable strain sensors for subtle and large strain detection of human motions.* Journal of Materials Chemistry C, 2018. **6**(19): p. 5140-5147.
42. Zhu, L., et al., *Highly sensitive, ultrastretchable strain sensors prepared by pumping hybrid fillers of carbon nanotubes/cellulose nanocrystal into electrospun polyurethane membranes.* ACS applied materials & interfaces, 2019. **11**(13): p. 12968-12977.
43. Sun, H., et al., *A Highly Sensitive and Stretchable Yarn Strain Sensor for Human Motion Tracking Utilizing a Wrinkle-Assisted Crack Structure.* ACS applied materials & interfaces, 2019. **11**(39): p. 36052-36062.
44. Jung, H., et al., *Nano-Cracked Strain Sensor with High Sensitivity and Linearity by Controlling the Crack Arrangement.* Sensors, 2019. **19**(12): p. 2834.
45. Amjadi, M., et al., *Parallel microcracks-based ultrasensitive and highly stretchable strain sensors.* ACS applied materials & interfaces, 2016. **8**(8): p. 5618-5626.
46. WhanáChoi, Y. and S. MoonáKim, *Crack-based strain sensor with diverse metal films by inserting an inter-layer.* RSC advances, 2017. **7**(55): p. 34810-34815.

47. Chen, S., et al., *Acid-Interface Engineering of Carbon Nanotube/Elastomers with Enhanced Sensitivity for Stretchable Strain Sensors.* ACS applied materials & interfaces, 2018. **10**(43): p. 37760-37766.
48. Han, Z., et al., *High-performance flexible strain sensor with bio-inspired crack arrays.* Nanoscale, 2018. **10**(32): p. 15178-15186.
49. Lee, S., et al., *A Highly Sensitive Bending Sensor Based on Controlled Crack Formation Integrated with an Energy Harvesting Pyramid Layer.* Advanced Materials Technologies, 2018. **3**(12): p. 1800307.
50. Xin, Y., et al., *Making a bilateral compression/tension sensor by pre-stretching open-crack networks in carbon nanotube papers.* ACS applied materials & interfaces, 2018. **10**(39): p. 33507-33515.
51. Miao, W., et al., *Micro-/nano-voids guided two-stage film cracking on bioinspired assemblies for high-performance electronics.* Nature communications, 2019. **10**(1): p. 1-8.
52. Zhang, J., et al., *Flexible and highly sensitive pressure sensors based on microcrack arrays inspired by scorpions.* RSC advances, 2019. **9**(39): p. 22740-22748.
53. Zhou, Y., et al., *Significant stretchability enhancement of a crack-based strain sensor combined with high sensitivity and superior durability for motion monitoring.* ACS applied materials & interfaces, 2019. **11**(7): p. 7405-7414.
54. Lambricht, N., T. Pardoen, and S. Yunus, *Giant stretchability of thin gold films on rough elastomeric substrates.* Acta materialia, 2013. **61**(2): p. 540-547.
55. Liu, Z., et al., *Thickness‐Gradient Films for High Gauge Factor Stretchable Strain Sensors.* Advanced Materials, 2015. **27**(40): p. 6230-6237.
56. Lacour, S.P., et al., *Mechanisms of reversible stretchability of thin metal films on elastomeric substrates.* Applied Physics Letters, 2006. **88**(20): p. 204103.
57. Leterrier, Y., et al., *Mechanical integrity of transparent conductive oxide films for flexible polymer-based displays.* Thin Solid Films, 2004. **460**(1-2): p. 156-166.
58. Graudejus, O., P. Görrn, and S. Wagner, *Controlling the morphology of gold films on poly (dimethylsiloxane).* ACS applied materials & interfaces, 2010. **2**(7): p. 1927-1933.
59. Liu, Z., et al., *Surface Strain Redistribution on Structured Microfibers to Enhance Sensitivity of Fiber‐Shaped Stretchable Strain Sensors.* Advanced materials, 2018. **30**(5): p. 1704229.
60. Yang, T., et al., *Structural engineering of gold thin films with channel cracks for ultrasensitive strain sensing.* Materials Horizons, 2016. **3**(3): p. 248-255.
61. Wang, S.H., et al., *Skin-Inspired Electronics: An Emerging Paradigm.* Accounts of Chemical Research, 2018. **51**(5): p. 1033-1045.
62. Amjadi, M., Y.J. Yoon, and I. Park, *Ultra-stretchable and skin-mountable strain sensors using carbon nanotubes–Ecoflex nanocomposites.* Nanotechnology, 2015. **26**(37): p. 375501.
63. Atalay, O., W.R. Kennon, and M.D. Husain, *Textile-based weft knitted strain sensors: Effect of fabric parameters on sensor properties.* Sensors, 2013. **13**(8): p. 11114-11127.
64. Choi, D.Y., et al., *Highly stretchable, hysteresis-free ionic liquid-based strain sensor for precise human motion monitoring.* ACS applied materials & interfaces, 2017. **9**(2): p. 1770-1780.
65. Mattmann, C., F. Clemens, and G. Tröster, *Sensor for measuring strain in textile.* Sensors, 2008. **8**(6): p. 3719-3732.
66. Wang, Y., X. Zhang, and D. Li, *Dynamic configuration of reduced graphene oxide in aqueous dispersion and its effect on thin film properties.* Chemical Communications, 2015. **51**(100): p. 17760-17763.
67. Yang, X., et al., *Ordered gelation of chemically converted graphene for next-generation electroconductive hydrogel films.* Angewandte Chemie - International Edition, 2011. **50**(32): p. 7325-7328.
68. Qiu, L., et al., *Controllable corrugation of chemically converted graphene sheets in water and potential application for nanofiltration.* Chemical Communications, 2011. **47**(20): p. 5810-5812.

69. Yang, X., et al., *Liquid-mediated dense integration of graphene materials for compact capacitive energy storage.* science, 2013. **341**(6145): p. 534-537.
70. Lee, J.-H., et al., *Fracture mechanism and electromechanical behavior of chemical vapor deposited graphene on flexible substrate under tension.* Carbon, 2017. **118**: p. 475-484.
71. Cao, C., et al., *Nonlinear fracture toughness measurement and crack propagation resistance of functionalized graphene multilayers.* Science advances, 2018. **4**(4): p. eaao7202.
72. Li, P., et al., *In situ tensile fracturing of multilayer graphene nanosheets for their in-plane mechanical properties.* Nanotechnology, 2019. **30**(47): p. 475708.
73. Jang, B., et al., *Asynchronous cracking with dissimilar paths in multilayer graphene.* Nanoscale, 2017. **9**(44): p. 17325-17333.
74. Zheng, S., et al., *Swelling of graphene oxide membranes in aqueous solution: characterization of interlayer spacing and insight into water transport mechanisms.* ACS nano, 2017. **11**(6): p. 6440-6450.
75. Chi, C., et al., *Facile preparation of graphene oxide membranes for gas separation.* Chemistry of Materials, 2016. **28**(9): p. 2921-2927.
76. Pham, V.H., et al., *Fast and simple fabrication of a large transparent chemically-converted graphene film by spray-coating.* Carbon, 2010. **48**(7): p. 1945-1951.
77. Hempel, M., et al., *A novel class of strain gauges based on layered percolative films of 2D materials.* Nano letters, 2012. **12**(11): p. 5714-5718.
78. Yamaguchi, H., et al., *Highly uniform 300 mm wafer-scale deposition of single and multilayered chemically derived graphene thin films.* ACS nano, 2010. **4**(1): p. 524-528.
79. Xu, Y., et al., *Polymer photovoltaic devices with transparent graphene electrodes produced by spin-casting.* Carbon, 2010. **48**(11): p. 3308-3311.
80. Liu, J., et al., *Graphene dip coatings: An effective anticorrosion barrier on aluminum.* Applied Surface Science, 2015. **327**: p. 241-245.
81. Lange, U., et al., *Hydrogen sensor based on a graphene–palladium nanocomposite.* Electrochimica Acta, 2011. **56**(10): p. 3707-3712.
82. Wang, J., et al., *Wetting‐Induced Climbing for Transferring Interfacially Assembled Large‐Area Ultrathin Pristine Graphene Film.* Advanced Materials, 2019. **31**(10): p. 1806742.
83. Li, X., et al., *Large‐area ultrathin graphene films by single‐step marangoni self‐assembly for highly sensitive strain sensing application.* Advanced Functional Materials, 2016. **26**(9): p. 1322-1329.
84. Deokar, G., et al., *Towards high quality CVD graphene growth and transfer.* Carbon, 2015. **89**: p. 82-92.
85. Sheng, J., et al., *Review of recent progresses on flexible oxide semiconductor thin film transistors based on atomic layer deposition processes.* Journal of Semiconductors, 2018. **39**(1): p. 011008.
86. Myny, K., *The development of flexible integrated circuits based on thin-film transistors.* Nature Electronics, 2018. **1**(1): p. 30-39.
87. Li, X., et al., *Large-area synthesis of high-quality and uniform graphene films on copper foils.* science, 2009. **324**(5932): p. 1312-1314.
88. Matsumoto, K., *Frontiers of graphene and carbon nanotubes: devices and applications*. 2015: Springer.
89. Muñoz, R. and C. Gómez‐Aleixandre, *Review of CVD synthesis of graphene.* Chemical Vapor Deposition, 2013. **19**(10-11-12): p. 297-322.
90. Schwander, M. and K. Partes, *A review of diamond synthesis by CVD processes.* Diamond and related materials, 2011. **20**(9): p. 1287-1301.
91. Zhang, Y., L. Zhang, and C. Zhou, *Review of chemical vapor deposition of graphene and related applications.* Accounts of chemical research, 2013. **46**(10): p. 2329-2339.
92. Vervuurt, R.H., W.M. Kessels, and A.A. Bol, *Atomic layer deposition for graphene device integration.* Advanced Materials Interfaces, 2017. **4**(18): p. 1700232.

93. Azpeitia, J., et al., *High-quality PVD graphene growth by fullerene decomposition on Cu foils.* Carbon, 2017. **119**: p. 535-543.
94. Narula, U., C.M. Tan, and C.S. Lai, *Growth mechanism for low temperature PVD graphene synthesis on copper using amorphous carbon.* Scientific reports, 2017. **7**(1): p. 1-13.
95. Tung, V.C., et al., *High-throughput solution processing of large-scale graphene.* Nature nanotechnology, 2009. **4**(1): p. 25.
96. Li, D., et al., *Processable aqueous dispersions of graphene nanosheets.* Nature nanotechnology, 2008. **3**(2): p. 101.
97. Adetayo, A. and D. Runsewe, *Synthesis and Fabrication of Graphene and Graphene Oxide: A Review.* Open Journal of Composite Materials, 2019. **9**(02): p. 207.
98. Konios, D., et al., *Dispersion behaviour of graphene oxide and reduced graphene oxide.* Journal of colloid and interface science, 2014. **430**: p. 108-112.
99. Robinson, J.T., et al., *Wafer-scale reduced graphene oxide films for nanomechanical devices.* Nano letters, 2008. **8**(10): p. 3441-3445.
100. He, Q., et al., *Fabrication of flexible MoS2 thin-film transistor arrays for practical gas-sensing applications.* Small, 2012. **8**(19): p. 2994-2999.
101. Pu, N.-W., et al., *Dispersion of graphene in aqueous solutions with different types of surfactants and the production of graphene films by spray or drop coating.* Journal of the Taiwan Institute of Chemical Engineers, 2012. **43**(1): p. 140-146.
102. Jing, X., W. Zhao, and L. Lan, *The effect of particle size on electric conducting percolation threshold in polymer/conducting particle composites.* Journal of materials science letters, 2000. **19**(5): p. 377-379.
103. Scher, H. and R. Zallen, *Critical density in percolation processes.* The Journal of Chemical Physics, 1970. **53**(9): p. 3759-3761.
104. Sheng, P., E. Sichel, and J. Gittleman, *Fluctuation-induced tunneling conduction in carbon-polyvinylchloride composites.* Physical Review Letters, 1978. **40**(18): p. 1197.
105. Simmons, J.G., *Generalized formula for the electric tunnel effect between similar electrodes separated by a thin insulating film.* Journal of applied physics, 1963. **34**(6): p. 1793-1803.
106. Stauffer, D. and A. Aharony, *Introduction to percolation theory*. 2014: Taylor & Francis.
107. Li, L., et al., *A superhydrophobic smart coating for flexible and wearable sensing electronics.* Advanced Materials, 2017. **29**(43): p. 1702517.
108. Su, X., et al., *Highly stretchable and conductive superhydrophobic coating for flexible electronics.* ACS applied materials & interfaces, 2018. **10**(12): p. 10587-10597.
109. Lipomi, D.J., et al., *Skin-like pressure and strain sensors based on transparent elastic films of carbon nanotubes.* Nature nanotechnology, 2011. **6**(12): p. 788.
110. Abdelhalim, A., et al., *Fabrication of carbon nanotube thin films on flexible substrates by spray deposition and transfer printing.* Carbon, 2013. **61**: p. 72-79.
111. Wang, Y., et al., *Graphene-directed supramolecular assembly of multifunctional polymer hydrogel membranes.* Advanced Functional Materials, 2015. **25**(1): p. 126-133.
112. Chen, H., et al., *Mechanically strong, electrically conductive, and biocompatible graphene paper.* Advanced Materials, 2008. **20**(18): p. 3557-3561.
113. Zhang, K., X. Yang, and D. Li, *Engineering graphene for high-performance supercapacitors: Enabling role of colloidal chemistry.* Journal of Energy Chemistry, 2018. **27**(1): p. 1-5.
114. Wang, Y., et al., *High-Rate and High-Volumetric Capacitance of Compact Graphene–Polyaniline Hydrogel Electrodes.* Advanced Energy Materials, 2016. **6**(11).
115. Cheng, C., et al., *Ion transport in complex layered graphene-based membranes with tuneable interlayer spacing.* Science advances, 2016. **2**(2): p. e1501272.
116. Park, Y., et al., *Microtopography-guided conductive patterns of liquid-driven graphene nanoplatelet networks for stretchable and skin-conformal sensor array.* Advanced materials, 2017. **29**(21): p. 1606453.

117. Mu, C., et al., *Flexible Normal‐Tangential Force Sensor with Opposite Resistance Responding for Highly Sensitive Artificial Skin.* Advanced Functional Materials, 2018. **28**(18): p. 1707503.
118. Nguyen, D.D., et al., *Superhydrophobic and superoleophilic properties of graphene-based sponges fabricated using a facile dip coating method.* Energy & Environmental Science, 2012. **5**(7): p. 7908-7912.
119. An, S.J., et al., *Thin film fabrication and simultaneous anodic reduction of deposited graphene oxide platelets by electrophoretic deposition.* The Journal of Physical Chemistry Letters, 2010. **1**(8): p. 1259-1263.
120. Sastry, M., et al., *DNA-mediated electrostatic assembly of gold nanoparticles into linear arrays by a simple drop-coating procedure.* Applied Physics Letters, 2001. **78**(19): p. 2943-2945.
121. Kočišová, E. and M. Procházka, *Drop‐coating deposition Raman spectroscopy of liposomes.* Journal of Raman Spectroscopy, 2011. **42**(8): p. 1606-1610.
122. Hu, P., et al., *Drop‐coating deposition and surface‐enhanced Raman spectroscopies (DCDRS and SERS) provide complementary information of whole human tears.* Journal of Raman spectroscopy, 2014. **45**(7): p. 565-573.
123. Takahashi, Y., et al., *Dip-coating of ITO films.* Journal of non-crystalline solids, 1997. **218**: p. 129-134.
124. Brinker, C., et al., *Fundamentals of sol-gel dip coating.* Thin solid films, 1991. **201**(1): p. 97-108.
125. Lu, N., et al., *Highly sensitive skin‐mountable strain gauges based entirely on elastomers.* Advanced Functional Materials, 2012. **22**(19): p. 4044-4050.
126. Pang, C., et al., *A flexible and highly sensitive strain-gauge sensor using reversible interlocking of nanofibres.* Nature materials, 2012. **11**(9): p. 795.
127. Boland, C.S., et al., *Sensitive, high-strain, high-rate bodily motion sensors based on graphene–rubber composites.* ACS nano, 2014. **8**(9): p. 8819-8830.
128. Yao, S. and Y. Zhu, *Wearable multifunctional sensors using printed stretchable conductors made of silver nanowires.* Nanoscale, 2014. **6**(4): p. 2345-2352.
129. Cheng, Y., et al., *A stretchable and highly sensitive graphene‐based fiber for sensing tensile strain, bending, and torsion.* Advanced Materials, 2015. **27**(45): p. 7365-7371.
130. Lee, S., et al., *Ag nanowire reinforced highly stretchable conductive fibers for wearable electronics.* Advanced Functional Materials, 2015. **25**(21): p. 3114-3121.
131. Gorantla, S., et al., *A universal transfer route for graphene.* Nanoscale, 2014. **6**(2): p. 889-896.
132. Bae, S.-H., et al., *Graphene-based transparent strain sensor.* Carbon, 2013. **51**: p. 236-242.
133. Yang, J., et al., *Wearable temperature sensor based on graphene nanowalls.* Rsc Advances, 2015. **5**(32): p. 25609-25615.
134. Liu, J., et al., *Exploiting a robust biopolymer network binder for an ultrahigh-areal-capacity Li–S battery.* Energy & Environmental Science, 2016. **10**.
135. Wassei, J.K. and R.B. Kaner, *Graphene, a promising transparent conductor.* Materials today, 2010. **13**(3): p. 52-59.
136. Chen, S.C., et al., *Defective Carbon-Based Materials for the Electrochemical Synthesis of Hydrogen Peroxide.* Acs Sustainable Chemistry & Engineering, 2018. **6**(1): p. 311-317.
137. Gross, D. and T. Seelig, *Fracture mechanics: with an introduction to micromechanics*. 2017: Springer.
138. Dikin, D.A., et al., *Preparation and characterization of graphene oxide paper.* Nature, 2007. **448**(7152): p. 457-460.
139. Le, M.-Q. and R.C. Batra, *Single-edge crack growth in graphene sheets under tension.* Computational Materials Science, 2013. **69**: p. 381-388.
140. Gao, Y. and P. Hao, *Mechanical properties of monolayer graphene under tensile and compressive loading.* Physica E: Low-dimensional Systems and Nanostructures, 2009. **41**(8): p. 1561-1566.
141. Liu, Y., et al., *Mechanical properties of graphene papers.* Journal of the Mechanics and Physics of Solids, 2012. **60**(4): p. 591-605.

142. Cordill, M. and A. Taylor, *Thickness effect on the fracture and delamination of titanium films.* Thin Solid Films, 2015. **589**: p. 209-214.
143. Tsui, T.Y., A.J. McKerrow, and J.J. Vlassak, *Constraint effects on thin film channel cracking behavior.* Journal of materials research, 2005. **20**(9): p. 2266-2273.
144. Shen, J., Z. Gai, and J. Kirschner, *Growth and magnetism of metallic thin films and multilayers by pulsed-laser deposition.* Surface science reports, 2004. **52**(5-6): p. 163-218.
145. Utriainen, M., et al., *Studies of metallic thin film growth in an atomic layer epitaxy reactor using M (acac) 2 (M= Ni, Cu, Pt) precursors.* Applied Surface Science, 2000. **157**(3): p. 151-158.
146. Chen, M., et al., *Controlled Fragmentation of Single-Atom-Thick Polycrystalline Graphene.* Matter, 2019.
147. Qiao, Y., et al., *Multilayer Graphene Epidermal Electronic Skin.* ACS nano, 2018. **12**(9): p. 8839-8846.
148. Nakamura, N. and H. Ogi. *Monitoring of morphological change of deposited metallic thin film through internal friction of noncontacting piezoelectric oscillator*. in *2017 IEEE International Ultrasonics Symposium (IUS)*. 2017. IEEE.
149. Amjadi, M., et al., *Stretchable, skin‐mountable, and wearable strain sensors and their potential applications: a review.* Advanced Functional Materials, 2016. **26**(11): p. 1678-1698.
150. Prado, L.A. and I.V. Yoshida, *Studies on the structural heterogeneities of poly (dimethylsiloxane) networks modified with poly (phenylsilsesquioxane) s using small-angle X-ray scattering and dynamical mechanical analysis.* Journal of non-crystalline solids, 2009. **355**(34-36): p. 1726-1732.
151. Qiu, L., D. Li, and H.-M. Cheng, *Structural Control of Graphene-Based Materials for Unprecedented Performance.* ACS nano, 2018. **12**(6): p. 5085-5092.
152. Gao, W., *The chemistry of graphene oxide*, in *Graphene oxide*. 2015, Springer. p. 61-95.
153. Bai, H., et al., *On the gelation of graphene oxide.* The Journal of Physical Chemistry C, 2011. **115**(13): p. 5545-5551.
154. Yang, X., et al., *Ordered gelation of chemically converted graphene for next‐generation electroconductive hydrogel films.* Angewandte Chemie International Edition, 2011. **50**(32): p. 7325-7328.
155. Woo, C.-S., et al., *Fabrication of flexible and transparent single-wall carbon nanotube gas sensors by vacuum filtration and poly (dimethyl siloxane) mold transfer.* Microelectronic Engineering, 2007. **84**(5-8): p. 1610-1613.
156. Lim, C., D.-H. Min, and S.-B. Lee, *Direct patterning of carbon nanotube network devices by selective vacuum filtration.* Applied Physics Letters, 2007. **91**(24): p. 243117.
157. Linghu, C., et al., *Transfer printing techniques for flexible and stretchable inorganic electronics.* npj Flexible Electronics, 2018. **2**(1): p. 1-14.
158. Chen, X.-D., et al., *High-quality and efficient transfer of large-area graphene films onto different substrates.* Carbon, 2013. **56**: p. 271-278.
159. Dong, W.J., et al., *Ultrafast and Chemically Stable Transfer of Au Nanomembrane Using a Water-Soluble NaCl Sacrificial Layer for Flexible Solar Cells.* ACS applied materials & interfaces, 2019. **11**(33): p. 30477-30483.
160. Song, L., et al., *Transfer printing of graphene using gold film.* ACS nano, 2009. **3**(6): p. 1353-1356.
161. Abraham, J., et al., *Tunable sieving of ions using graphene oxide membranes.* Nat Nanotechnol, 2017. **12**(6): p. 546-550.
162. Chen, L., et al., *Ion sieving in graphene oxide membranes via cationic control of interlayer spacing.* Nature, 2017. **550**(7676): p. 380-383.
163. Kim, S., et al., *Highly crosslinked, chlorine tolerant polymer network entwined graphene oxide membrane for water desalination.* Journal of Materials Chemistry A, 2017. **5**(4): p. 1533-1540.
164. Hontoria-Lucas, C., et al., *Study of oxygen-containing groups in a series of graphite oxides: physical and chemical characterization.* Carbon, 1995. **33**(11): p. 1585-1592.

165. Wang, Z., et al., *Micropatterning of organic semiconductor microcrystalline materials and OFET fabrication by "hot lift off".* Journal of the American Chemical Society, 2003. **125**(50): p. 15278-15279.
166. Xiong, Z., C. Liao, and X. Wang, *Reduced graphene oxide diffraction gratings from duplication of photoinduced azo polymer surface-relief-gratings through soft-lithography.* Journal of Materials Chemistry C, 2015. **3**(24): p. 6224-6231.
167. Subedi, D., *Contact angle measurement for the surface characterization of solids.* Himalayan Physics, 2011. **2**: p. 1-4.
168. Liu, S., et al., *Fast and controllable fabrication of suspended graphene nanopore devices.* Nanotechnology, 2012. **23**(8): p. 085301.
169. Clint, J.H., *Adhesion and components of solid surface energies.* Current Opinion in Colloid & Interface Science, 2001. **6**(1): p. 28-33.
170. Dupré, A. and P. Dupré, *Théorie mécanique de la chaleur*. 1869: Gauthier-Villars.
171. Wu, S., *Polar and nonpolar interactions in adhesion.* The Journal of Adhesion, 1973. **5**(1): p. 39-55.
172. Lu, J.-Y., et al., *The evolution in graphitic surface wettability with first-principles quantum simulations: the counterintuitive role of water.* Physical Chemistry Chemical Physics, 2018. **20**(35): p. 22636-22644.
173. Petersen, S.V. and D. Li, *Controlled gelation of graphene towards unprecedented superstructures.* Chemistry-A European Journal, 2017.
174. Terdalkar, S.S., et al., *Nanoscale fracture in graphene.* Chemical Physics Letters, 2010. **494**(4-6): p. 218-222.
175. Zhang, B., L. Mei, and H. Xiao, *Nanofracture in graphene under complex mechanical stresses.* Applied Physics Letters, 2012. **101**(12): p. 121915.
176. Zhang, T., X. Li, and H. Gao, *Fracture of graphene: a review.* International Journal of Fracture, 2015. **196**(1-2): p. 1-31.
177. Suk, J.W., et al., *Mechanical properties of monolayer graphene oxide.* ACS nano, 2010. **4**(11): p. 6557-6564.
178. Rogers, J.A., R. Ghaffari, and D.-H. Kim, *Stretchable bioelectronics for medical devices and systems*. 2016: Springer.
179. Kim, T.K., J.K. Kim, and O.C. Jeong, *Measurement of nonlinear mechanical properties of PDMS elastomer.* Microelectronic Engineering, 2011. **88**(8): p. 1982-1985.
180. Shintake, J., et al., *Ultrastretchable strain sensors using carbon black‐filled elastomer composites and comparison of capacitive versus resistive sensors.* Advanced Materials Technologies, 2018. **3**(3): p. 1700284.
181. Liu, Y., et al. *A stretchable and transparent SWNT strain sensor encapsulated in thin PDMS films*. in *2013 Transducers & Eurosensors XXVII: The 17th International Conference on Solid-State Sensors, Actuators and Microsystems (TRANSDUCERS & EUROSENSORS XXVII)*. 2013. IEEE.
182. Hu, J.-y. and S. Jiang, *Study on Encapsulating technique and strain sensing characteristic of FBG temperature sensor.* JOURNAL OF OPTOELECTRONICS LASER, 2006. **17**(3): p. 311.
183. Vella, D., et al., *The macroscopic delamination of thin films from elastic substrates.* Proceedings of the National Academy of Sciences, 2009. **106**(27): p. 10901-10906.
184. Cordill, M.J., et al., *Fracture and delamination of chromium thin films on polymer substrates.* Metallurgical and Materials Transactions A, 2010. **41**(4): p. 870-875.
185. Hashimoto, A., et al., *Atomic correlation between adjacent graphene layers in double-wall carbon nanotubes.* Physical review letters, 2005. **94**(4): p. 045504.
186. 郭涛, *脆性薄膜的失效及其对基体的影响*. 2018, 北京科技大学.
187. Roylance, D., *Introduction to fracture mechanics.* 2001.
188. Anderson, T.L. and T.L. Anderson, *Fracture mechanics: fundamentals and applications*. 2005: CRC press.

189. Anderson, T.L., *Fracture mechanics-fundamentals and applications.* NASA STI/Recon Technical Report A, 1991. **92**.
190. Liu, Q., et al., *High-performance strain sensors with fish-scale-like graphene-sensing layers for full-range detection of human motions.* ACS nano, 2016. **10**(8): p. 7901-7906.
191. Soldano, C., A. Mahmood, and E. Dujardin, *Production, properties and potential of graphene.* Carbon, 2010. **48**(8): p. 2127-2150.
192. Liu, G., W. Jin, and N. Xu, *Graphene-based membranes.* Chemical Society Reviews, 2015. **44**(15): p. 5016-5030.
193. Liu, M., et al., *Thickness-dependent mechanical properties of polydimethylsiloxane membranes.* Journal of micromechanics and microengineering, 2009. **19**(3): p. 035028.
194. Seghir, R. and S. Arscott, *Extended PDMS stiffness range for flexible systems.* Sensors and Actuators A: Physical, 2015. **230**: p. 33-39.
195. Khan, U., et al., *Size selection of dispersed, exfoliated graphene flakes by controlled centrifugation.* Carbon, 2012. **50**(2): p. 470-475.
196. 汪国睿, *石墨烯界面力学行为的表征与调控研究*. 2017, 中国科学技术大学.
197. Lopez-Polin, G., J. Gomez-Herrero, and C. Gómez-Navarro, *Confining crack propagation in defective graphene.* Nano letters, 2015. **15**(3): p. 2050-2054.
198. Budarapu, P.R., et al., *Crack propagation in graphene.* Journal of Applied Physics, 2015. **118**(6): p. 064307.
199. Wang, Y., et al., *Wearable and highly sensitive graphene strain sensors for human motion monitoring.* Advanced Functional Materials, 2014. **24**(29): p. 4666-4670.
200. Won, S.M., et al., *Multimodal Sensing with a Three-Dimensional Piezoresistive Structure.* ACS nano, 2019.
201. Gong, S., et al., *Tattoolike polyaniline microparticle-doped gold nanowire patches as highly durable wearable sensors.* ACS applied materials & interfaces, 2015. **7**(35): p. 19700-19708.
202. Liu, H., et al., *Electrically conductive polymer composites for smart flexible strain sensors: a critical review.* Journal of Materials Chemistry C, 2018. **6**(45): p. 12121-12141.
203. Hu, N., et al., *Piezoresistive strain sensors made from carbon nanotubes based polymer nanocomposites.* Sensors, 2011. **11**(11): p. 10691-10723.
204. Maxian, O., D. Pedrazzoli, and I. Manas-Zloczower, *Modeling the electrical percolation behavior of hybrid nanocomposites based on carbon nanotubes and graphene nanoplatelets.* Materials Research Express, 2015. **2**(9): p. 095013.
205. Li, J. and J.-K. Kim, *Percolation threshold of conducting polymer composites containing 3D randomly distributed graphite nanoplatelets.* Composites Science and Technology, 2007. **67**(10): p. 2114-2120.
206. Hu, N., et al., *Tunneling effect in a polymer/carbon nanotube nanocomposite strain sensor.* Acta Materialia, 2008. **56**(13): p. 2929-2936.
207. Hicks, J., A. Behnam, and A. Ural, *A computational study of tunneling-percolation electrical transport in graphene-based nanocomposites.* Applied Physics Letters, 2009. **95**(21): p. 213103.
208. Wang, G., et al., *Measuring interlayer shear stress in bilayer graphene.* Physical review letters, 2017. **119**(3): p. 036101.
209. Jiang, T., R. Huang, and Y. Zhu, *Interfacial sliding and buckling of monolayer graphene on a stretchable substrate.* Advanced Functional Materials, 2014. **24**(3): p. 396-402.
210. Ryu, S., et al., *Extremely elastic wearable carbon nanotube fiber strain sensor for monitoring of human motion.* ACS nano, 2015. **9**(6): p. 5929-5936.
211. Li, L., et al., *Ultrastretchable Fiber Sensor with High Sensitivity in Whole Workable Range for Wearable Electronics and Implantable Medicine.* Advanced Science, 2018. **5**(9): p. 1800558.
212. Hwang, B.-U., et al., *Transparent stretchable self-powered patchable sensor platform with ultrasensitive recognition of human activities.* ACS nano, 2015. **9**(9): p. 8801-8810.

213. Pan, F., et al., *3D Graphene Films Enable Simultaneously High Sensitivity and Large Stretchability for Strain Sensors.* Advanced Functional Materials, 2018. **28**(40): p. 1803221.
214. Boland, C.S., et al., *Sensitive electromechanical sensors using viscoelastic graphene-polymer nanocomposites.* Science, 2016. **354**(6317): p. 1257-1260.
215. Wang, D.-Y., et al., *High performance flexible strain sensor based on self-locked overlapping graphene sheets.* Nanoscale, 2016. **8**(48): p. 20090-20095.
216. Roh, E., et al., *Stretchable, transparent, ultrasensitive, and patchable strain sensor for human–machine interfaces comprising a nanohybrid of carbon nanotubes and conductive elastomers.* ACS nano, 2015. **9**(6): p. 6252-6261.
217. Xiao, X., et al., *High ‐strain sensors based on ZnO nanowire/polystyrene hybridized flexible films.* Advanced materials, 2011. **23**(45): p. 5440-5444.